Institut für Tierwissenschaften
Abteilung Biochemie der Rheinischen Friedrich-Wilhelms-Universität Bonn

---

Vitamin K dependent γ-carboxylation in chronic kidney disease

Inaugural-Dissertation

zur

Erlangung des Grades

Doktor der Ernährungswissenschaften
(Dr. troph)

der
Landwirtschatlichen Fakultät
der
Rheinischen Friedrich-Wilhelms-Universität

Bonn
vorgelegt im Juli 2013

von Nadine Kaesler

aus
Aachen

Referent:	Prof. Dr. rer. nat. Brigitte Schmitz
Koreferenten:	Prof. Dr. rer. nat. Simone Diestel PD. Dr. med. Vincent Brandenburg
Tag der mündlichen Prüfung:	19.11.2013
Erscheinungsjahr:	2014

Veröffentlichungen im Rahmen dieser Arbeit

I Originalarbeiten

Kaesler N, Schettgen T, Mutucumarana VP, Brandenburg V, Jahnen-Dechent W, Schurgers LJ, Krüger T.: A fluorescent method to determine vitamin K-dependent gamma-glutamyl carboxylase activity. *Anal Biochem*. 2012 Feb 15;421(2):411-6. doi: 10.1016/j.ab.2011.11.036. Epub 2011 Dec 2.

Kaesler N, Magdeleyns E, Herfs M, Schettgen T, Brandenburg V, Vermeer C, Floege J, Schlieper G, Krüger T: Impaired vitamin K recycling in uremia is rescued by vitamin K supplementation; *Kidney International*, in press

Kaesler N, Krüger T: Vitamin K, mehr als nur Koagulation, akzeptiert bei Ernährung und Medizin 03/2013

Kaesler N, Immendorf S, Ouyang C, Herfs M, Magdeleyns E, Carmeliet P, Floege J, Krüger T, Schlieper G: Gas6 Protein and its Role in Vascular Calcification; under revision, *PLOSone*

II Kongressbeiträge und Meetings

a) Vorträge

The Vitamin K cycle and vascular calcification

- Fellows Meeting, Abbvie Symposium on behalf of the 50th ERA.EDTA, Istanbul, Turkey, 2013

"Gas6 protein and its role in vascular calcification"

- 45th Annual Meeting of the American Society of Nephrology, Kidney Week, San Diego, USA, 2012

"Reduced γ-carboxylase Activity in Uremia - a Possible Mechanism of Uremic Vascular Calcification"

- Fellows Meeting, Abbott Symposium on behalf of the 49th ERA-EDTA, Paris, France, 2012

- 4th Conference of Fat Soluble Vitamins, Kalabaka, Greece, 2012

b) Ausgewählte Poster

"Increased level of vitamin K in $ApoE^{-/-}$ and $LDL^{-/-}$ mice", 20th Congress of Nutrition, Granada, Spain, 2013

"Gas6 protein and its role in vascular calcification"

- International Society of Nephrology (ISN) Nexus, Kidney and Bone, Copenhagen, Denmark, 2012

"Reduced Activity of the gamma-Carboxylase in Uremia – Possible Mechanism of Uremic Vascular Calcification"

- 49th ERA-EDTA, Paris, France, 2012; winner of Travel Grant
- 44th Annual Meeting of the American Society of Nephrology, Kidney Week, Philadelphia, USA, 2011

Summary

Vascular calcification is present in atherosclerosis, ageing, chronic kidney diseases and diabetes and is strongly associated with an increased morbidity and mortality. Calcification of arteries occurs at the tunica intima and the tunica media. Thereby, vascular smooth muscles cells (VSMC) transdifferentiate into an osteoblastic phenotype. In contrast to the antiquated opinion that calcification of soft tissues is a passive process it is now known that actively regulated processes play a major role. Modifiable calcification inhibitors were identified of which matrix gla protein (MGP) is regarded as the most potent one being expressed in the vascular wall. MGP gets posttranslationally gamma carboxylated at 5 glutamic acid residues, which achieve calcium binding properties. This carboxylation step requires reduced vitamin K as a cofactor. It is provided and recycled in the so called vitamin K cycle, which consists of the vitamin K epoxid reductase (VKOR), DT-diaphorase and γ-glutamyl carboxylase (GGCX). The VKOR is inhibitable by warfarin and other coumarins. High levels of uncarboxylated MGP (ucMGP) were found in VSMC after treatment with vitamin K antagonists like warfarin, which is frequently used for anticoagulation. Besides MGP, other vitamin K dependent proteins are known. One is the Gas6 protein, which is also expressed by VSMC, but its role is not yet fully understood. Gas6 binds to the Axl receptor, a receptor tyrosine kinase which gets autophosphorylated after binding to its ligand. Gas6 offers one n-terminal carboxylation site. The effects of uremia on vitamin K recycling via the vitamin K cycle are unknown.

Aim of this thesis was to characterize the activities of three enzymes of the vitamin K cycle and the role of vitamin K dependet Gas6 protein under uremic conditions.

First, a fluorescence method for the quantification of GGCX activity *in vitro* in tissue samples was developed. This method employs a fluorescein isothiocyanate (FITC) labelled Glu containing hexapeptide which gets carboxylated by the GGCX. The generated Gla-peptide can be easily quantified using a reversed phase HPLC setup. For further proteomic analysis mass spectrometry was applied.

Second, the influences of uremia and pharmacological doses of vitamin K supplementation on the activity of the vitamin K cycle and extraosseous calcification were investigated. Uremia was induced in rats by adenine diet, in part supplemented with vitamin K_1 or K_2 for 4 or 7 weeks. After 4 weeks of adenine, the activity of the vitamin-K cycle enzyme GGCX but not DT diaphorase or VKOR was reduced. Serum levels of ucMGP increased, indicating functional vitamin K deficiency. No histological calcification was detected at this stage but aortic and renal calcium content increased. Seven weeks of adenine induced histological

calcification in the aorta, heart and kidneys. The addition of vitamin K restored the intrarenal gamma-carboxylase activity and over-stimulated it in the liver and aorta. Moreover, vitamin K treatment decreased tissue calcium content. Uremic functional vitamin K deficiency, at least results from a reduction of the gamma-carboxylase activity which possibly contributes to calcification.

Third, the influence of Gas6 protein on vascular calcification was investigated in murine *in vitro* VSMC culture and different *in vivo* models using a) Warfarin diet, b) uninephrectomy or c) electrocautery of the kidney as well d) ageing mice.

In vitro VSMC exposed to warfarin calcified and showed increased apoptosis without differences between wildtype (WT) and $Gas6^{-/-}$ mice. *In vivo*, after electrocautery, serum calcium increased similarly in WT and $Gas6^{-/-}$ mice but no significant difference in aortic calcium content was observed between the groups. In all groups von Kossa staining revealed only a weak positive vascular staining in WT and $Gas6^{-/-}$ mice. In ageing mice no significant differences in vascular calcification could be identified between $Gas6^{-/-}$ and WT mice. No differences were found in left ventricular (LV) mass, stroke volume or pulse wave velocity (PWV) in all treatment groups. $Gas6^{-/-}$ mice showed no up regulation of MGP. This does not support a role of Gas6 in the pathogenesis of vascular calcification.

Zusammenfassung

Vaskuläre Kalzifizierung tritt als eine Begleiterscheinung von Atherosklerose, Alter, chronischen Nierenerkrankungen und Diabetes auf und geht mit einer stark erhöhten Morbidität und Mortalität einher. Arterielle Kalzifizierungen erfolgen in der Tunica intima und der Tunica media. Hier transdifferenzieren glatte Gefäßmuskelzellen (vascular smooth muscle cells, VSMC) in einen osteoblastären Phänotyp. Entgegen der tradierten Auffassung, dass die Gewebeverkalkung ein passiver Prozess ist, weiß man nun, dass es sich um einen aktiv regulierten Prozess handelt. Es konnten regulierbare Verkalkungsinhibitoren identifiziert werden. Ein potenter Kalzifizierungsinhibitor ist das Matrix Gla Protein (MGP), welches insbesondere in der Gefäßwand von VSMC exprimiert wird. MGP wird an 5 Glutamatresten posttranslational γ-carboxyliert, wodurch eine Kalziumbindung ermöglicht wird. Zur γ-Carboxylierung wird reduziertes Vitamin K als Cofaktor benötigt. Dieses wird im sogenannten Vitamin K Zyklus bereitgestellt und recycelt. Die beteiligten Enzyme sind die Vitamin K Epoxid-Reduktase (VKOR), DT-Diaphorase und γ-glutmayl-Carboxylase (GGCX). Die VKOR wird durch Coumarine wie Warfarin inhibiert.

Erhöhte Level an uncarboxyliertem MGP (ucMGP) werden in VSMCs nach Warfarin Exposition gefunden, welches weitverbreitet therapeutisch als Antikoagulanz Einsatz findet. Neben MGP sind weitere Vitamin K abhängige Proteine bekannt. Hierzu zählt auch das Gas6 Protein, welches ebenfalls von VSMC exprimiert wird, aber dessen Funktion noch nicht vollständig geklärt ist. Gas6 bindet an den Axl-Rezeptor, eine Rezeptor-Tyrosinkinase die nach Ligandenbindung autophosphoryliert wird. Gas6 verfügt über einen n-terminale Gla Rest. Das Ziel dieser Arbeit war die Charakterisierung der Enzymaktivitäten im Vitamin K Zyklus und die Rolle des Vitamin K abhängigen Gas6 Proteins in der experimentellen Urämie.

Dazu wurde zunächst eine Fluoreszenz-gestützte Methode entwickelt, zur Bestimmung der GGCX Aktivität in Gewebeproben. Verwendet wurde ein Fluorescein Isothiocanat (FITC) gekoppeltes Glu-haltiges Hexapeptid, welches durch die GGCX carboxyliert wird. Ein reversed phase (rp) HPLC gestütztes Setup ermöglicht eine einfache Qunatifizierung des generierten Gla-Peptids. Zur weiterführenden Proteom-Analyse wurde eine Massenspektometrie durchgeführt.

Zweitens wurde der Einfluss einer Urämie sowie die Verabreichung pharmakologischer Dosen Vitamin K auf die Enzyme des Vitamin K Zyklus und extraossäre Kalzifikation untersucht. Durch Gabe von Adenin über einen Zeitraum von 4 oder 7 Wochen wurde in Ratten eine Urämie induziert, teilweise unter Supplemtentation mit Vitamin K_1 oder K_2. Nach

4-wöchiger Adenin Behandlung war die Aktivität der GGCX reduziert, nicht jedoch der DT-Diaphorase oder der VKOR. Die Serumwerte von ucMGP waren erhöht, woraus auf eine funktionale Vitamin K Defizienz geschlossen werden kann. Histologisch konnte keine Kalzifiaktion nachgewiesen werden, es zeigten sich jedoch erhöhte renale und aortale Calcium Gehalte. Eine 7-wöchige Verabreichung von Adenin induzierte histologische Kalzifikation von Aorta, Herz und Niere. Durch Zugabe von Vitamin K wurde die erniedrigte renale GGCX Aktivität zurückgesetzt und in Leber und Aorta überstimuliert. Darüber hinaus senkte Vitamin K den Gehalt an Calcium im Gewebe. Möglicherweise resultiert die funktionale Vitamin K Defizienz in urämischen Patienten zum Teil aus einer erniedrigten GGCX Aktivität mit einhergehenden Kalzifikationen.

Drittens wurde der Einfluss des Gas6 Proteins auf die Gefäßkalzifikation in murinen *in vitro* VSMC Kultur und in verschiedenen *in vivo* Modellen untersucht: a) Warfarin Diät b) Uninephrektomie c) Elektrokoagulation der Niere sowie d) alternde Mäuse. *In vivo* erhöhte sich nach Elektrokauterisation der Serum Calcium Gehalt in WT und $Gas6^{-/-}$ ohne signifikanten Unterschied zwischen den Gruppen. In allen Gruppen zeigte sich lediglich eine schwach positive vaskuläre *von Kossa* Färbung in WT und $Gas6^{-/-}$ Mäusen. In alternden, unbehandelten Mäusen gab es keine signifikanten Unterschiede bezüglich vaskulärer Kalzifikation zwischen WT und $Gas6^{-/-}$ Mäusen. Echokardiographisch zeigten sich keine Unterschiede in der linksventrikulären (LV) Masse, Schlagvolumen oder Pulswellengeschwindigkeit (PWV) in allen behandelten Gruppen. In $Gas6^{-/-}$ Mäusen lag keine Heraufregulierung von MGP vor. Diese Daten unterstüzen keine Rolle von Gas6 in der Pathogenese der vaskulären Kalzifikation.

Table of contents

I List of Tables

II List of Figures

III List of Formulas

IV Abbreviations

A	Adenine
bp	base pairs
BSA	Bovine Serum Albumin
B-mode	Brightness mode
C	Cytosine
CAPS	N-cyclohexyl-3-aminopropanesulfonic acid
CKD	Chronic Kidney Disease
DAPI	4’,6-Diamidino-2-Phenylindole
DNA	Desoxyribonucleic Acid
DTT	Dithiotreitol
E	Extinction
EC	Electrocautery
EDTA	Ethylendiamintetraacetate
EDV	(left ventricular) end diastolic volume
EF	Ejection Fraction
ELISA	Enzyme Linked Immunosorbent Assay
ESD	(left ventricular) end systolic volume
FAD	Flavin Adenine Dinucleotide
FITC	Fluorescein Isothiocyanate
FLEEL	Phe-Leu-Glu-Glu-Leu
FLEFLK-FITC	Phe-Leu-Glu-Phe-Leu-Lys-Fluorescein Isothiocyanate
G	Guanine
GAPDH	Glycerinaldehyde-3-phosphat dehydrogenase
GFR	Glomerular Filtration Rate
GGCX	Gamma Glutamyl Carboxylase
Gla	Gamma-carboxy glutamic acid
Glu	Glutamic acid
HEPES	2-(4-(2-Hydroxyethyl)-1-piperazinyl)-ethansulfon acid
K_1<O	Vitamin K1 epoxide
kcat	catalytic production of product
KM	Michaelis constant
LVID	Left Ventricular Inner Diameter
LVM	Left Ventricular Mass
LVPW	Left Ventricular Posterior Wall
LVSW	Left Ventricular Septal Wall
MGP	Matrix Gla Protein
MK4	Menaquinone 4
M-mode	Motion mode
MS	Mass Spectrometry
MTT	3-(4,5-Dimethylthiazol-2-yl)-2,5-Diphenyltetrazolium Bromide
MW	Molecular Weight
NADPH	Nicotinamide Adenine Dinucleotide Phosphate
NEM	N-Ethylmaleimide

Ocn	Osteocalcin
PBS	Phosphate Buffered Saline
PCR	Polymerase Chain Reaction
PIVKA	Prothrombin/ Protein Induced by Vitamin K Absence
PWV	Pulse Wave Velocity
RNA	Ribonucleic Acid
rp-HPLC	reversed phase High Performance Liquid Chromatography
S	Substrate
SD	Standard Deviation
SV	Stroke Volume
T	Thymine
TFA	Trifluoroacetic acid
TUNEL	Terminal deoxynucleotidyl transferase dUTP nick end labeling
ucMGP	uncarboxylated Matrix Gla Protein
UniNx	Uninephrectomy
V_{ACC}	Pulse wave Velocity over the Arteria Carotis Communis
VKOR	Vitamin K Epoxid Reductase
Vmax	Maximum Velocity
VSMC	Vascular Smooth Muscle Cells
WT	Wildtype

1.1 General Introduction

Fat soluble vitamin K exists in 4 major different forms, all based on the 2-methyl 1,4-naphtochinon (K_3). The phylloquinone (K_1; Figure 1), a 3 phytyl substituent, is located in membranes of chloroplasts. It is the major component of vitamin K uptake in human nutrition.

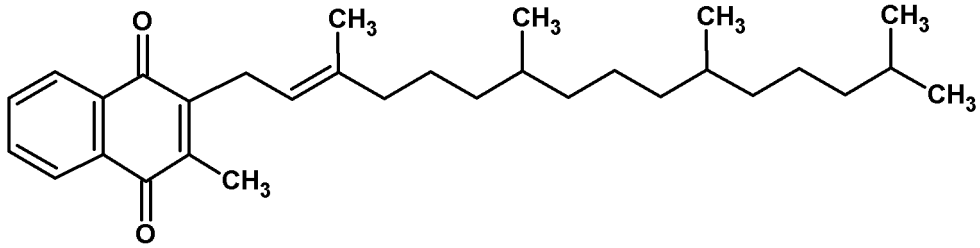

Figure 1: Chemical structure of phylloquinone (Vitamin K_1)

High contents of vitamin K_1 can be found for example in herbs (cress: 600 µg/100 g; chive: 570 µg/100 g), green leafy vegetables (corn salad: 200; chard 441 µg/100 g) or broccoli (129 µg/100 g) (1). Menaquinones (K_2) contain an unsaturated isoprenoid side chain at the C3 position (MK4 - MK10, Figure 2).

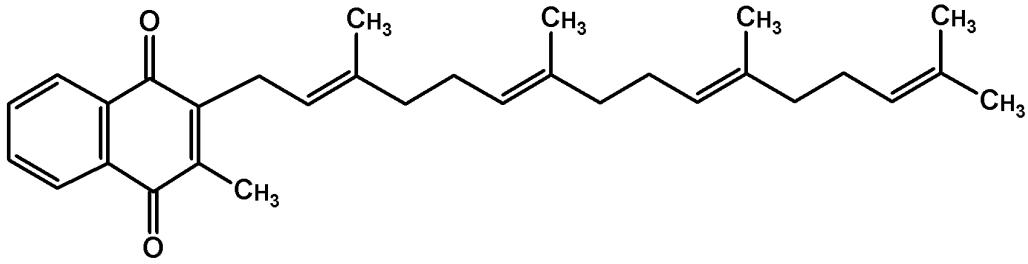

Figure 2: Chemical structure of menaquinone 4 (MK4)

They are formed by bacterial fermentation, for example by *bacillus subtilis* in natto (2). Natto, made from fermented soy beans, is the richest known source of vitamin K_2. Menadione (K_3) and menadione esther (K_4) are synthetic compounds and play only a role in animal nutrition. Vitamin K_1 is mainly found in the liver to serve as a cofactor for γ-carboxylation of the blood coagulation factors II, VII, IX, X, protein C and S (3). Vitamin K_2 is mainly distributed in extrahepatic tissues (4) and contributes to γ-carboxylation of vitamin K dependent proteins like MGP, Osteocalcin (Ocn) or Gas6. The function of all vitamin K dependent proteins is mediated by binding of calcium to the γ-carboxylated form (5). Increased amounts of uncarboxylated prothrombin (PIVKA), Ocn and MGP were detected in dialysis patients compared to healthy controls (6;7). This indicates a functional vitamin K deficiency in this

population. The origin of the functional vitamin K deficiency in CKD is only partially understood. Reduced vitamin K intake has been described in dialysis patients (7) but we reasoned that this cannot fully explain the marked functional vitamin K deficiency.

Low levels of carboxylated MGP predict mortality in such patients (6;8). MGP knockout mice develop spontaneous calcification of arteries (9). The mechanism by which MGP inhibits vascular calcification may involve BMP-2 antagonism and a direct calcium-complexing effect (10). MGP is expressed predominantly by vascular smooth muscle cells (VSMC) in the arterial media and chondrocytes. It contains five glutamic acid residues that can be γ-carboxylated (Glu → Gla) by the vitamin K-dependent γ-carboxylase (GGCX). MGP potently inhibits precipitation of hydroxyapatite crystals in uremia. Abnormalities in mineral metabolism and vascular calcification are highly present in chronic kidney diseases (CKD) (11). Increased ucMGP is associated with increased coronary artery calcification (12). Calcification can occur at the intimal (atherosclerosis) or at medial layer (arteriosclerosis) of an arterial vessel wall (13). In CKD, defined as a decreased kidney function with a glomerular filtration rate < 60 mL/min per 1.73 m^2 (14), the arterial tunica media gets predominantly calcified (13). It can be visualized by computed tomography (13;15). An increased coronary artery calcification score is highly related to mortality in haemodialysis patients, independent of the traditional risk factors (16). Possible unique contributors to the development of vascular calcification in CKD are an increased calcium-phosphate product, parathyroid hormone and as well as reduced levels of inhibitors of vascular calcification like fetuin-A and insufficient activity of MGP (17).

In contrast to MGP, the role of Gas6 in vascular calcification is not well established. Vitamin-K dependent carboxylation of Gas6 is essential for its binding to the Axl receptor (18). Tyrosine phosphorylation of Axl induces cell proliferation (19). Gas6 is known to protect endothelial cells and VSMC against apoptosis (20;21), the latter is known to be associated with vascular calcifications. Another potential link between Gas6 and vascular calcification is demonstrated by *in vitro* data showing that phosphate- induced calcification of VSMC is associated with a downregulation of Gas6 expression (21). In addition, antiapoptotic effects and protection of calcification of VSMC by statins were mediated through Gas6 mRNA stabilization (21). So far no *in vivo* data are available on the role of Gas6 in vascular calcification. To clarify this, I assessed Gas6 knockout ($Gas6^{-/-}$) mice and $Gas6^{-/-}$ derived VSMC in *in vitro* and *in vivo* vascular calcification models.

Existing animal models contribute to a better understanding of the pathogenesis in vascular calcification processes. Experimental uremia can be created by reducing the kidney mass (uninephrectomy, 5/6 nephrectomy, electrocautery), which mimics the progressive nephron loss occurring in patients with chronic renal failure (22;23). Noninvasively, dietary adenine causes an overload of the converting adenine phosphoribosyltransferase and leads to deposition of 2,8 dihydroxyadenosine crystals in the tubulo-interstitium of the kidney (22;23). Another approach to induce vascular calcification is oral administration of coumarins like warfarin (Figure 3) or phenprocoumon. This was shown both in rats (24) and humans (25) (26). Coumarins directly inhibit the activity of the vitamin K oxidoreductase (VKOR; EC 1.1.4.1)(27). This leads to an insufficient activation of blood coagulation factors, a desirable effect for patients with artificial heart valves or after thromboembolism. But the drawback is a lesser γ-carboxylation of extrahepatic proteins like the vessel derived calcification inhibitor MGP. Replacing coumarins with alternative thrombin inhibitors is under actual debate (28;29). In turn, a high intake of vitamin K_2 (MK4) was capable of regressing warfarin-induced medial calcification in Wistar rats (30).

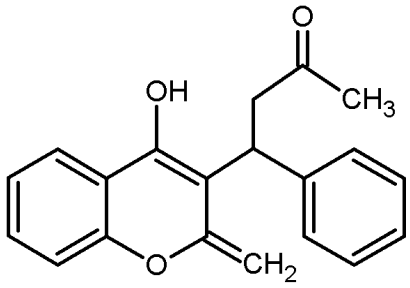

Figure 3: Chemical structure of warfarin

The GGCX (EC code 4.1.1.90) is an intrinsic membrane protein located in the endoplasmic reticulum and requires vitamin K as a cofactor (31). It utilizes both reduced vitamin K (KH_2) and vitamin K with KH_2 being the more potent one (32) (Figure 4). The amino terminus is located on the cytoplasmic side and its carboxyl terminus on the lumen (33). The enzyme carboxylates specific protein bound glutamate residues at the gamma position resulting in an extra negative charge and thus potent calcium binding site (34).

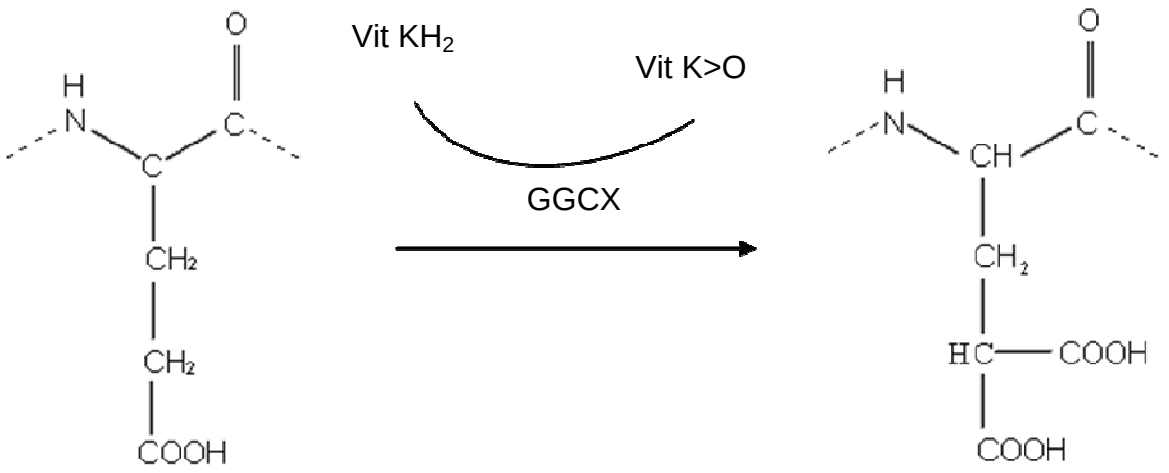

Figure 4: The gamma-carboxylation step: A peptide gets γ-carboxylated by the GGCX, which requires the reduced form of vitamin K (Vit KH_2) as a cofactor. KH_2 is epoxidized to vitamin K epoxide (Vit K>O).

Multiple proteins require γ-carboxylation to achieve full bioactivity (35). The pro-sequence, which is the enzyme binding site, is a homologous region of several vitamin K dependent proteins (3). Some known proteins containing this pro-sequence and thus being targets for the GGCX are prothrombin, protein S and extrahepatic osteocalcin, Gas6 and MGP (5). Besides the availability of vitamin K and KH_2, the GGCX activity is also dependent on the concentration of substrate and $NaHCO_3$ (36). The enzymatic reaction produces the unusual aminoacid Gla and vitamin K epoxide (K>O) as products, whereby K>O is recycled to K and KH_2 by the warfarin sensitive VKOR (37;38). The latter product is also generated by a warfarin insensitive antidotal enzyme (39) the DT-diaphorase (EC 1.6.99.2 also called NADPH-quinone oxidoreductase). The DT diaphorase using NAD(P)H as an electron acceptor uses vitamin K as a substrate and is independent to the dithiotreitol pathway, which antagonises the effects of warfarin (40;41). The DT-diaphorase is predominantly active in the liver and offers an alternative pathway to provide vitamin KH_2. Dicoumarol (Figure 5) inhibits the purified DT-diaphorase by binding to the oxidized form of the enzyme (42).

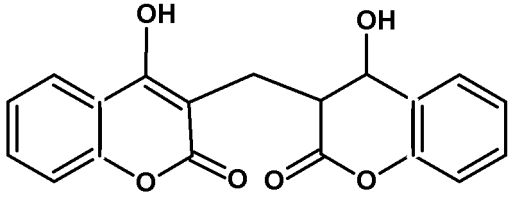

Figure 5: Chemical structure of dicoumarol

These three enzymes form the so called vitamin K cycle (Figure 6) (43;44).

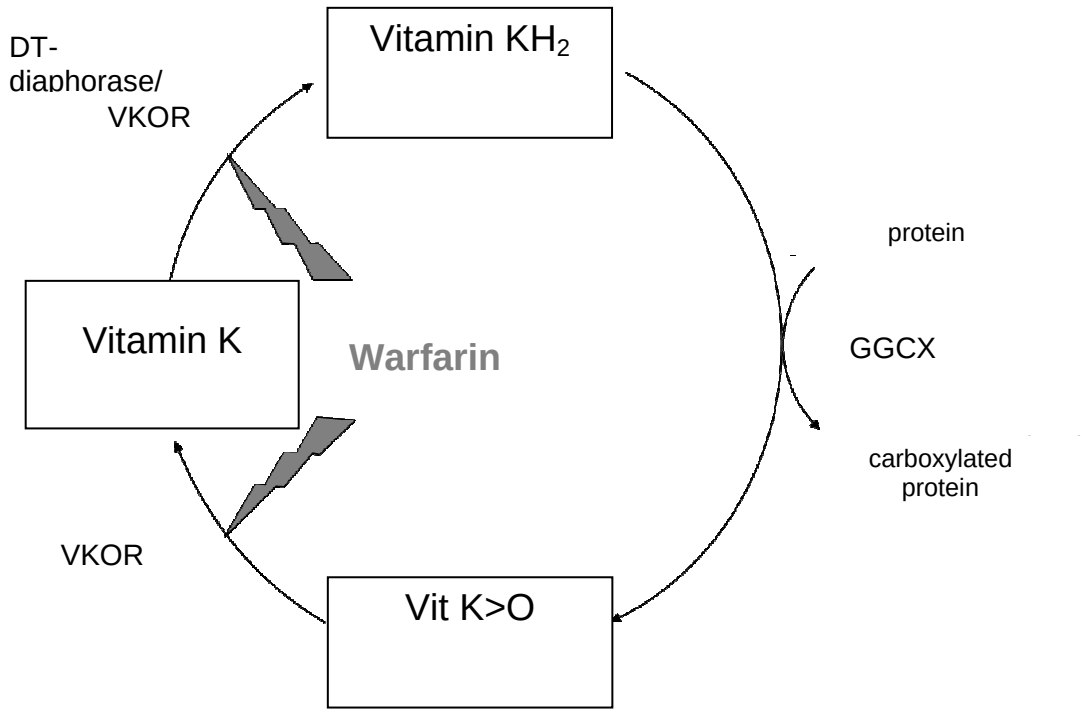

Figure 6: The vitamin K cycle (modified from Stafford, 2005 (43)). The required cofactor vitamin KH_2 for the γ-carboxylation by the GGCX is stepwise recycled by 2 additional enzymes: the VKOR, which is directly inhibitable by warfarin and the DT-diaphorase.

In 1975, Emson and Suttie developed a method for measuring the GGCX activity by incorporation of radioactive $H^{14}CO_3^-$ in the synthetic peptide Phe-Leu-Glu-Glu-Leu (short: FLEEL) which is based on the sequence of prothrombin (31). Ulrich and colleagues tested 16 peptide sequences as enzyme substrates and found FLEEL to be the most active one (45). The peptides were hydrolyzed and purified by anion exchange HPLC. Quantification was achieved using a setup based upon a liquid scintillation for detection (46). Protocols describe the addition of propeptide in approaches with purified enzyme (47) or in tissues without propeptide (31;32;48). *In vitro*, GGCX is inhibited by N-Ethylmaleimide (NEM) (49) and 5-Mercapto-1-Methyl-Thiotetrazole (5-MMT), which is used as a part of antibiotics (moxalactam) (50).

1.2 Aims

1. Establishment of an appropriate method for safe and reproducible detection of γ-glutamyl-carboxylase activity in different tissues
2. Development of a model for uremia and vascular calcification in rats
3. Investigation of the vitamin K cycle under the conditions of uremia in rats
4. Analysis of the influence of oral vitamin K supplementation on vascular calcification
5. Investigation of the influence of oral vitamin K supplementation on vitamin K dependent enzyme activities
6. Examination of the influence of uremic toxins on the activity of the γ -glutamyl carboxylase activity
7. To clarify the role of Gas6 protein in vascular calcification processes

2 MATERIALS AND METHODS

2.1 Chemicals

Acetic Acid	Merck, Darmstadt, Germany
Acetonitrile, HPLC grade	AppliChem, Darmstadt, Germany
Agarose	Cambrex, ME, USA
Agilent RNA 6000 Nano Kit	Agilent, Böblingen, Germany
$AgNO_3$	Merck, Darmstadt, Germany
ALT lysis buffer	Qiagen, Hilden, Germany
Ambion RNase Zap	Life Technologies, Darmstadt, Germany
BCA Pierce Protein Determination Kit	Fisher Scientific GmbH, Schwerte, Germany
BSA	Serva, Heidelberg, Germany
Calcium Phosohate	Sigma Aldrich, Munich, Germany
CAPS	Sigma Aldrich, Munich, Germany
Collagenase	Sigma Aldrich, Munich, Germany
Complete Mini Protease Inhibitor Cocktail	Roche, Diagnostics, Mannheim, Germany
Dicoumarol	AppliChem, Darmstadt, Germany
Diethylether, HPLC grade	Sigma Aldrich, Munich, Germany
Digitonin	AppliChem, Darmstadt, Germany
DNase	Qiagen, Hilden, Germany
DTT	AppliChem, Darmstadt, Germany
EDTA	AppliChem, Darmstadt, Germany
Elastase	Sigma Aldrich, Munich, Germany
Ethanol	Apotheke, Universiätsklinikum Aachen, Germany
Ethanol HPLC grade	Sigma Aldrich, Munich, Germany
Ethidiumbromide	Sigma Aldrich, Munich, Germany
FAD	AppliChem, Darmstadt, Germany
Fermentas gene Ruler DNA ladder SM 0313	Fisher Scientific GmbH, Schwerte, Germany
FLEFLK-FITC	Biomatik, Ontario, Canada
Formalin	Merck, Darmstadt, Germany
Formic acid	Merck, Darmstadt, Germany
Gentamycin	Sigma Aldrich, Munich, Germany
GGCX TaqMan® gene expression assay RN00582138	Life Technologies, CA, USA
Glucose-6-phosphate	AppliChem, Darmstadt, Germany
Glucose-6-phosphate-dehydrogenase	AppliChem, Darmstadt, Germany
H_2O_2	AppliChem, Darmstadt, Germany
HEPES	AppliChem, Darmstadt, Germany
Histofix	Carl Roth, Karlsruhe, Germany
Imidazole	AppliChem, Darmstadt, Germany
In situ Cell Death Detection Kit	Roche, Basel, Switzerland
Indoxylsulphate	AppliChem, Darmstadt, Germany

Isoflurane	Abbott, IL, USA
Isopropanol	Sigma Aldrich, Munich, Germany
KCl	AppliChem, Darmstadt, Germany
Ketamin 10%	CEVA Tiergesundheit, Düsseldorf, Germany
Liquid nitrogen	Apotheke, Universiätsklinikum Aachen, Germany
Meandione	AppliChem, Darmstadt, Germany
Meanquinone 4	Sigma Aldrich, Munich, Germany
Methanol	AppliChem, Darmstadt, Germany
$MnCl_2$	Carl Roth, Karlsruhe, Germany
MTT	Merck, Darmstadt, Germany
Na2HCO3	Merck, Darmstadt, Germany
NaCl	AppliChem, Darmstadt, Germany
NaCl, 0.9%	Delta Select, Pfullingen, Germany
NADPH	AppliChem, Darmstadt, Germany
$NaHCO_3$	Merck, Darmstadt, Germany
NaOH	Merck, Darmstadt, Germany
Paraffin	Carl Roth, Karlsruhe, Germany
PBS	Gibco, Gaithersburg, MD, USA
PCR beads Ready to go	GE Healthcare, Munich, Germany
p-Cresol	AppliChem, Darmstadt, Germany
Penicillin	Sigma Aldrich, Munich, Germany
Phylloquinone	Sigma Aldrich, Munich, Germany
Picric Acid	Sigma Aldrich, Munich, Germany
Proteinase K	Qiagen, Hilden, Germany
qPCR Core Kit for SYBR Green I RT SN10-05	Eurogentec, Cologne, Germany
qPCR Core Kit for SYBR Green I RT SN10-05	Eurogentec, Cologne, Germany
Randox Cresophthalein Assay	Randox Laboratories, Crumlin, UK
Reverse Transcriptase Core Kit RT-RTCK-05	Eurogentec, Cologne, Germany
Reverse Transcriptase Core Kit RT-RTCK-05	Eurogentec, Cologne, Germany
RNA later	Qiagen, Hilden, Germany
RNeasy Mini Kit	Qiagen, Hilden, Germany
Rotihistol	Carl Roth, Karlsruhe, Germany
Safranin-O	Sigma Aldrich, Munich, Germany
Sirius Red	Sigma Aldrich, Munich, Germany
Smooth Muscle Cell (SMC) Growth Medium 2	PromoCell GmbH, Heidelberg, Germany
Sodium citrate	Merck, Darmstadt, Germany
Sodiumthiosulfate	Sigma Aldrich, Munich, Germany
Streptomycin	Sigma Aldrich, Munich, Germany
Sucrose	Carl Roth, Karlsruhe, Germany
Supplement Pack for SMCs	PromoCell GmbH, Heidelberg, Germany
Tetra-butyl-ammoniumphosphate	Sigma Aldrich, Munich, Germany
Tissue Tek	Sakura, Alphen, Netherlands
Trifluoroacetic acid	Carl Roth, Karlsruhe, Germany

Tris-Cl	BioRad, Munich, Germany
TritonX	AppliChem, Darmstadt, Germany
Trypsin/ EDTA	GIBCO, Gaithersburg, MD, USA
Tween 20	Sigma Aldrich, Munich, Germany
Urea	BioRad, Munich, Germany
Vectashield with DAPI	Vector Laboratories, CA, USA
Warfarin	Sigma Aldrich, Munich, Germany
Xylazin 2%	Medistar, Ascheberg, Germany
Xylol	AppliChem, Darmstadt, Germany

2.2 Instruments

7500 Real-Time PCR TagMan® system	Life Technologies, CA, USA
Agilent 1100 Series HPLC apparatus	Agilent Technoligies, Böblingen, Germany
Agilent auto sampler G 1313A,	Agilent Technoligies, Böblingen, Germany
Agilent binary gradient pump G 1312A	Agilent Technoligies, Böblingen, Germany
Agilent vacuum degasser G 1379A	Agilent Technoligies, Böblingen, Germany
Balance Sartorius 2007 MP	Sartorius AG, Göttingen, Germany
Centrifuge 4K15	Sigma Aldrich, Munich, Germany
Centrifuge 5417R	Eppendorf, Hauppauge, NY, USA
CODA blood pressure system	Kent Scientific, Torrington, Connecticut, USA
Cooling plate COP 30	Medite GmbH, Burgdorf, Germany
Cryotome Leica Jung CM3000	Leica Biosysteme, Nussloch. Germany
Erbotom ACC 450	Erbe, Tübingen, Germany
Freezer Jouan VXE600	Fisher Scientific GmbH, Schwerte, Germany
HPLC autoinjector L-7200	Merck Hitachi, Tokyo, Japan
HPLC column oven L-7350	Merck Hitachi, Tokyo, Japan
HPLC fluorescence detector L-7480	Merck Hitachi, Tokyo, Japan
HPLC interface D-7000	Merck Hitachi, Tokyo, Japan
HPLC pump L-7100	Merck Hitachi, Tokyo, Japan
HPLC UV detector L-7400	Merck Hitachi, Tokyo, Japan
Incubator Heracell	Fisher Scientific GmbH, Schwerte, Germany
Lyophilisator, Christ Loc 1mALPHA 1-4	Martin Christ, Osterode am Harz, Germany
Max RP HPLC C12 column	Phenomenex, Aschaffenburg, Germany
Microscope	Olympus Deutschland GmbH, Hamburg, Germany
Microscope Leica DM 6000 B	Leica Biosysteme, Nussloch. Germany
MilliQ Water system	Millipore GmbH, Schwalbach, Germany
MS1 Minishaker	IKA, Staufen, Germany
Multifuge 3L-R	Heraeus Instruments, Hanau, Germany
Orbital Shaker	Forma Scientific Inc., Marietta, OH, USA
Paraffin Section Mounting Bath	Barnstead International, Iowa, USA
pH-Fix 0-14	Carl Roth, Karlsruhe, Germany
Qiagen tissue lyser	Qiagen, Hilden, Germany
Rotary Microtome Slee Cut 5062	SLEE medical GmbH, Mainz, Germany
Sciex API 3000 LC/MS/MS system	Life Technologies, CA, USA
Tecan sunrise microplate absorbance reader	Tecan, Männedorf, Switzerland
Therma Sonic Gel warmer	Parker Laboratories, Fairfield, NJ, USA
Thermocylcer PTC-100	MJ Research Inc., Quebec, Canada
Tissue embdding station Leica 1160	Leica Biosysteme, Nussloch. Germany
Tissue processor Slee mtm	SLEE medical GmbH, Mainz, Germany
Ulracentrifuge Optima L-100 XP	Beckman Coulter GmbH, Krefeld, Germany
Vacuum hybrid pump RL 6	Vacubrand, Wertheim, Germany
Vevo 770	Visualsonics, Ontario, Canada
Vitros 250	Ortho Clinical Diagnostics, NY, USA

2.3 Materials

Blood sample tube with serum gel, 1.1 ml	Sarstedt AG und Co, Nümbrecht, Germany
Cell culture flask, T25, T75	Becton Dickinson, Heidelberg, Germany
Cell scraper	Becton Dickinson, Heidelberg, Germany
Centrifugation tube	Beckman Coulter GmbH, Krefeld, Germany
Costar Stripette, 5 ml, 10 ml, 25 ml	Fisher Scientific GmbH, Schwerte, Germany
Cover glass	Engelbrecht GmbH, Edermünde, Germany
Depilatory cream	Veet, Reckitt Benckiser, Hull, UK
Dewar	KGW Isotherm, Karlsruhe, Germany
Disposable Scalpels, No 15, No 23	Feather, Osaka, Japan
Electrocoagulation Ball Tip	Erbe, Tübingen, Germany
Embedding cassettes	Carl Roth, Karlsruhe, Germany
Eppendorf pipettes	Eppendorf AG, Hamburg, Germany
F-Air canister	Harvard Apparatus, Holliston, MA, USA
Filter, 0.2 µM	Millipore GmbH, Schwalbach, Germany
Flange cap N11	Macherey Nagel, Düren, Germany
Forceps	Fine Science Tools GmbH, Heidelberg, Germany
Glass pipettes	Sarstedt AG und Co, Nümbrecht, Germany
HPLC C-12 Synergy 4 µm Max-RP 80A column	Phenomenex, Aschaffenburg, Germany
HPLC C-12, 4 x 3 mm, guard column	Phenomenex, Aschaffenburg, Germany
Micro Inserts, 200 µl	Macherey Nagel, Düren, Germany
Microlance 21G	Becton Dickinson, Heidelberg, Germany
Microscope slide Superfrost plus	Fisher Scientific GmbH, Schwerte, Germany
Microtiterplate, 12-well, 96-well	Becton Dickinson, Heidelberg, Germany
Microtome Blade, N35, C35	Feather, Osaka, Japan
Pipetboy	IBS Integra Biosciences GmbH, Fernwald, Germany
Pipette tips	Carl Roth, Karlsruhe, Germany
Rat Restrainer	Kent Scientific, Torrington, Connecticut, USA
Round bottom flask	Carl Roth, Karlsruhe, Germany
Safety Multifly Canuele	Sarstedt AG und Co, Nümbrecht, Germany
Scissors	Fine Science Tools GmbH, Heidelberg, Germany
SepPak C18 cartridge	Waters GmbH, Eschborn, Germany
Silk, 3-0 Mersilene, Ethicon	Johnson & Johnsons, St Stevens-Woluwe, Belgium
Stainless steel beads 5 mm	Qiagen, Hilden, Germany
Syringes, plastic, 1 ml;	Becton Dickinson, Heidelberg, Germany
Syringes, plastic, 10 ml; 20 ml	Terumo, Eschborn, Germany
Tissue Tek Cryomold	Sakura, Alphen, Netherlands
Tubes 1.5; 2 ml	Eppendorf AG, Hamburg, Germany
Tubes 15mL, 50 ml	Greiner Bio-One GmbH, Frickenhausen, Germany
Tubes, N11, 1.5 ml, glass	Macherey Nagel, Düren, Germany

Ultrasound Gel	A + M Handelsvertretung, Versmold, Germany

2.4 Software

ChemSketch 12.01	ACD labs, Ontario, Canada
Coda	Kent Scientific, Torrington, Connecticut, USA
Diskus	C.H. Hilgers, Königswinter, Germany
Graph Pad Prism 5.01	GraphPad Software, Inc., CA, USA
Image J 1.43u	National Institute of health, MD, USA
Merck-Hitachi D-7000 HSM	Merck Hitachi, Tokyo, Japan
Origin Pro 8	OriginLab Corporation, MA, USA
Vevo	Visualsonics, Ontario, Canada

2.5 Methods for Aim 1

2.5.1 Peptide design

The synthetic fluorescence labelled hexapeptide FLEFLK-FITC (purity > 90%) was synthesized by Biomatik Corporation, Ontario Canada. The peptide was designed in order to contain only one carboxylation site instead of two, with good purification and solubility properties. The lysine residue is required to link the fluorescence marker (FITC) to the side chain of the peptide (Figure 7).

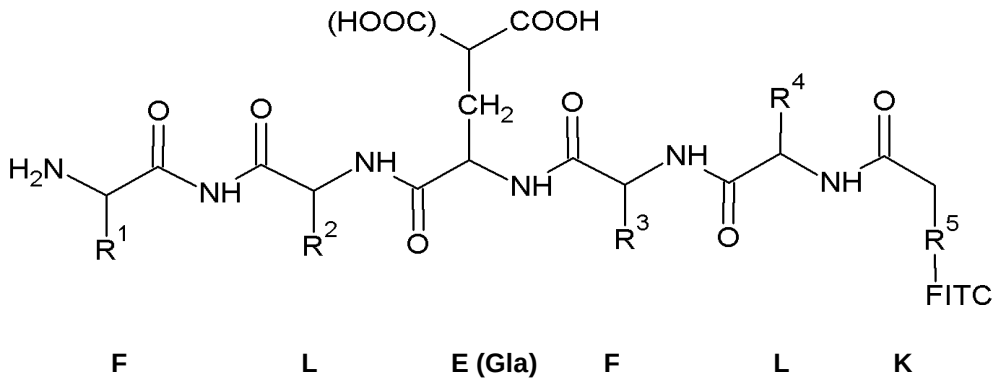

Figure 7: Chemical structure of the FITC labelled hexapeptide FLEFLK. The brackets indicate the site of γ-carboxylation.

2.5.2 Animals

Animals received food and water ad libitum. They were housed in a 12h day and night cycle (Institut für Versuchstierkunde, Aachen, Germany).

All animals were treated in accordance with the requirements of the Federation of the European Laboratory Animals Science Associations approved by the Landesamt für Natur, Umwelt und Verbraucherschutz NRW, Germany (Permit No 84-02.04.2011.A144). For preparation of microsomes healthy, male WISTAR rats (purchased from Charles River, Sulzfeld, Germany) weighing 462 +/- 30 g were used. Animals were sacrificed under isoflurane anaesthesia by heart puncture and exsanguination. Before harvesting, organs were perfused *in vivo* with 20 ml ice-cold PBS.

2.5.3 Preparation of microsomes

After removal the liver, kidneys and aortas were immediately snap frozen in liquid nitrogen and stored at -80°C. To isolate the enzyme rich microsomes 300-400 mg of liver or kidney

was used. Aortas were pooled (3 ± 1 aortas) up tp 150 mg in total. All tissue samples were cut into small pieces and homogenized in a Qiagen tissue lyser in 3 x volume of 300 mM sucrose buffer (10 mM HEPES, 0.1 mM EDTA and protease inhibitor cocktail) for 2 x 2 min at 24 Hz with two 5 mm steel beads. Afterwards the homogenate was centrifuged at 1,600 × g, for 10 min at 4°C. The pellet was discarded and the supernatant was collected and centrifuged for 20 min at 10,000 × g. The post-mitochondrial fraction was ultracentrifuged at 100,000 × g for 1 h at 4°C. The pelleted microsomal fractions were dissolved in 0.3 ml sucrose buffer in a protein concentration of 5-15 mg/ml, aliquoted and flash frozen for storage at -80°C. Microsomes from aortas were diluted in 100 µl sucrose buffer.

2.5.4 Protein determination

Protein content of microsomes from rat liver, kidney or aorta was determined by the BCA Pierce kit accordong to the manufacturer's protocol. Each 25 µl sample was measured in duplicates. BSA standard concentrations were 2, 1.5, 1, 0.75, 0.5, 0.25, 0.125 and 0.025 mg/ml. The samples were incubated for 30 min at 37°C. The absorption was measured at 562 nm on a Tecan sunrise microplate absorbance reader.

2.5.5 GGCX activity assay from microsomes

The assay was performed in sealed tubes at 20°C. A total reaction volume of 0.125 ml contained 250 µg microsomal protein, 0.5% (w/v) CAPS, 5 mM DTT, 2.5 mM $NaHCO_3$, 10 mM $MnCl_2$, 100 µg/ml vitamin K_1H_2, at pH 7.0. The pipetting scheme was 1) 64 µl of 250 µg microsomal protein, 2) 12.5 µl of 50 mg/ml CAPS, 3) 2 µl of 625 mM DTT, 4) 12.5 µl of 25 mM $NaHCO_3$, 5) 12.5 µl of 100 mM $MnCl_2$ and 6) 12.5 µl of 1 mg/ml vitamin K_1H_2 . All substrates were added in aqueous solution, except vitamin K_1H_2, which was diluted 1 mg/ml in ethanol. The reaction was started by adding 2 mM FLEFLK-FITC, always protected from light. After 30 min the reaction was stopped by adding 2 x volume of ice-cold methanol. All samples were kept on ice until injection. For enzyme kinetics the reaction was stopped at 0, 15, 60 and 120 min. The microsomal protein contents were 50, 125, 250, 500 and 750 µg. Used concentrations of the substate FLEFLK-FITC were, 0.5, 1, 2, 4 and 5 mM. To inhibit enzyme activity, 10 mM NEM was added to the reaction mixture prior to adding the substrate FLEFLK-FITC (2 mM). Vitamin K_1 was reduced to KH_2 by incubation in a mixture of 20 mM DTT, 50 mM NaCl and 2 mM Tris at 37°C for 24 h in the dark. (47). The resulting K_1H_2 was extracted with 100% ether, diluted up to 1 mg/ml in ethanol and stored at -80°C in argon atmosphere. All chemicals used here were HPLC grade.

2.5.6 Purification of FLELFK-FITC after in vitro carboxylation

Purification of the carboxylated peptide was achieved by the method of Mc Tigue (46). The reaction mixture of the GGCX assay was centrifuged at 10,000 × g for 15 min. For mass spectrometry (MS) measurements, the supernatant was dissolved in 10 ml SI-buffer (250 mM sucrose, 25 mM imidazole, 5 mM tetra-butyl-ammoniumphosphate), loaded onto a Waters SepPak C18 cartridge and washed with additional 10 ml of SI-buffer. The peptide was eluted in 4 ml methanol, which was evaporated by drying at 50°C in argon flow. For final HPLC measurements, samples were centrifuged at 10,000 × g for 15 min at 4°C. The supernatant was collected and the remaining residue was washed twice with a water-acetonitrile solution (4:1) and pooled with the supernatant to a total volume of 1 ml.

2.5.7 Reversed phase HPLC

The D-7000 Merck-Hitachi HPLC consisted of a pump (L-7100), an autoinjector (L-7200), a column oven (L-7350), a fluorescence detector (L-7480) and an interface (D-7000). 50 µl of each sample was injected. A linear gradient from 100% of 0.1% (v/v) TFA in H_2O up to 100 % 0.1% TFA (v/v) in acetonitrile was set at a continuous flow of 0.5 ml/min. For separation, a Phenomenex C-12 Synergy 4 µm Max-RP 80A column including a C-12, 4 x 3 mm, Phenomenex guard column was used. Fluorescence detection was optimized for FITC at 494 nm excitation and 521 nm emission The pressure limit was set at 350 bar. Each run was recorded for 30 minutes on the Merck-Hitachi D-7000 HSM software. The peptide was quantified by using internal and external standards.

2.5.8. Mass spectrometric confirmation by LC/ESI-MS

Liquid chromatography was carried out on an Agilent 1100 Series HPLC apparatus consisting of an auto sampler G 1313A, a binary gradient pump G 1312A and an Agilent vacuum degasser G 1379A. The gradient of the mobile phase, column and injection volume were equal to the rp-HPLC setup. The mass spectrometric detection was performed on an Applied Biosystems Sciex API 3000 LC/MS/MS system in ESI-positive mode. An electrospray needle voltage of + 4,500 V in the positive ion mode and nitrogen as nebulizer were used The turbo heater gas (450°C) was set to a pressure of 65 psi and the curtain gas was set to 58 psi. Mass spectra were acquired in full scan mode between m/z 350-1,250. Resolution of the mass spectrometer was set to “unit”. Peptide molecular weights were calculated using chemSketch.

2.5.9 $^{14}CO_2$ incorporation

The $^{14}CO_2$ incorporation of FLEEL is the standard assay to determine GGCX activity by a liquid scintillation counter. The $^{14}CO_2$ incorporation by FLEFLK-FITC was measured by Vasantha P. Mutucumarana at the University of North Carolina at Chapel Hill, North Carolina, USA, as described previosly (51). The radioactive assay was performed for 1 h 20 min. The kcat/KM of the $^{14}CO_2$ incorporation into FLEFLK-FITC was calculated by conversion of the Michaelins Menten equation (Formular 1a-f).

Formular 1a $v = Vmax [S] / (KM + [S])$

Formular 1b $Vmax = kcat [E]$

Formular 1c $v = kcat [E] [S] / (KM + [S])$

at low [S], that is when Km >> [S},

Formular 1d $v = kcat [E] [S] / KM$

Formular 1e $v / [S\} = slope = kcat [E\} / KM$

Formular 1f $slope / [E] = kcat / KM$

2.6. Methods for Aims 2-6

2.6.1 Rats and diets

Male Wistar rats (Charles River, Sulzfeld, Germany) weighing 365 ± 18 g were fed a standard diet containing 5 µg/g Vitamin K_1 and water *ad libitum*. They were fed the diets shown in Figure 3 (all diets were from Altromin, Lage, Germany; Table 1). Diets a) - d) were applied for 4 weeks as a model for kidney failure with no overt vascular calcification, diets e) - h*)* as a model of severe calcification for 7 weeks. 7 weeks of adenine diet included a 2-week interphase on an adenine-free diet in week 5 and 6 for recovery of the animals. Vitamin K_2 diet contained 100 mg/kg MK4 (diets c, d, f) or 500 md/kg (diet g). Vitamin K_1 was added to 100 mg/kg (diet h) (Figure 8, Table 1). Organ harvesting was performed as described under 2.5.2.

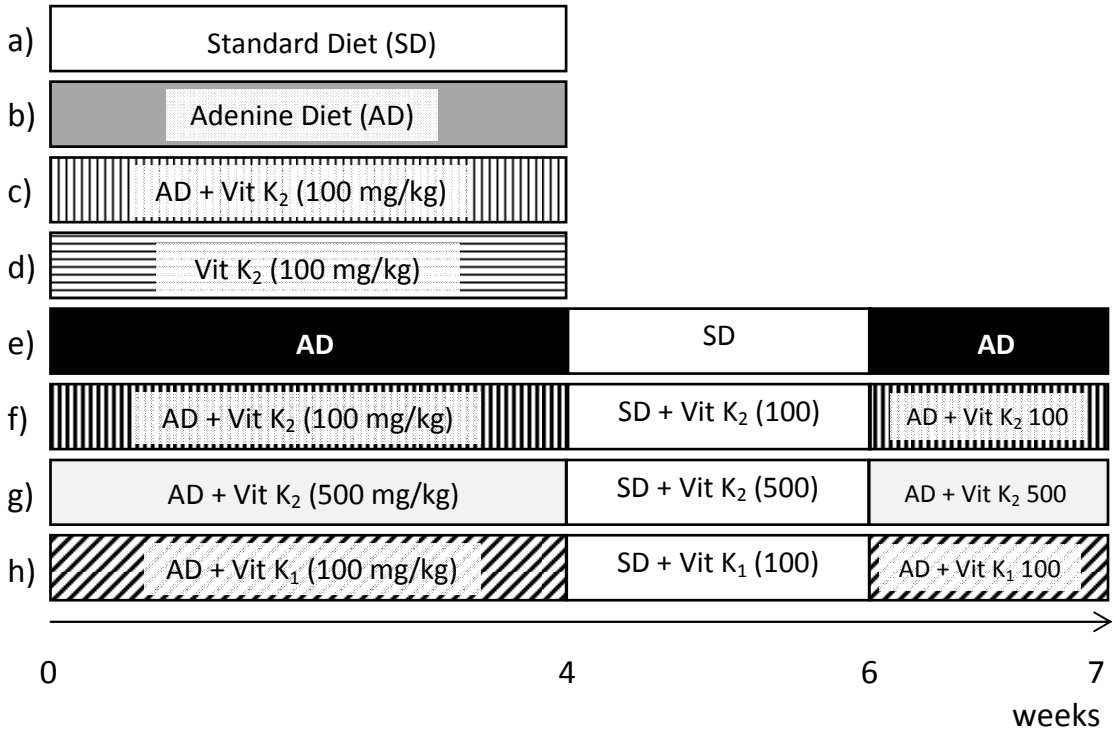

Figure 8: Overview of the 8 different rat treatment groups. Seven weeks of treatment contained a 2-week interphase without adenine supplementation.

Table 1: Composition of diets and treatment duration

	I diets composition [g/kg]							
Group	**Protein**	**Energy [kcal/kg]**	**Fat**	**Fibre**	**K_1 [mg/kg]**	**K_2 [mg/kg]**	**Adenine**	**Weeks**
a)	173.46	3720	50.3	0.06	5	-	-	4
b)	173.46	3720	50.3	0.06	5	-	7.5	4
c)	173.46	3720	50.3	0.06	5	100	7.5	4
d)	173.46	3720	50.3	0.06	5	100	-	4
e)	25	3671	50.6	1.8	5	-	7.5	7
f)	25	3671	50.6	1.8	5	100	7.5	7
g)	25	3671	50.6	1.8	5	500	7.5	7
h)	25	3671	50.6	1.8	100	-	7.5	7

2.6.2 Blood pressure

Blood pressure was measured in rats non-invasively by determining the tail blood volume with a volume recording sensor and an occlusion tail cuff on a Kent Scientific CODA system at weeks 0, 2, 4 and 7. Rats were placed into a restrainer and the warming plate was set on 37°C. The Coda software was programmed on 5 cycles for acclimatisation and 10 cycles to obtain values. The systolic blood pressure is measured directly whereas the diastolic blood pressure is calculated by the software. Rats were trained before assessing values.

2.6.3 Biochemistry

Blood from rats was collected at after 0 and 4 weeks by tail vein puncture. Therefore, rats were placed into a restrainer and the tail was warmed with 38°C tap water. One of the 3 tail veins was punctured with a safety multifly canuele. At the end point (4 or 7 weeks), blood was collected by puncture of the left ventricle. Serum was obtained by spinning the blood sample tube at 2,000 x g for 10 min at 4°C. To collect the urine, animals were placed into metabolic cages for 24 h prior sacrifice (Institut für Versuchstierkunde, Aachen, Germany). Serum and urine parameters were measured by Vitros 250, Ortho Clinical Diagnostics, NY, USA clinical routine laboratory diagnostics (Institut für Versuchstierkunde, Aachen, Germany). Glomerular filatration rate (GFR) was calculated as followes:

Formula 2: $$GFR[ml/\min] = \frac{c_{creaurine} * V_{urine}}{t * c_{creaserum}}$$

$C_{creaurine}$: concentration of creatinine in urine [µmol/l]

V_{urine}: Volume of urine [ml]

t: time [min]

$c_{creaserum}$: concentration of creatinine in serum [µmol/l]

2.6.4 MGP ELISA

MGP diagnostics were performed at VitaK BV, Maastricht, NL.

Total uncarboxylated MGP was measured in serum by competitive ELISA by a monoclonal antibody (MGP sequence 35-49; VitaK BV, Maastricht, the Netherlands), as described previously (52).

2.6.5 Enzyme activities

Enzyme activites were tested using microsomes which were obtained as described under 2.5.3. Each microsomal fraction was split to be tested in three enzyme activity assays, GGCX, VKOR and DT-diaphorase. Microsomes from aorta were only tested for GGCX activity due to the low amount of microsomal protein.

2.6.5.1 GGCX activity assay

GGCX assay was performed as described under 2.5.5. The amount of microsomal protein was 250 µg and the reaction time was 30 min. For a selective influence on the γ-carboxylase activity, microsomes from healthy rats were first incubated with the uremic toxins urea (50 mM, 500 mM), indoxylsulfate (250 µM, 500 µM) or p-cresol (100 µM) at room temperature for 30 min. Quantification of carboxylated FLEFLK-FITC was performed by rp-HPLC setup referring to 2.5.6.

2.6.5.2 VKOR activity assay

The VKOR activity was measured by conversion of vitamin K_1 2, 3 epoxide (K_1<O) to vitamin K_1 (37). The reaction mixture, with a total volume of 200 µl contained 500 µg microsomal protein in sucrose buffer and 8 µl 5 mM K_1<O. The reaction was started by the addition of 5 µl 200 mM DTT and stopped after 60 min incubation at 30°C in the dark by 500 µl 0.05 M $AgNO_3$ in isopropanol. The samples were centrifuged at 5,000 x g for 5 min. The

supernatant was taken for HPLC measurements. The HPLC system consisted of a pump (L-7100), an autoinjector (L-7200), a column oven (L-7350), a UV- detector (L-7400) and an interface (D-7000) connected in line. Vitamin K_1 was separated in reversed phase HPLC on a Max RP C12 column. Isocratic methanol at pH 5 (acidified with acetic acid) was used as a mobile phase with a continuous flow rate of 1 ml/min. The pressure limit was set at 350 bar. Vitamin K_1 and vitamin K_1>O were detected at 246 nm. Each run was recorded for 12 min. Vitamin K was quantified by external standards. For epoxidation, vitamin K_1 was diluted in hexane and mixed with 0.5 M NaOH, 0.2 M Na_2CO_3 and 5% H_2O_2 for 12 h at 37°C in the dark. Vitamin K_1>O quality was monitored by HPLC measurements.

2.6.5.3 DT-diaphorase activity assay

DT-diaphorase activity was analyzed in rat kidney and liver by the standard assay (53) with NADPH as electron donor and menadione as electron acceptor (Figure 9).

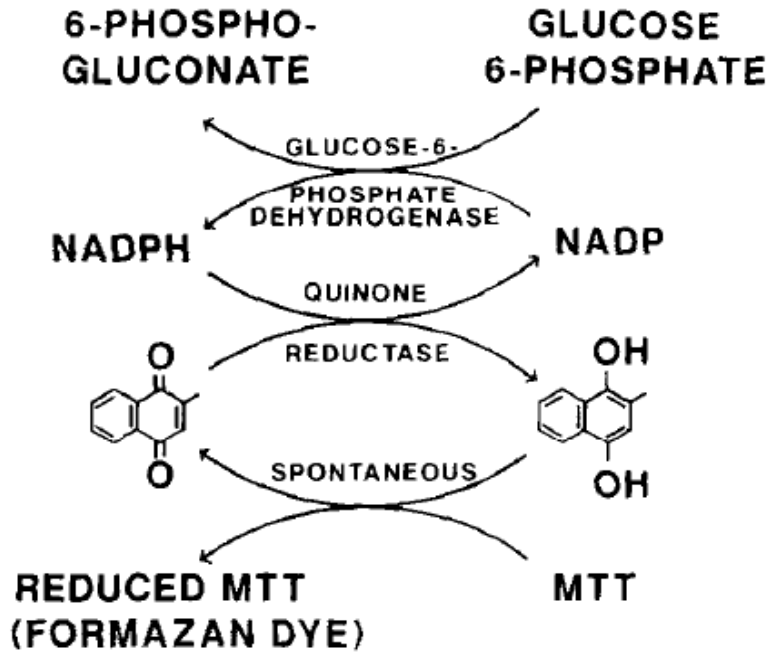

Figure 9: Principle of the DT-diaphorase activity assay (from Prochaska 1987) (53).

NADPH is generated by the conversion from glucose-6-phosphate to 6-phosphogluconate by glucose-6-phosphate dehydrogenase and is required as a cofactor for the DT-diaphorase (Quinone-reductase). Thereby, menadione is reduced to menadiol by the DT-diaphorase. MTT is reduced nonenzymatically by menadiol and forms a blue colour which is detected at 610 nm (53).

A total volume of 150 ml reaction mixture contained 7.5 ml 0.5 M Tris-Cl (pH 7.4), 100 mg BSA, 1 ml 1.5% Tween-20, 0.1 ml 7.5 mM FAD, 1 ml 150 mM glucose-6-phosphate, 90 µl 50 mM NADPH, 300 U yeast glucose-6-phosphate-dehydrogenase and 45 mg MTT. The assay was carried out in the presence and absence of 3 mM dicoumarol and 50 µM menadione with 250 µg microsomal protein (Figure 10).

	1	2	3	4	5	6	7	8	9	10	11	12
a	b1	S1	S2	S3	S1	S2	S3	S1	S2	S3		
b	b2	S4	...	...	S4	...	...	S4	....	....		
c	b3											
d	....											
e												
f												
g												
h			...	S24		...	S24		...	S24		

1-4: RM
5-7: RD
8-10: R

Figure 10: Pipetting scheme of the 96-well plate for DT-diaphorase activity assay.
b = nonenzymatic blank; S1-S24: sample number; RM = reaction mixture with menadione (timepoint t 5min); D: reaction mixture with menadione and dicoumarol (to determine the unspecific activity not inhibitable by dicoumarol); R: reaction mixture without menadione (representing timepoint t0)

The reaction was stopped after 5 min at 20°C by 3 mM dicoumarol and 5 mM KCl. The DT-diaphorase activity was calculated as the specific activity inhibited by dicoumarol. Reduced MTT as the formazan dye was detected at 610 nm on a Tecan sunrise microplate absorbance reader. To calculate the difference of reduced MTT extinction (δE) the arithmetic mean of the blank (B) is subtracted from each value first (i: sample number 1-24) and afterwards timepoint t0 from the extinction at timepoint 5 min (according to formula 3).

Formula 3: $$\delta E = (Si_{t5min} - B) - (Si_{t0} - B)$$

The extinction of the unspecific activity (SiD), also corrected for the mean of the blank, can be subtracted from the activity at timepoint t5 to calculate the extinction of the specific DT diaphorase activity (δE_{spec}) (according to formula 4).

Formula 4: $$\delta E_{spec} = \delta E - (SiD - B)$$

The concentration of the formazan dye reduced MTT (δc) can be calculated from the Beer Lambert law (formula 5).

Formula 5: $$\partial c[M] = \frac{\delta E_{spec}}{(\varepsilon * d)}$$

ε = extinction coefficient of MTT at 610 nm = 11.3 mM/cm
d = thickness of the sample = 0.7 cm

The final result is depicted as specific activity per minute per g protein (formula 6).

Formula 6: $$\text{DT-diaphorase activity [mol/min/g]} = (\delta c/5) * 4$$

2.6.6 Calcium determination

The extent of vascular and tissue calcium content was measured colorimetrically. Frozen samples weighing between 30-70 mg (aorta) or 100-250 mg (kidney, lung, heart) were lyophilised on a Christ Loc 1mALPHA 1-4 coupled with a vacuum hybrid pump RL 6 over night. Dried samples were weighed and incubated in 500 µl 10% formic acid over night to elute the calcium. For quantification of calcium deposition of VSMC, cells were washed twice with calcium-free PBS and incubated over night in 10% formic acid. 25 µl of each sample was measured twice in the Randox cresolphthalein assay. The working solution consisted of equal parts solution 1 (2-amino-2methyl-1-propan-1-ol 3.5mol/l, pH 10.7) and solution 2 (containing the chromogen O-chresolphthalein 0.16 mmol/l). Calcium standards were 10, 5, 2.5, 0.625 and 0 mg/dl. Absorption was measured at 550 nm on a Tecan sunrise microplate absorbance reader. Results were depicted in mg calcium per g dry tissue.

2.6.7 Histochemistry

Kidney, lung, and thoracic aorta were fixed in 4% paraformaldehyde (Roti®-Histofix) for at least 24 h at room temperature. Dehydration of the samples was performed on an automated tissue processor (Slee tissue processor, Interdisziplinäres Zentrum für klinische Forschung IZKF, Aachen, Germany). Afterwards the samples were embedded in paraffin blocks. 4 µm thick sections were cut on a rotary microtome (Slee, Mainz, Germany). Microscope slides were incubated for 12 h at 37°C before staining. The base of the heart was embedded in tissue tek for cryosectioning. 10 µm thick sections were cut on a cryotome.

Deparaffinization of the slices was performed by washing 3 x 5 min Xylol, 3 x 2 min 96% ethanol, 2 x 2 min 75% ethanol, 10 seconds in water.

Localisation of the calcification was visualized by *von Kossa* staining (54). Therefore, deparaffined sections were immersed in 1% aqueous $AgNO_3$ solution for 5 min. After washing, samples were incubated in a solution of 5% $NaCO_3$ and 9.25% formalin for 1 min. After a second rinse, sections were developed using 5% sodiumthiosulfate for 5 min and counterstained in 0.1% safranin-O followed by a final rinse using tap water. Dehydration was performed by washing in 70% ethanol for 1 min, 95% ethanol for 1 min, 3 x 5 min in xylol. Stained slices were covered with Roti®-Histol and a cover glass. Quantification of von Kossa positive areas was performed with the help of imageJ software. Results are depicted in % positive area of total area.

UcMGP was visualized in aortic tissues by incubation with the anti-GluMGP antibody (55), performed at the VitaK BV, Maastricht, NL.

2.6.8 Real time PCR

RNA was harvested from RNAlater® (Qiagen, Hilden, Germany) stabilized liver, abdominal aorta and heart using the Qiagen RNeasy mini kit. Purity and RNA concentration were analyzed with the Agilent RNA 6000 Nano Kit. 200 ng RNA was used for reverse transcriptase performed on a thermocycler in four steps: 1) 10 min at 25°C, 2) 3 min at 48°C, 3) 5 min 95°C and 4) cool down.

The qPCR Core Kit for SYBR Green I was applied for a two-step quantification on an Real-Time PCR TagMan® system. The GGCX TaqMan® gene expression assay was performed from cDNA received from rat liver. GAPDH was used as a housekeeping gene. The following rat GAPDH primers were used:

sense: ACAAGATGGTGAAGGTCGGT,

antisense: AGAAGGCAGCCCTGGTAACC,

probe: CGGATTTGGCCGTATCGGACGC 3.

2.7. Methods for Aim 7

2.7.1 Mice

Two breeding pairs of Gas6$^{-/-}$ mice were kindly provided by Peter Carmeliet (University of Leuven, Belgium). Gas6$^{-/-}$ were backcrossed for more than 10 generations on a C57BL/ background, which served as a wildtype (WT) control.

2.7.2 VSMC culture

VSMC were isolated from the thoracic aorta of healthy adult C57BL/6 and Gas6$^{-/-}$ mice. Therefore, mice were killed with an overdose of isoflurane. The abdomen and the thorax were opened with sterile instruments. Organs were perfused with 10 ml cold PBS via puncture of the left ventricle. The iliac artery was incised to enable an out flow of blood and PBS. Liver, intestine, lung, kidney and spleen were removed to dissect the aorta. The thoracic aorta was cleaned from fat and surrounding tissue. After harvesting, aortas were washed twice with PBS and then incubated with 2 g/l collagenase and 1% elastase containing cell culture medium for 1 h at 37°C. Aortas were cut into small pieces, washed twice with PBS and seed into T25 cell culture flasks. The smooth muscle cell basal medium was supplemented with fetal calf serum (0.05 ml/ml), epidermal growth factor (0.5 ng/ml), basic fibroblast growth factor (2 ng/ml), insulin (5 µg/ml) and finally 1% penicillin streptomycin and 0.1% gentamycin. Cell culture medium was changed twice each week. Cells were grown to 85% confluence untill passaging. Passages from 3-5 were used for calcification experiments in 12 well plates. Calcification medium contained 3 mM calcium phosphate or 10 nM warfarin plus 3 mM calcium phosphate. To induce calcification cells were cultured for 5 to 7 days. A negative control (d_0) was included in each experiment to normalize the obtained values; calcium deposits were depicted as changes in %.

2.7.3 Protein determination

The adherent cells were diluted in 200 µl lysis buffer (0.8% Digitonin, 2 mM EDTA, pH 7.8) using a cell scraper. Protein content in VSMC was determinded as described under 2.5.4.

2.7.4 TUNEL-assay

Apoptosis measurements were performed with the Roche *in situ* cell death detection kit. All samples were fixed in methanol for 10 min at room temperature. VSMC were permeabilised by an aqueous solution of 0.1% sodium citrate and 0.1% Triton X for 2 min on ice. Cells were counterstained with DAPI (Vectashield®, containing 1.5 µg/ml DAPI). For positive control

cells were preincubated with DNase for 10 min at room temperature. For a negative control the terminal transferase was omitted.

Stained slices were photographed on a Leica microscope at a 100 x magnification. Semiquantitative analysis of positive stained area was measured with ImageJ software.

2.7.5 Mice: Surgery and diets

Mice were divided into six groups: two healthy groups at the age of a) 8-10 weeks and b) 34-36 weeks and four treatment groups: c) warfarin d) Uninephrectomy (UNiNx) and e) electrocautery (EC). For the surgical groups (UniNx and EC) the rodent chow (AB diets, Woerden, The Netherlands) was supplemented to 0.95% calcium and 1.65% phosphate. The warfarin chow contained 3 g/kg. The warfarin diet or surgery was started at the age of 8-10 weeks and the diets were continued for 8 weeks. UniNx was performed at the age of 8 weeks. All surgery was performed under Ketamin/ Rompun (0.2 ml 10% Ketamin, 0.25 ml 2% Xylazin, 0.25% NaCl) anaesthesia. Anaesthesia was injected intraperitoneally at a dosage of 2 µl/g body weight 10 min earlier. The depth of anaesthesia was checked by a gentle skin pinch. The surgery was started after desinfection with an incision on the left flank. The kidney was exposed and after ligation of the ureter, renal artery and vein with non resorbable silk-removed. After one week of recovery, high phosphate diet was initiated (Figure 11). For more severe kidney damage, electrocautery of the right kidney at the age of 8 weeks plus uninephrectomy of the left kidney 2 weeks later was performed. For electrocautery, punctual lesions were set on the renal cortex with a 2 mm diameter electrocoagulation ball tip over all areas of the kidney. The 1 mm deep punctuate lesions were spaced 2 mm apart (56) (Figure 12). After 2 weeks, the contralateral kidney was removed and after one additional week the high phosphate diet was started (Figure 11). In all experiments female animals were used, except in ageing mice where both gender were analyzed. Tissue was harvested as described under 2.6.

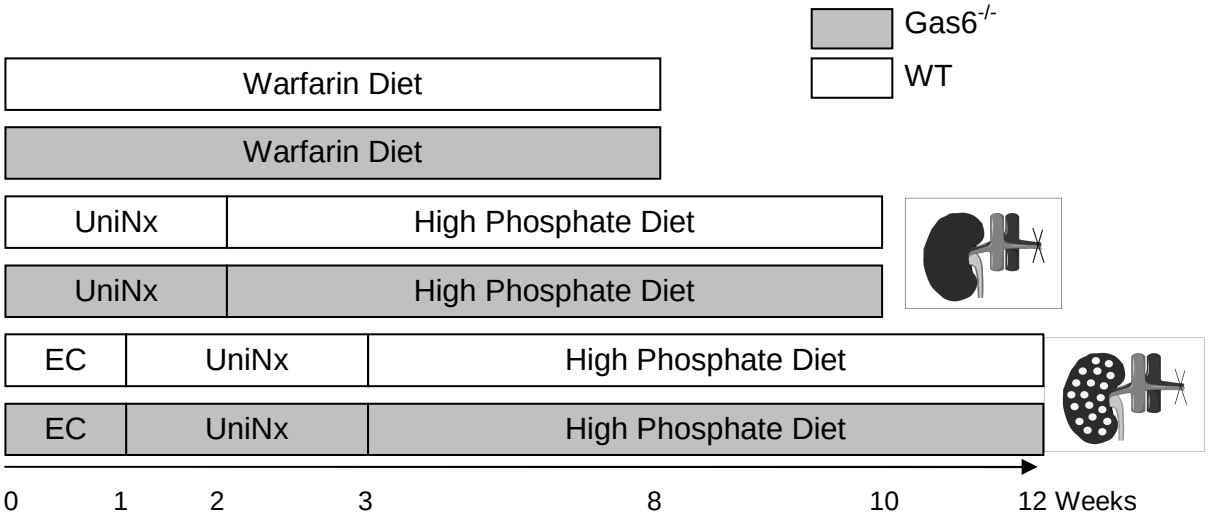

Figure 11: Experimental design of the *in vivo* mouse experiments.

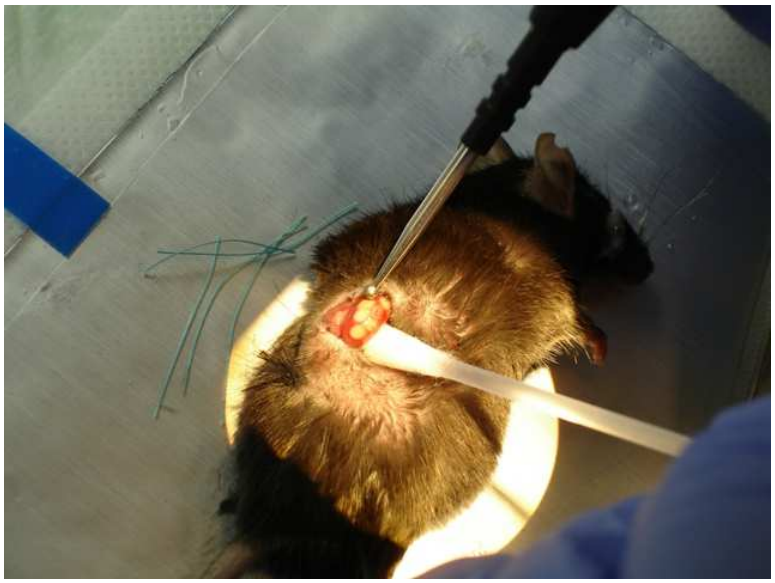

Figure 12: Electrocauterisation of the right kidney; punctuate lesions are set on the renal cortex.

2.7.6 Genotyping

DNA was isolated from snap frozen WT and Gas6$^{-/-}$ mice liver tissues from each treatment group at different timepoints throughout the breeding time of the experiment. The liver was homogenized in a ball mill in ALT lysis buffer at 20 Hz for 2 minutes. Protein was digested by incubation for 45 min at 56°C with proteinase K. Further DNA isolation was performed with the Qiagen QIAmp DNA Mini Kit. Ready to go PCR beads were used for cDNA synthesis. DNA was amplified on a thermocycler (step 1) 94°C 2 min, step 2) 94°C 30 sec,

step 3) 58°C 30 sec, step 4) 72°C 30 sec, step 5) go to step 2 for 34 times, step 6) 72°C 10 min, step 7) hold). Primer sequences made by Invitrogen (Invitrogen, CA, USA) were:
Mgas6 1S: 5' GAG-TGC-CGT-GAT-TCT-GGT-C 3';
Mgas6 2A: 5' CCA-CTA-AGG-AAA-CAA-TAA-CTG 3'.
The PCR product was seperated on a 1% agarose gel (2 g agarose, 200 mL TAE buffer) at 130 V in TAE buffer (50 x TAE: 18.61 g/l (0.05 M) EDTA Na2 2 H2O; 60.05 g/l (1 M) acetic acid and 242.28 g/l (2 M) TRIS) for 45 min. Bands were visualized with ethidium bromide and identified with the 1 kb DNA ladder Fermentas GeneRuler™.

2.7.7 Biochemistry

Blood from mice was collected by puncture of the left ventricle during sacrifice and collected in a serum tube. Serum and urine diagnositics were performed as described under 2.6.3.

2.7.8 Calcium determination

VSMC were washed twice with calcium free PBS and each well was incubated 10% formic acid over night. Quantification of VSMC and tissue calcium content (aorta, heart, kidney) was performed as described under 2.6.6.

2.7.9 Echocardiography

Transthoracic echocardiography was performed on the Visulasonics high resolution micro-imaging system Vevo 770 using the RMV 704 scanhead. Therefore, mice were anaesthetised with isoflurane and placed on a warming plate at 37°C. The thorax was fully depilated. Breathing and heart frequency were monitored, continuously. A long axis view loop was recorded in the brightness mode (B-mode). Left ventricular (LV) mass was calculated in the motion mode (M-mode) in the long axis view (Figure 13) from the Devereux formula:

Formula 7: $$LVM\ [mg] = 1.04*[(LVID+LVPW+LVSW)^3-LVID^3]$$

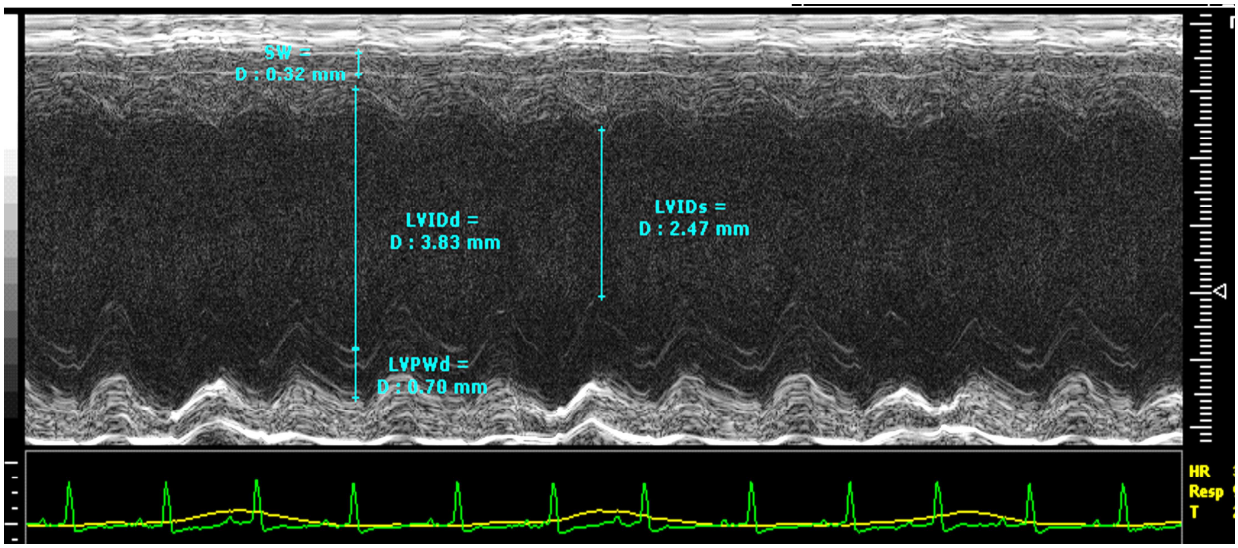

Figure 13: M-mode of the long axis view. The left ventricular inner diameter is measured in the systole (LVIDs) and the diastole (LVIDd), as well as the thickness of the septal wall (SW) and the left ventricular posterior wall in the diastole (LVPWd).

The short axis view is obtained by a 90 degree rotation of the scanhead (RMV 704) in the B-mode. Ejection fraction (EF) as an index for global left ventricular systolic function was measured by the Simpson`s method. Therefore, the heart was divided into 4 equal sections along the longitudinal axis (Simpson 1-4) and for each a short axis view loop was taken. The endocardial area was measured in each picture of the short axis view in the systole and in the diastole to obtain the end diastolic (EDV) and end systolic volumes (ESV) (Figure 14).

Formula 8:

$$EF[\%] = \frac{SV}{EDV} * 100$$

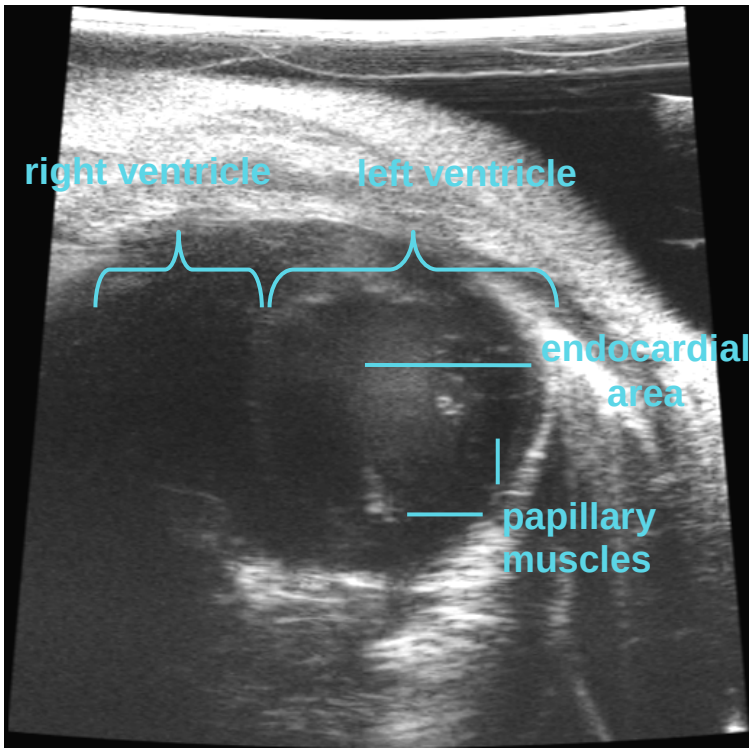

Figure 14: Short axis view of the diastole to measure the endocardial area (here Simpson 3) of the left ventricle.

Stroke volume (SV) was estimated as the difference between the LV end-systolic and end-diastolic volumes as follows:

Formula 9: $$SV[\mu L] = EDV - ESV$$

Pulse-wave velocity (PWV) in the right common carotid artery was measured using the transit-time method in a two-dimensional mode. In the carotid artery, the proximal pulse wave signal was obtained 1 mm behind the origin of the subclavian artery, the distal signal 1 mm before the carotid bifurcation (Figure 15). The transit time was found by subtracting the distal arrival time between the R-wave peak and the foot of velocity upstroke from the similarly determined proximal arrival time:

Formula 10 $$PWV[mm/ms] = \frac{\Delta d}{(Pt_{dist} - Pt_{prox})}$$

Pt is the time point of the proximal or distal pulse wave signal and Δd is the distance between the two measurements.

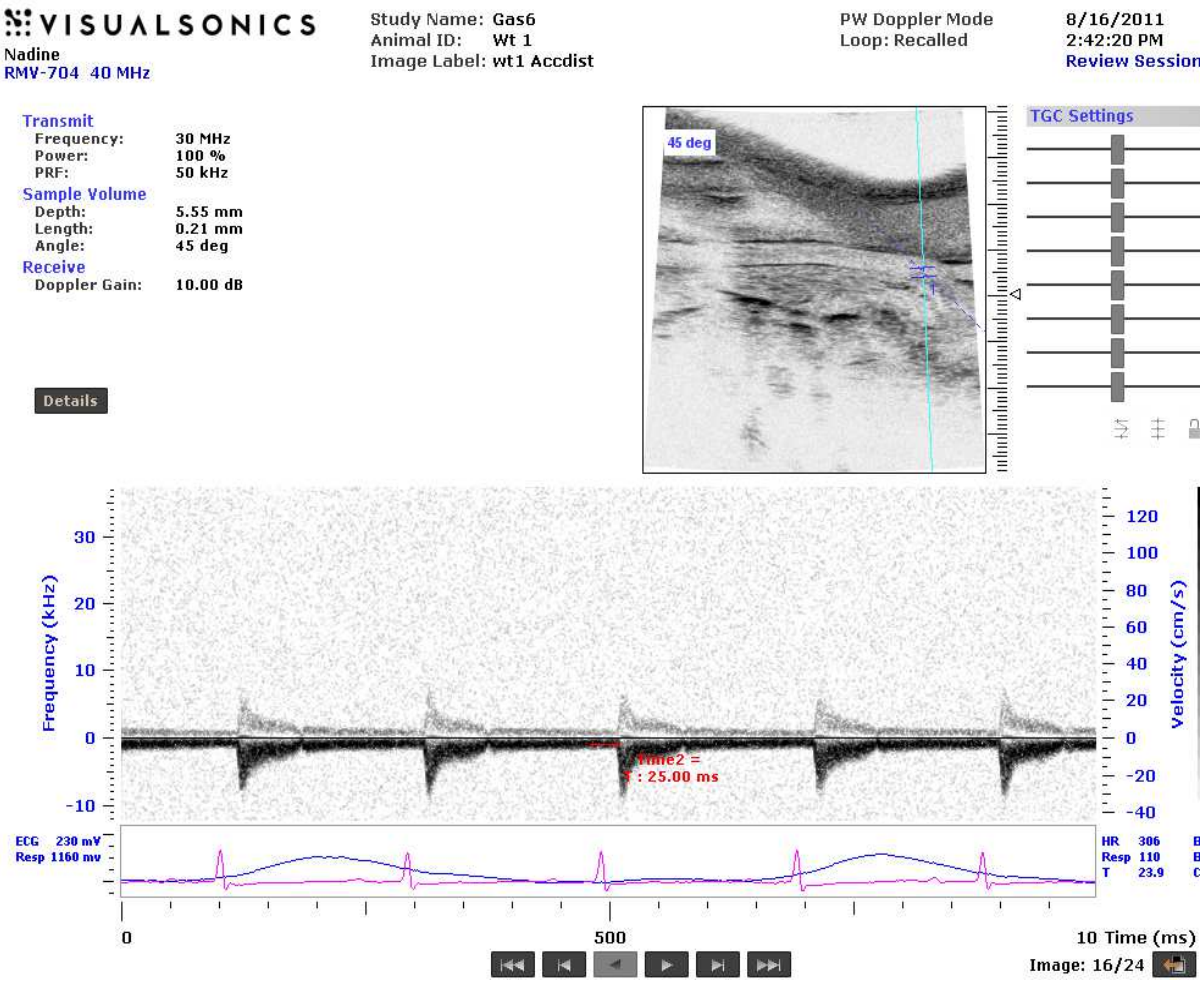

Figure 15: Assessment of the PVW in the arteria carotis communis. The doppler mode for the distal point is placed 1 mm before the bifurcation (small box) at an angel of 45 degrees. Then, the time between the ECG and the pulse wave can be measured (big box).

2.7.8 Histochemistry

Von Kossa staining was performed as described under 2.6.7.

Sirius red staining for collagen was performed in cryo sections from heart tissues from warfarin treated mice. Samples were incubated in 5 w/v % Sirius red for one hour in picric acid at room temperature. Afterwards the samples were washed twice in acidified ethanol (70 v/v %; pH 3.5).

2.7.9 Real time PCR

Real time PCR was performed as described under 2.6.8.

Quantification of MGP gene expression was performed from cDNA from $Gas6^{-/-}$ and WT mice aortas with external standards for MGP ($8.8 * 10^6$ – 8.8 * 10) and GAPDH ($6.4 * 10^6$ – 6.4 * 10).

MGP probe was AGAGTCCAGGAACGCAACAAGCCTGC,
sense primer GCAGAGGTGGCGAGCTAAAG and
antisense primer AGCGCTCACACAGCTTGTAGTC (57).
Corresponding murine GAPDH probe was AAGGCCGAGAATGGGAAGCTTGTCATC,
sense primer AAGTGGTGATGGGCTTCCC and
antisense primer GGCAAATTCAACGGCACAGT.

2.8 Statistical analysis

The difference between the treatment groups was assessed by one-way ANOVA followed by Tukey`s multiple comparison test. Equal variances were tested with Bartlett`s method. D`Agostino and Pearson normality test was performed to check for Gaussian distribution. Statistical significance was defined as $p < 0.05$. Linear correlations were calculated in Origin Pro8 software.

3. RESULTS

3.1 Results for aim 1

3.1.1 Peptide Design

The properties of the designed hexapeptide FLEFLK-FITC was tested on rp-HPLC coupled with UV-detection and in LC/MS/MS measurements before and after in vitro carboxylation.

3.1.1.1 Detection of the uncarboxylated FLEFLK-FITC

The lipophilic FLEFLK-FITC was detected after 19.44 min rp-HPLC (Figure 16) and 19.55 min in MS measurements (Figure 17).

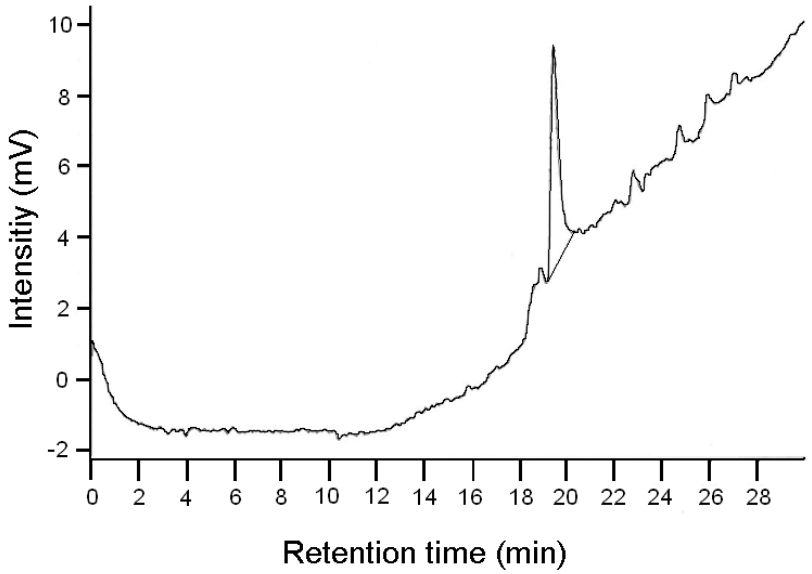

Figure 16: Rp-HPLC chromatogram of the purified reaction mixture at t=0. FLEFLK-FITC peak was detected after a retention time of 19.44 min.

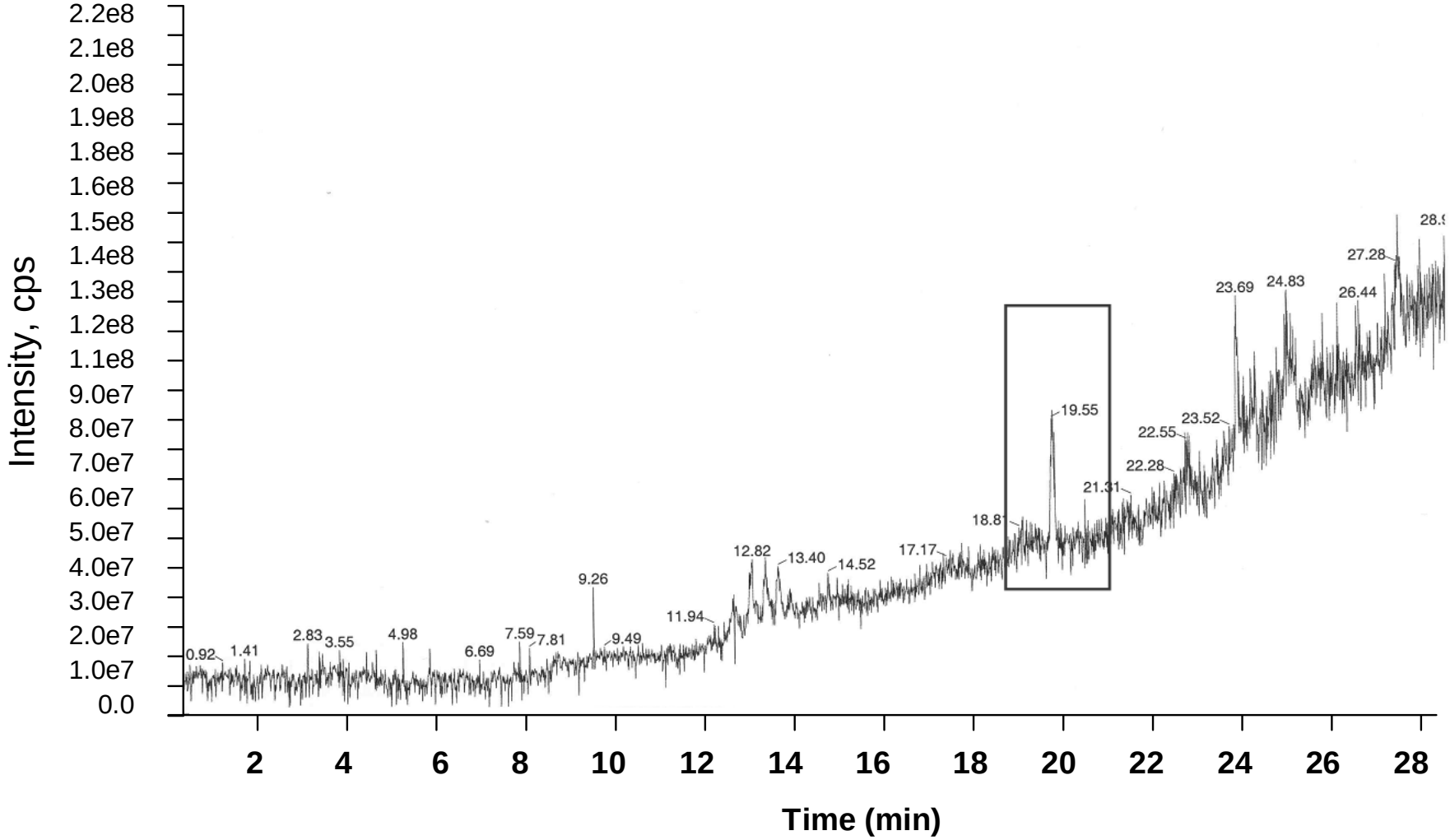

Figure 17: MS chromatogram of unmodified FLEFLK-FITC peptide solution with a distinct peak at 19.55 min (box).

There were no differences between the HPLC and MS patterns of the pure, diluted Glu-peptide and the purified reaction mixture at t = 0. The detection limit of uncarboxylated FLEFLK-FTIC in HPLC measurements was <10 ng/ml. There was a linear correlation of FLELFK-FITC between 10 ng -5 µg (R^2 = 0.99) (Figure 18).

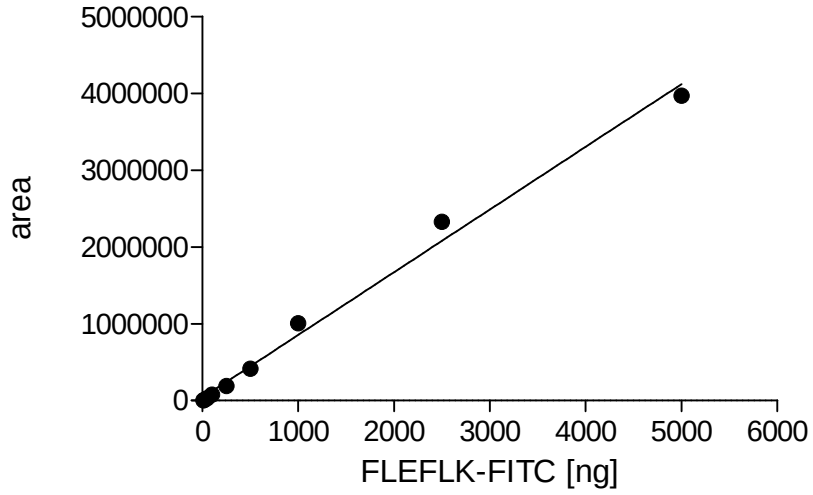

Figure 18: Linear correlation of the peak area and the amount of uncarboxylated FLEFLK-FITC. Used concentrations were 10 ng, 25 ng, 50 ng, 100 ng, 250 ng, 500 ng, 1 µg, 2.5 µg and 5 µg.

The MS pattern was in accordance with the manufacturer's analysis with distinct peaks at 390, 594, 926 and 1,186 m/z (Figure 19), the last matching the stated peak of highest mass corresponding to the molecular mass of the intact FITC-labelled peptide (Table 2).

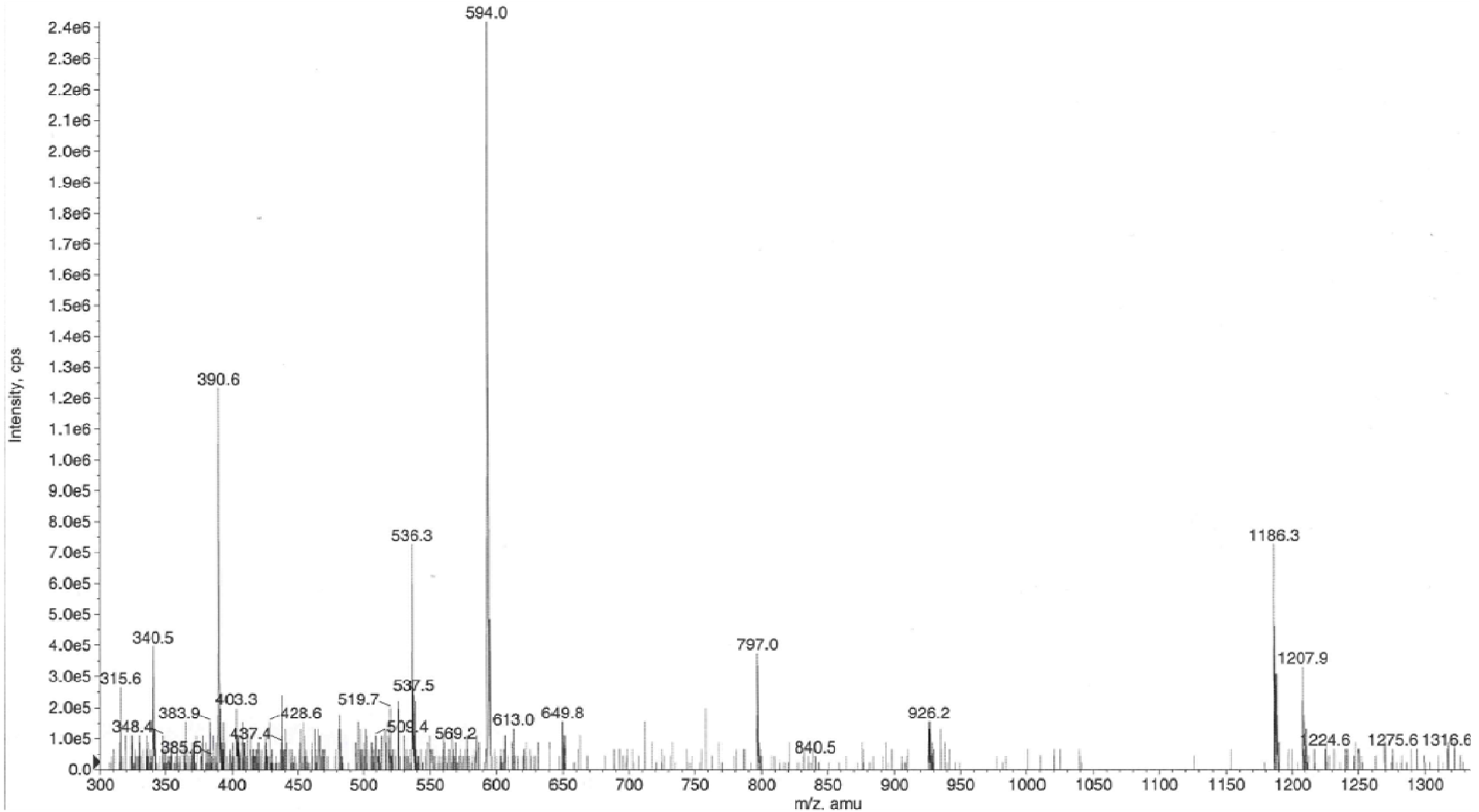

Figure 19: MS spectrum of FLELFK-FITC at 19.55 min

The 390 m/z fragment is expected to be FITC and the 594 m/z fragment could not be further identified. The purity of the peptide in reversed phase-HPLC analysis was 91%. The remaining 9% mainly include peptide fragments, salt and water, as supplied by the manufacturer.

3.1.1.2 C*haracterization of the carboxylated FLEFLK-FITC*

After running the carboxylase assay on the FLEFLK-FITC probe peptide, the lipophilic, hydrophobic FLGlaFLK-FITC product peptide showed a shorter retention time in reversed phase HPLC and was detected at 15.66 min in HPLC (Figure 20) and at 15.76 in MS measurements (Figure 21). Here, the in vitro reaction time was increased from 30 to 60 minutes in order to increase the amount of carboxylated peptide. In MS distinct peaks appear at 394, 438, 523, 577, 582 and 1,229 m/z (Figure 22, Table 2). The carboxylated peptide was stable over 24 h at 4°C in the dark.

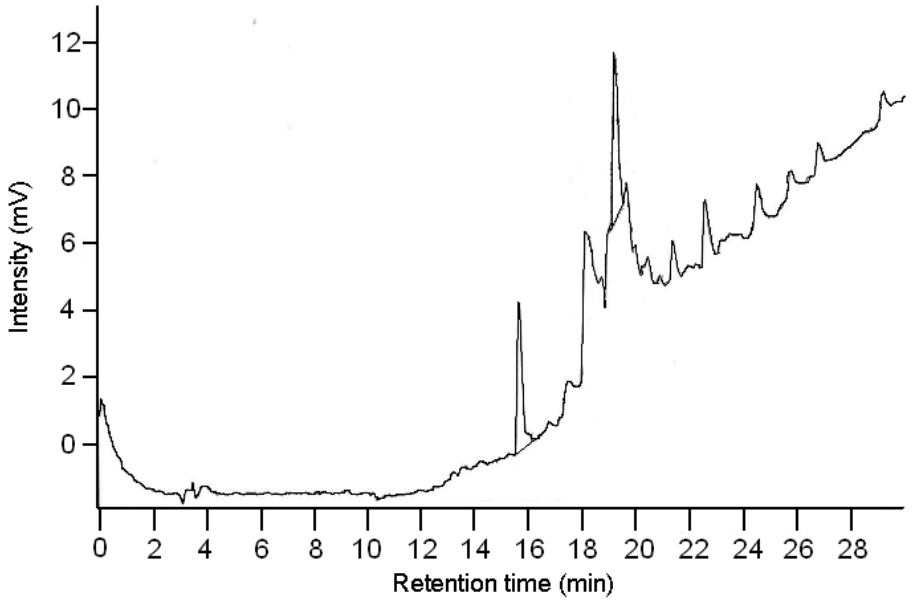

Figure 20: HPLC chromatogram of the reaction mixture at t = 30 min. A distinct peak appears at 15.66 min representing the carboxylated FLEFLK-FITC peptide as identified by LC/ESI-MS; a smaller peak at 19.24 min represents the uncarboxylated peptide (referring to figure 16).

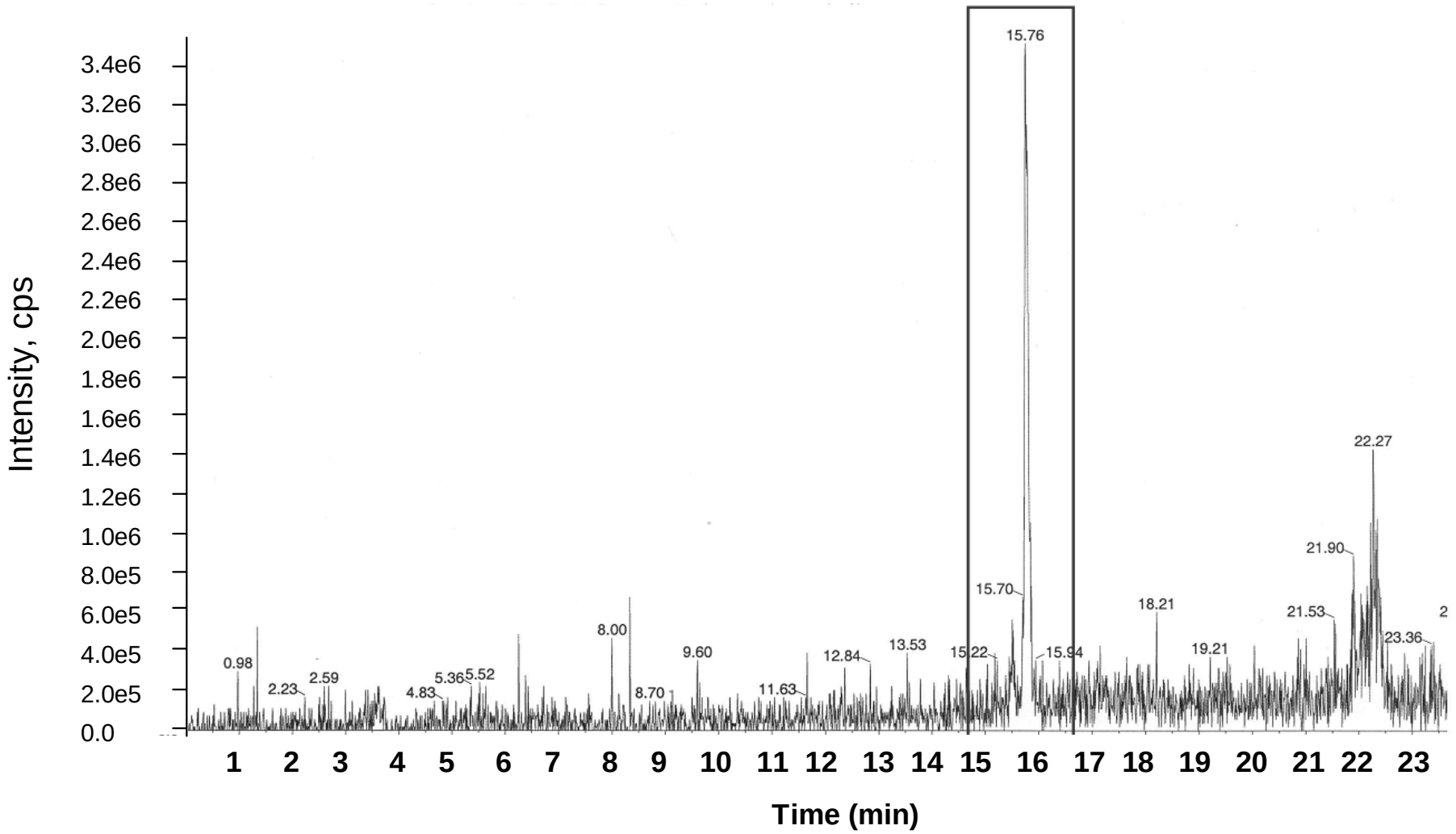

Figure 21: LC/MS chromatogram of the carboxylated FLELFK-FITC at *in vitro* reaction time t = 60, a distinct peak appears at 15.76 min (box).

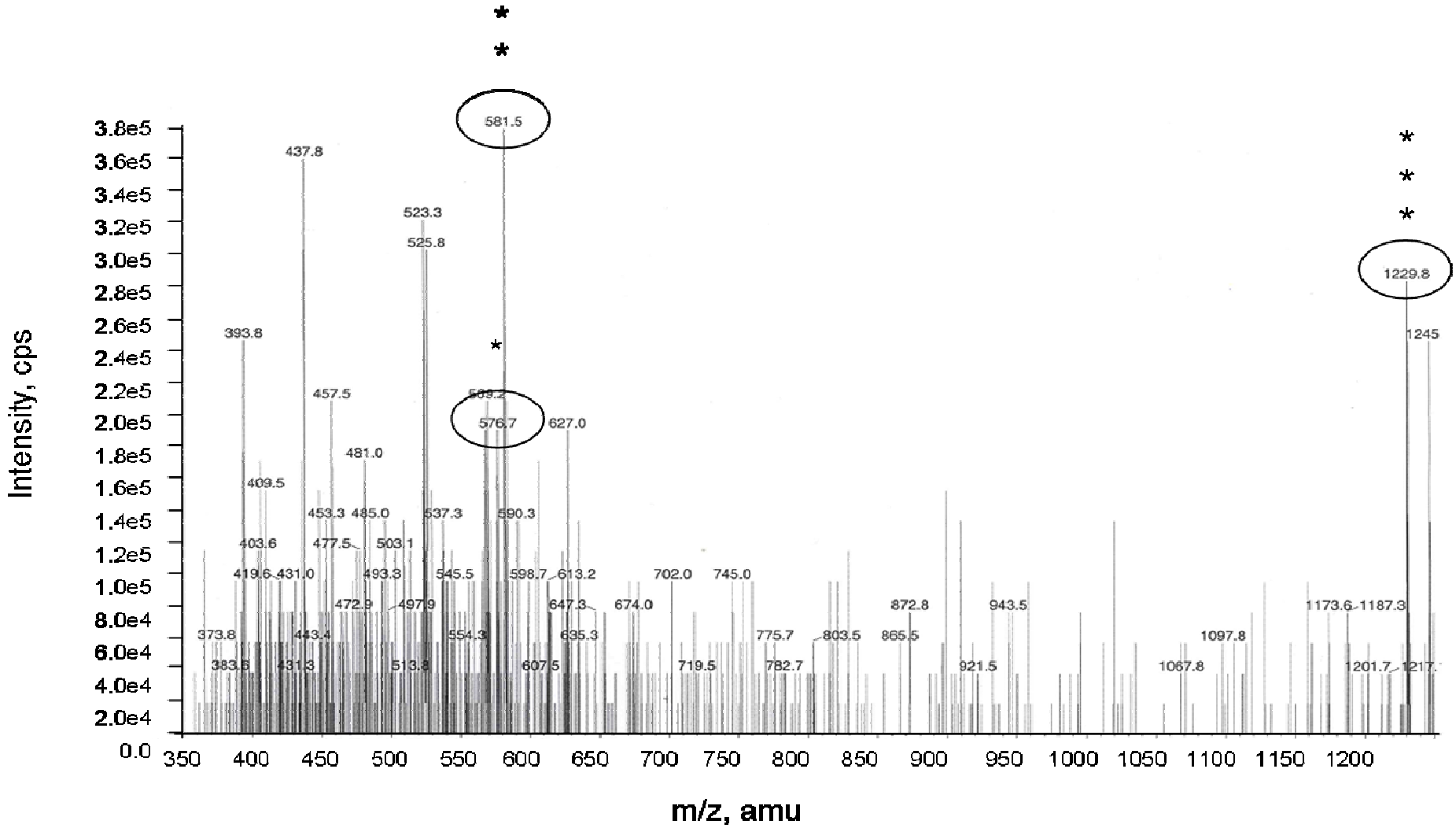

Figure 22: Mass spectrum of the carboxylated peptide at run time 15.76 min (referring to box figure 21). Asterisks indicate peaks representing carboxylated peptides (referring to table 2).

Table 2: Molecular weights of MS fragments

Fragments		
intact peptides	**calculated MW [g/mol]**	**measured MW [g/mol]**
Phe-Leu-**Gla**-Phe-Leu-Lys-FITC	1229.4	1229.8***
Phe-Leu-Glu-Phe-Leu-Lys-FITC	1185.3	1186.1
MS fragments		
Glu-Phe-Leu-Lys-FITC	924.0	925.8
Phe-Leu-Glu-Phe-Leu-Lys	795.0	796.8
Phe-Leu-Glu-Phe-Leu	650.8	649.8
Gla-Phe-Leu-Lys	577.6	576.7*
Phe-Leu-Glu-Phe	537.6	536.3
Phe-Leu-**Gla**-Phe	581.6	581.5**
Gla-Phe-Leu	433.5	437.8
Phe-Leu-Lys	391.5	393.8
FITC	390.4	390.3

List of unmodified FLEFLK-FITC and carboxylated FLEFLK-FITC with possible cleaved peptides generated by MS electrospray ionisation resembling positively charged fragments. Asterisks indicate carboxylated peptides corresponding to figure 22.

3.1.2 GGCX activity method

The GGCX activity was determined in microsomal preparations (9-21 mg/ml total protein) from kidney and liver tissues of healthy male rats fed a standard diet. The enzyme reaction was linear between 15 and 120 min ($R^2 = 0.98$) (Figure 23).

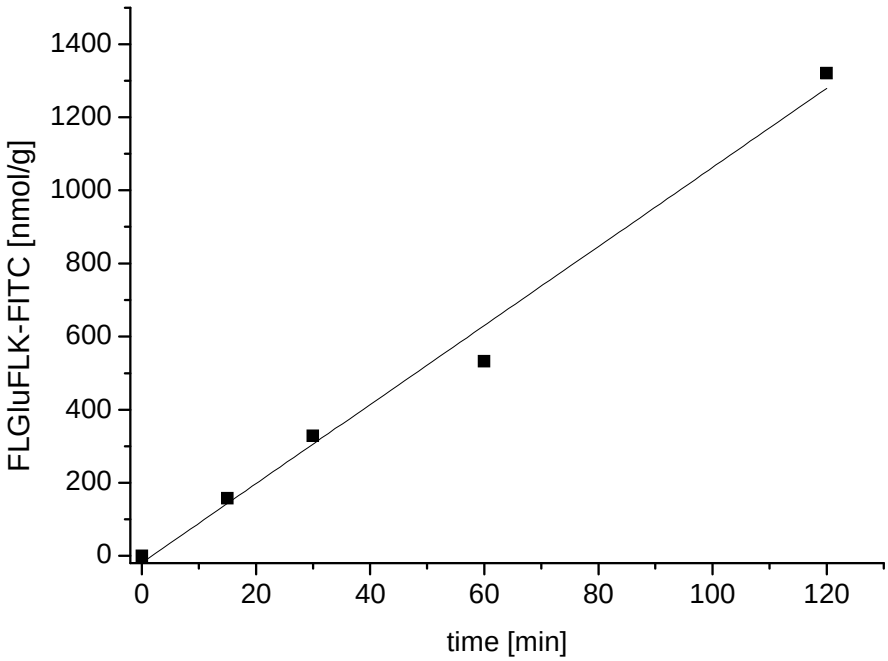

Figure 23: Linear correlation between *in vitro* reaction time and formed FLGluFLK-FITC (R^2 = 0.98).

A variation in the microsomal protein content resulted in a linear slope (R^2 = 0.99) between 50 and 750 µg microsomal protein (Figure 24).

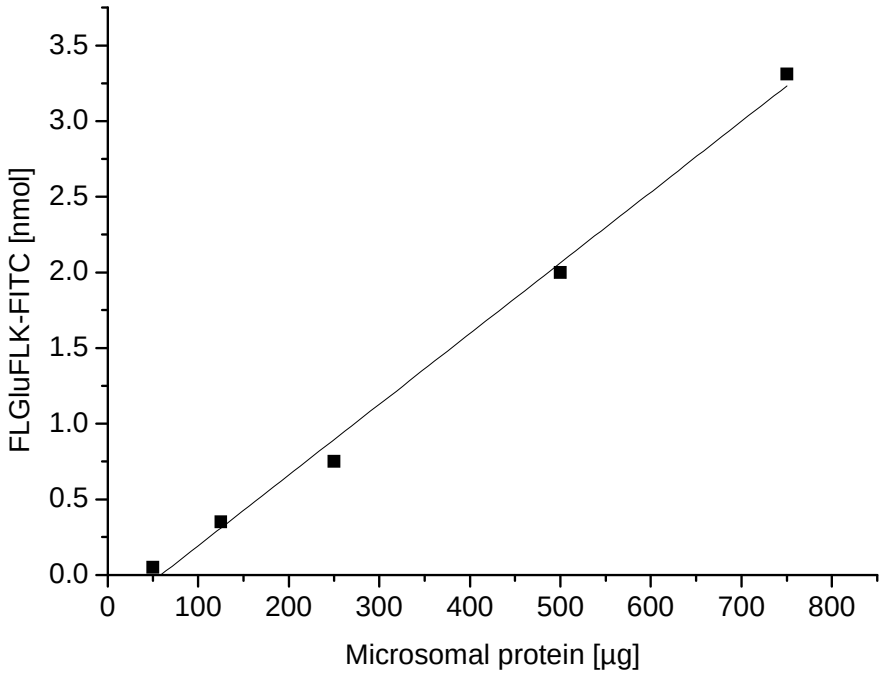

Figure 24: Linear correlation between the amount of microsomal protein and GGCX activity.

A variation in substrate however did not follow Michaelis Menten kinetics (data not shown).

The GGCX activity in liver microsomes was 481 ± 245 nmol/min/g protein and in kidney microsomes 412 ± 42 nmol/min/g protein. Treatment with NEM reduced the activity to 17.6 ± 10.7 in liver samples and 62.0 ± 49.0 nmol/min/g microsomal protein in kidneys (Figure 25).

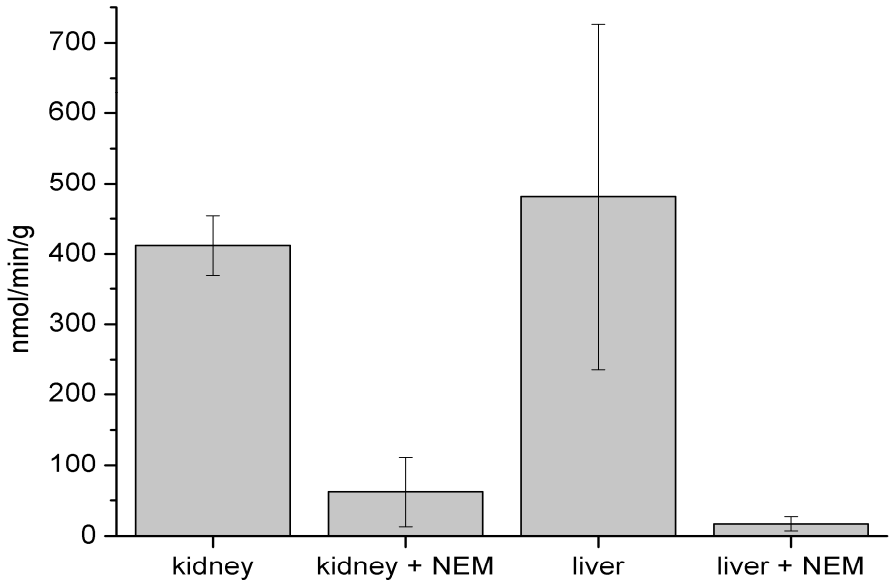

Figure 25: GGCX activity in rat liver and kidney without and with specific NEM inhibition (n = 7 and n = 3, respectively).

3.1.3 $^{14}CO_2$ incorporation

FLELFK-FITC showed incorporation of $^{14}CO_2$ during *in vitro* γ-carboxylation with a linear increase with increasing peptide concentrations from 0.3 -2.2 µM (Figure 26).

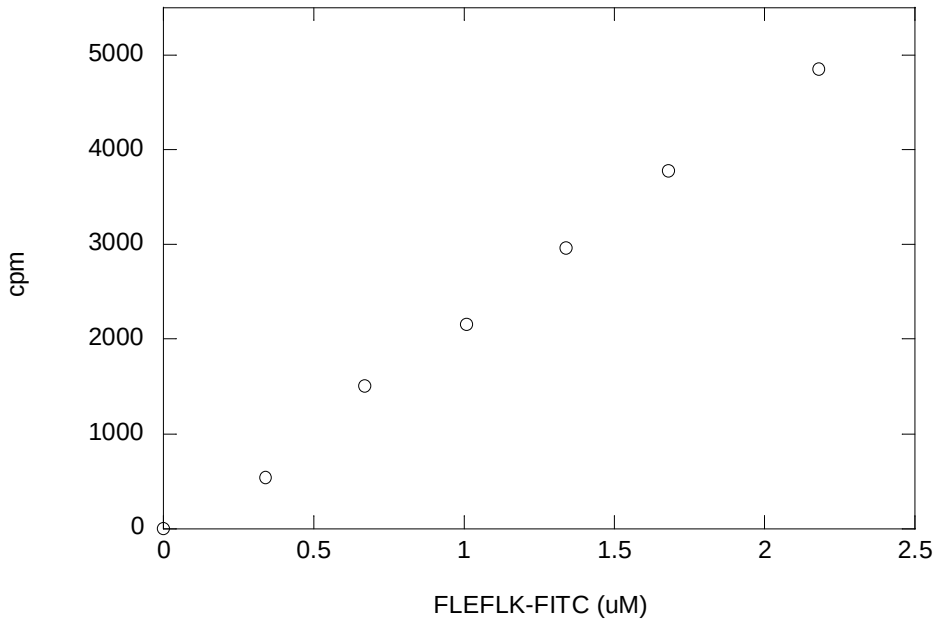

Figure 26: $^{14}CO_2$ incorporation of FLEFLK-FITC in the GGCX assay

Based on the slope of the curve, the calculated kcat/Km value for FLEFLK-FITC was 3.5 fold higher than reported for FLEEL (5068 vs. 1413 $h^{-1}mM^{-1}$) (58). Using the radioactive assay, increasing amounts of acetonitrile inhibit the GGCX activity (Figure 27).

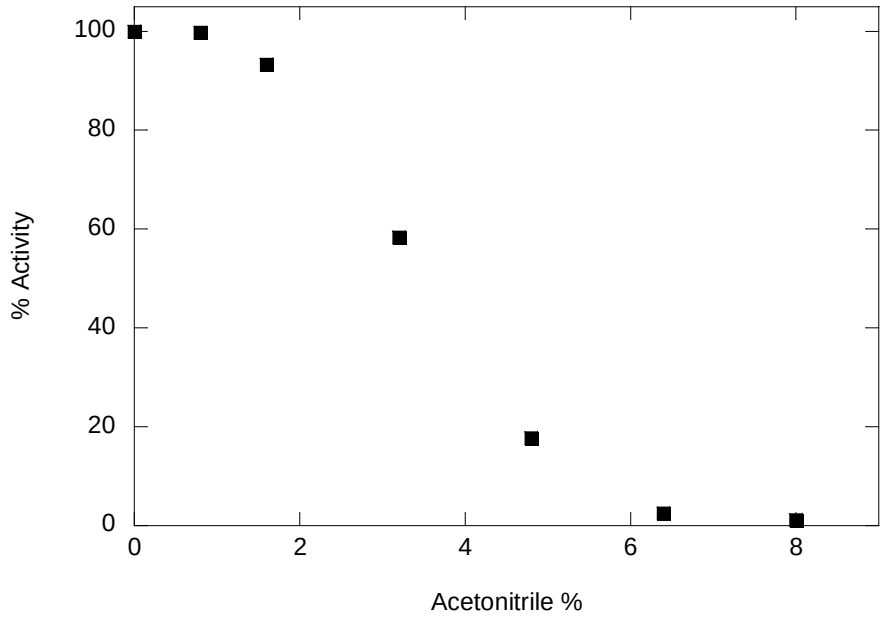

Figure 27: Effect of acetonitrile on GGCX activity.

3.2 Results for aims 2-6

3.2.1 Blood pressure

Systolic blood pressure levels measured in rats at the beginning and the end of each treatment period were unchanged in all groups (Figure 28). No changes were observed in diastolic blood pressure (for group e, CKD from 74 ± 5 mmHg at week 0 to 85 ± 10 mmHg at week 7).

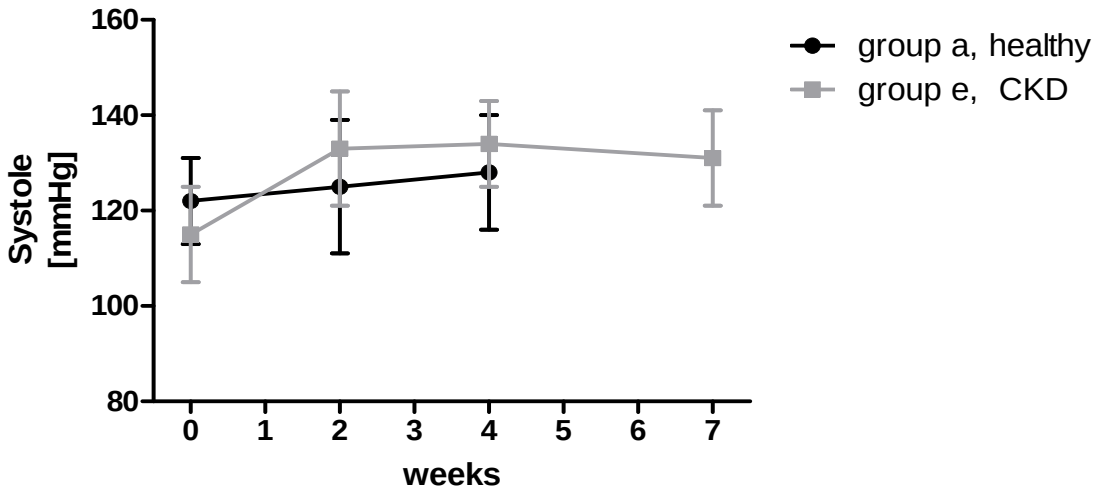

Figure 28: Time course of systolic blood pressure levels in CKD rats compared to healthy controls (group a); increase in CKD group (group e) is not significant.

3.2.2 Biochemistry

After 4 weeks of adenine treatment (group b), we observed a 6-fold increase in serum creatinine (Figure 29 and Table 3) and a 7-fold increase in serum urea (Table 3). Adenine diet combined with low protein diet led to slightly higher creatinine (Figure 29) and phosphate (Figure 30) levels in serum after 4 weeks, compared to adenine diet with normal protein.

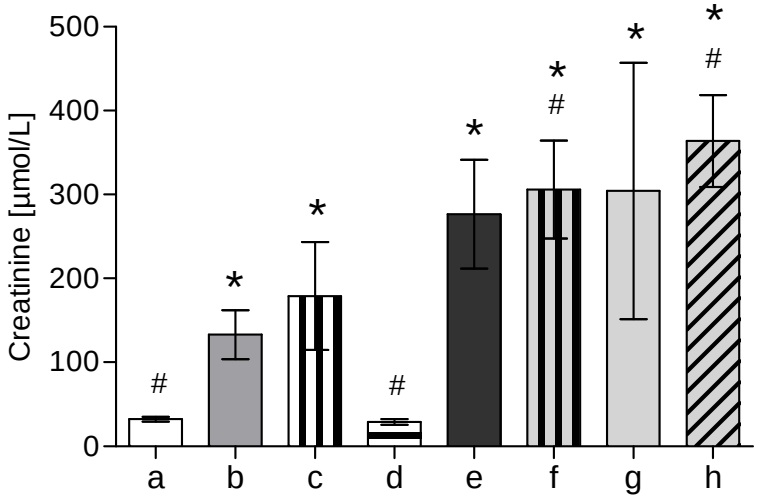

	a	b	c	d	e	f	g	h
Adenine	-	+	+	-	+	+	+	+
Protein [%]	17.35	17.35	17.35	17.35	2.5	2.5	2.5	2.5
K1 [mg/kg]	5	5	5	5	5	5	5	100
K2 [mg/kg]	-	-	100	100	-	100	500	-
Weeks	4	4	4	4	4	4	4	4

Figure 29: Creatinine levels in rat serum after 4 weeks of treatment. Increase was significant in all adenine fed groups.

*: significant to group a) healthy control; #: significant to group b) adenine treatment.

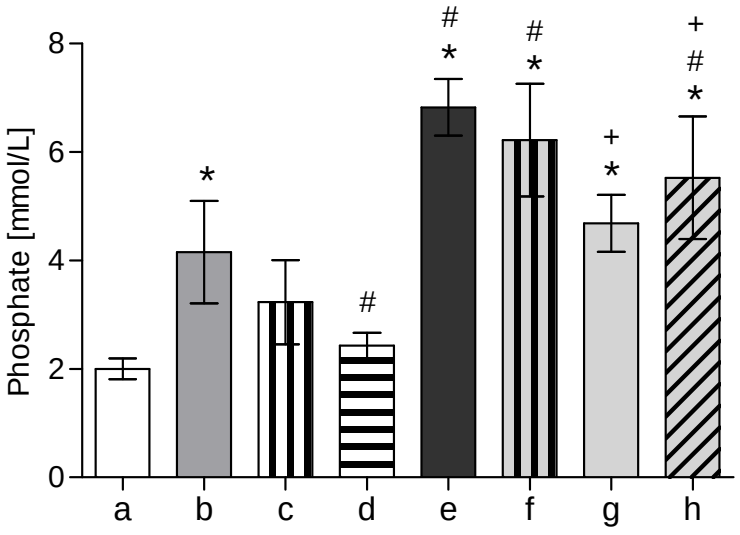

	a	b	c	d	e	f	g	h
Adenine	-	+	+	-	+	+	+	+
Protein [%]	17.35	17.35	17.35	17.35	2.5	2.5	2.5	2.5
K1 [mg/kg]	5	5	5	5	5	5	5	100
K2 [mg/kg]	-	-	100	100	-	100	500	-
Weeks	4	4	4	4	4	4	4	4

Figure 30: Phosphate in rat serum after 4 weeks of treatment. The low protein diet lead to higher levels even after 4 weeks of diet compared to normal protein diet.

*: significant to group a) healthy control; #: significant to group b) adenine; +: significant to group e) adenine with low protein.

After 7 weeks of treatment, serum phosphate levels in the vitamin K_2 high dose group (500 mg/kg + adenine) were significantly lower than in CKD (after 7 weeks of adenine based on low protein, Table 3). Serum calcium was unchanged in all groups at every time point (Table 3).

Table 3: Final biochemical results in rat serum

Serum Group	Urea [mmol/L]	Creatinine [µmol/L]	Calcium [mmol/L]	Phosphate [mmol/L]
a)	6.23 (± 1.67)#	32.40 (± 3.08)#	2.46 (± 0.11)	2.08 (± 0.18)#
b)	29.16 (± 7.16)*	173.60 (± 63.23)*	2.45 (± 0.16)	4.16 (± 0.94)*
c)	32.03 (± 7.36)*	133.17 (± 29.09)*	2.51 (± 0.21)	3.23 (± 0.78)* #
d)	4.09 (± 0.98)#	29.00 (± 3.20)#	2.57 (± 0.07)	2.42 (± 0.24)#
e)	36.37 (± 17.63)*	388.44 (± 115.43)*	2,53 (± 0.30)	6.57 (± 1.79)*
f)	31.30 (± 9.60)*	356.83 (± 92.50)*	2.62 (± 0.18)	6.06 (± 1.15)*
g)	34.42 (± 28.26)*	317.71 (± 93.48)*	2.66 (± 0.40)	5.22 (± 2.02)*
h)	42.81 (± 30.80)*	429.71 (± 120.01)*	2.94 (± 0.57)	6.75 (± 1.75)*

*: significant to group a) healthy control; # significant to group b) CKD 4 weeks

Renal creatinine excretion and GFR (Figure 31) were reduced in all adenine fed groups (Table 4).

Table 4: Final biochemical results in rat 24 h urine

Urine Group	Creatinine [µmol/L]	Protein [mg/dL]	Phosphate [mmol/L]
a)	9964 (± 8889.5)#+	26.71 (± 4.39)	58.79 (± 69.45)
b)	1792.3 (±232.7)*	38.5 (±6.22)	15.44 (± 6.03)
c)	1327.2 (±319.9)*	38.33 (±8.91)	14.33 (± 5.34)
d)	10433.6 (±6612.1)*#+	25 (±2.74)	59.83 (± 38.23)
e)	2367.3 (±488.4)*	40.28 (± 13.77)	21.82 (± 2.96)
f)	1817.4 (±368.5)*	45.33 (±33)	17.92 (± 4.47)
g)	2099.3 (±1001.5)*	29.66 (±8.09)	18.78 (± 12.46)
h)	2222.7 (±585.9)*	37.3 (±11.1)	17.19 (± 3.94)

*: significant to group a) healthy control; # significant to group b) CKD 4 weeks; + significant to group e) CKD 7 weeks

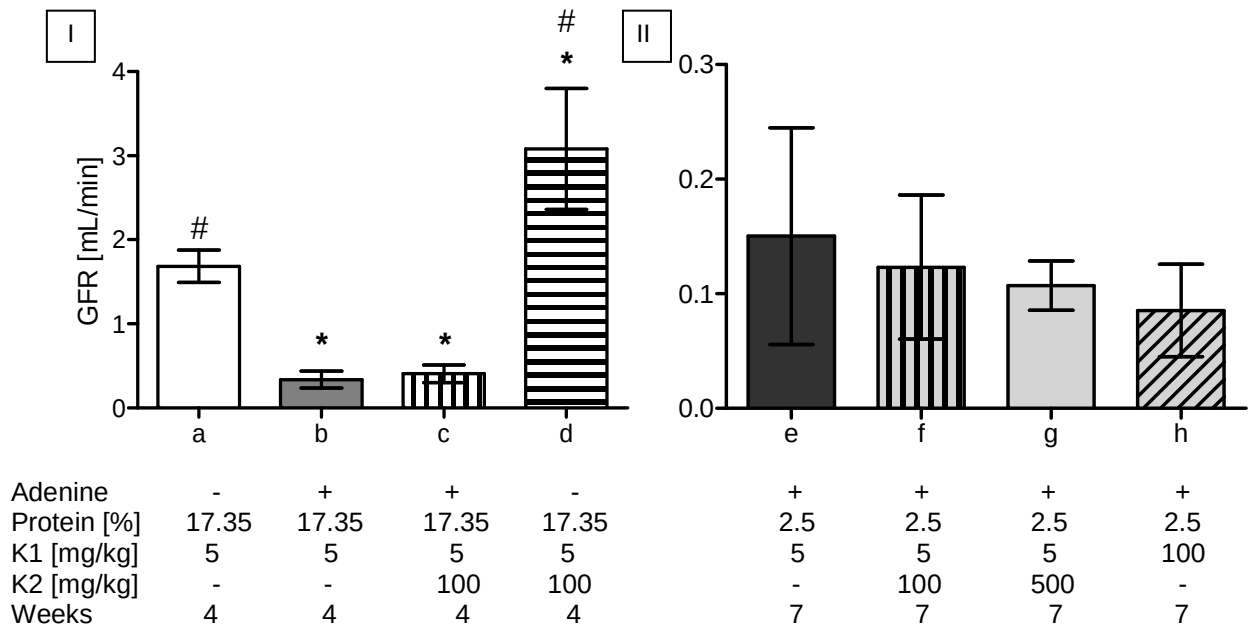

Figure 31: Glomerular Filtration rate (GFR) is reduced in adenine fed rats I) after 4 weeks; II) after 7 weeks of treatment; *: significant to group a) healthy control; #: significant to group b) 4 weeks of adenine.

Significantly higher levels of ucMGP were measured in the 4-week CKD group b (Figure 32 I). After 7 weeks, no significant differences in ucMGP levels were detected (Figure 32 II).

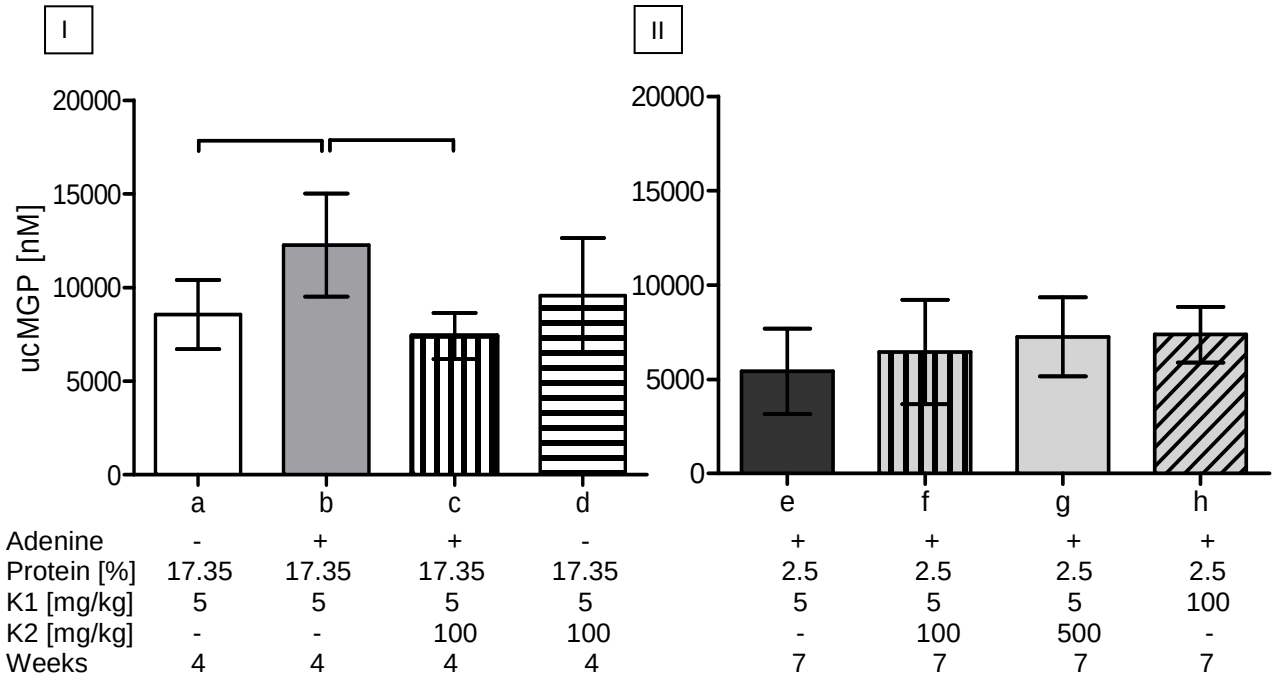

Figure 32: UcMGP measured in rat serum a) after 4 weeks; b) after 7 weeks of treatment. The only significant increase is seen after 4 weeks of adenine diet.

3.2.3 Enzyme acticvities

3.2.3.1 GGCX activity

Compared to group a) (healthy non-CKD controls) GGCX was significantly less active in the uremic groups (b and c) in kidney (Figure 33I) and liver tissue after 4 weeks of adenine treatment (Figure 33III). After 7 weeks of adenine treatment, the activity was even further reduced in kidney tissues (Figure 33II). A high dosage of vitamin K_2 or vitamin K_1 increased GGCX activity in kidney tissue after 7 weeks back to baseline values and was even higher in liver tissue (Figures 33II, 33IV). Reduced GGCX activity was also found in aortic tissue after 7 weeks (Figure 34) and exceeded values from healthy and untreated animals (160.7 ± 54.71 nmol/g/min) by high intake of either vitamin K_1 or K_2. No difference due to vitamin K treatment was detected in aortic tissue after 4 weeks of adenine diet.

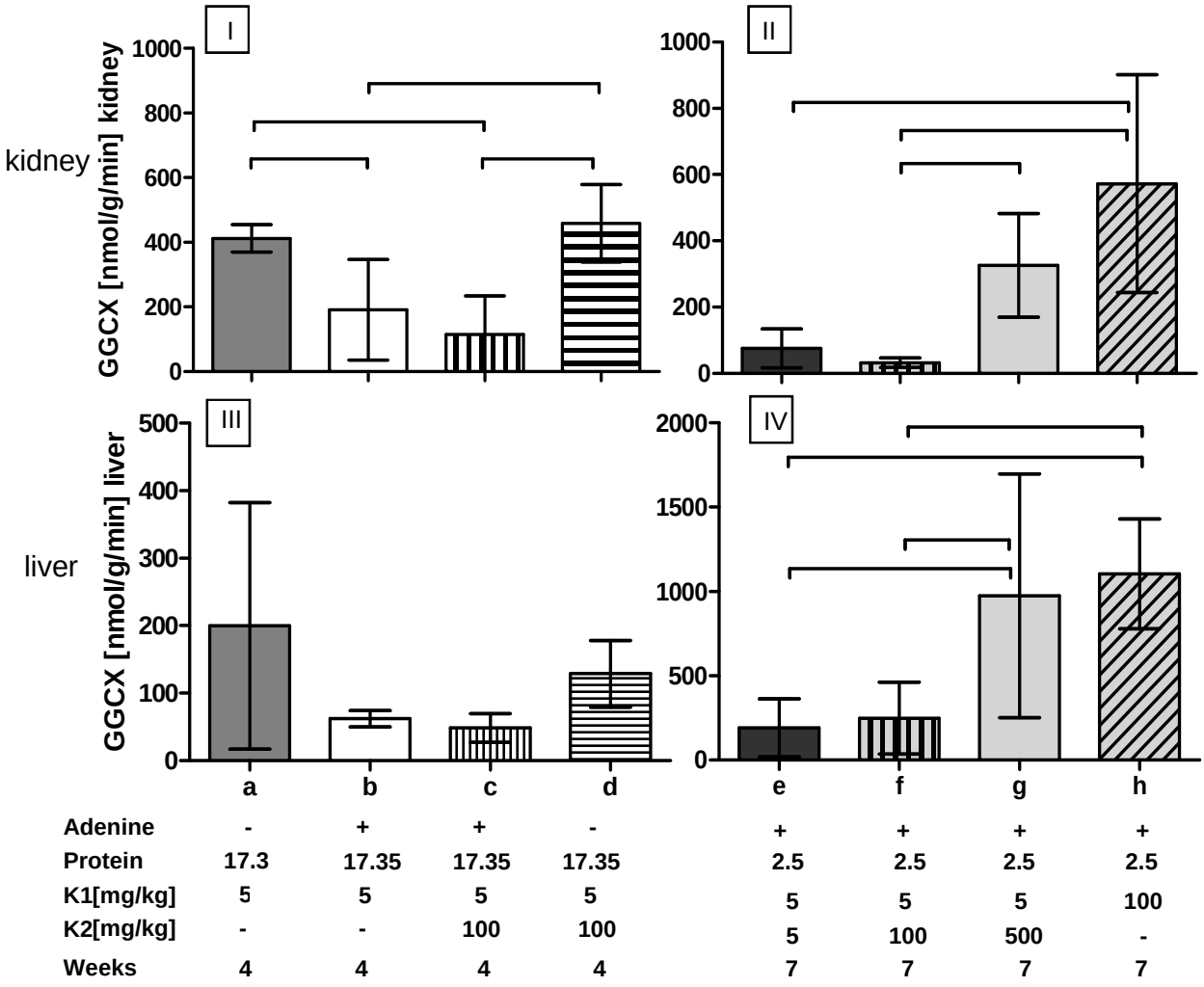

Figure 33: GGCX activity (mean ± SD) in kidneys [I after 4 weeks, II after 7 weeks] and liver [III after 4 weeks, IV after 7 weeks of adenine diet].

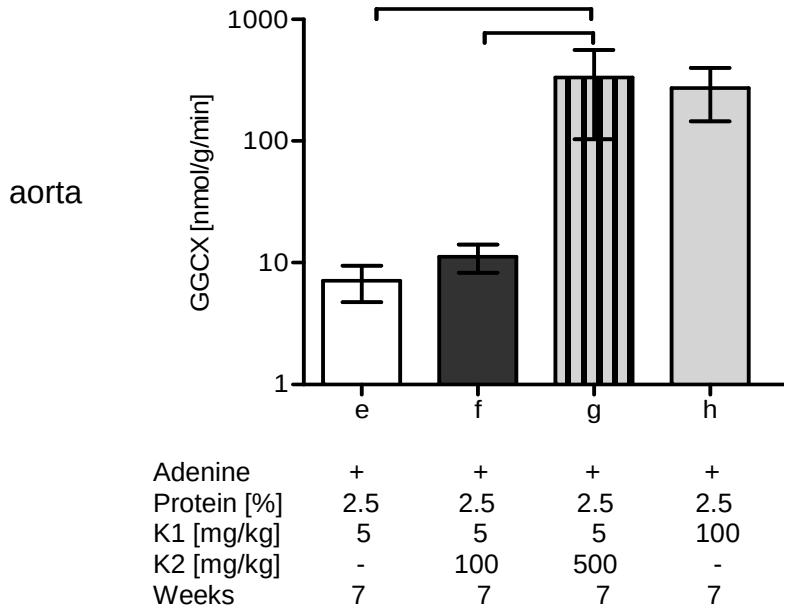

Figure 34: GGCX activity in aortas after 7 weeks (mean ± SD) of adenine diet.

Urea is supposed to modify molecular enzyme activities by carbamylation of lysine residues. *In vitro* co-incubation of 50 mM urea with microsomes from healthy animals did not lead to a reduction of GGCX activity (Figure 35).

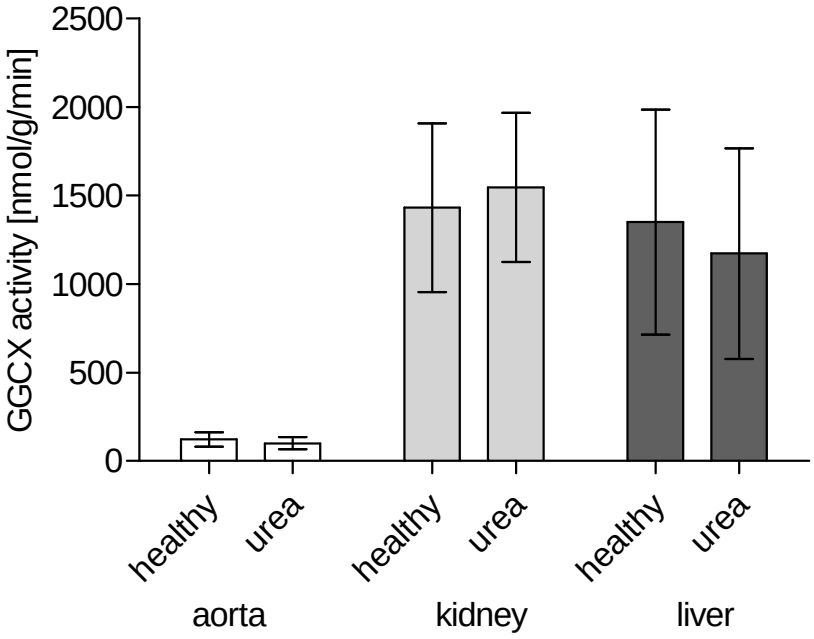

Figure 35: *In vitro* incubation with 50 mM urea prior GGCX activity assay, microsomes were isolated from healthy aorta, kidney and liver. No influence was seen by supplementation of urea to the carboxylation mixture.

Also no changes in enzyme activity were found after *in vitro* incubation with p-cresol or indoxylsulfate (data not shown).

3.2.3.2 VKOR activity

To determine VKOR activity, the measurement of vitamin K in rp-HPLC was established, first. Vitamin K_1 was eluted in the rp-HPLC setup at 8.7 min (Figure 36) with a detection limit < 0.5 ng/ml. Between 0.5 - 50 ng/ml the correlation between the area under the curve and the injected vitamin K_1 concentration was linear with $R^2 = 0.99$ (Figure 37).

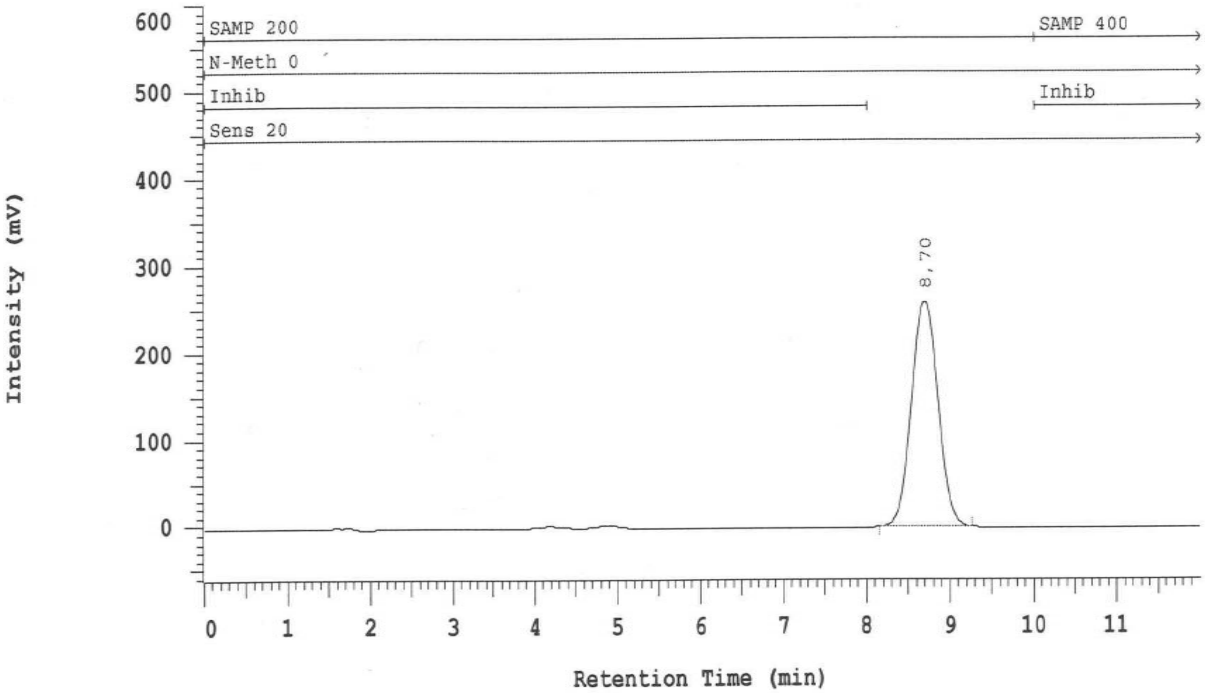

Figure 36: Vitamin K_1 peak at 8.7 min in rp-HPLC setup; Amount of Vitamin K_1: 50 ng/mL, Injection volume 50 µl.

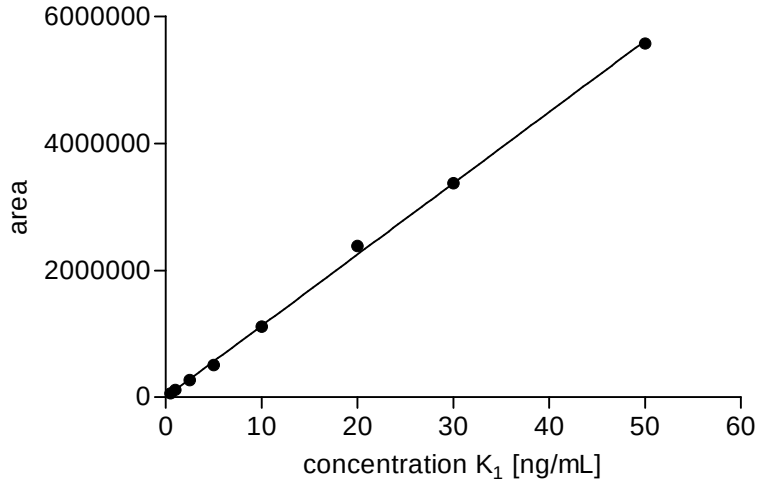

Figure 37: Linear correlation of Vitamin K_1 and area under the curve in rp-HPLC setup; used concentrations were: 0.5, 1, 2.5, 5, 10, 20, 30 50 ng/ml.

K_1>O was eluted at 6.3 min with a detection limit < 10 ng/ml. Vitamin K_1>O was stable for at least 6 months at -20°C (99% purity) measured by rp-HPLC. VKOR activity did not differ significantly between the groups and ranged between 0.6 and 2.6 µmol/g/min in kidney tissue and from 0.5 and 7.1 µmol/g/min in liver tissue (Table 5).

Table 5: VKOR activity in rat kidney and liver (mean ± SD)

	VKOR [µmol/g/min]	
group	**kidney**	**liver**
a)	1.43 (± 0.82)	2.05 (± 1.98)
b)	1.52 (± 0.40)	6.91 (± 9.97)
c)	1.28 (± 0.78)	4.81 (± 8.39)
d)	2.10 (± 0.72)	7.14 (± 10.18)
e)	0.57 (± 0.11)	2.01 (± 0.25)
f)	2.55 (± 0.99)	0.5 (± 0.32)
g)	1.66 (± 0.84)	2.5 (± 2.63)
h)	2.09 (± 0.74)	1.77 (± 1.40)

3.2.3.3 DT–diaphorase activity

DT-diaphorase activity was significantly higher in kidneys and liver in the 4-week CKD model (group b) (3.6 fold and 2.7 fold, respectively, Figure 38I and 38III). After 7 weeks of

additional vitamin K_1 or K_2 treatment in the severe calcification groups (groups g, h), DT-diaphorase activity was reduced to baseline values in the liver (Figure 38IV).

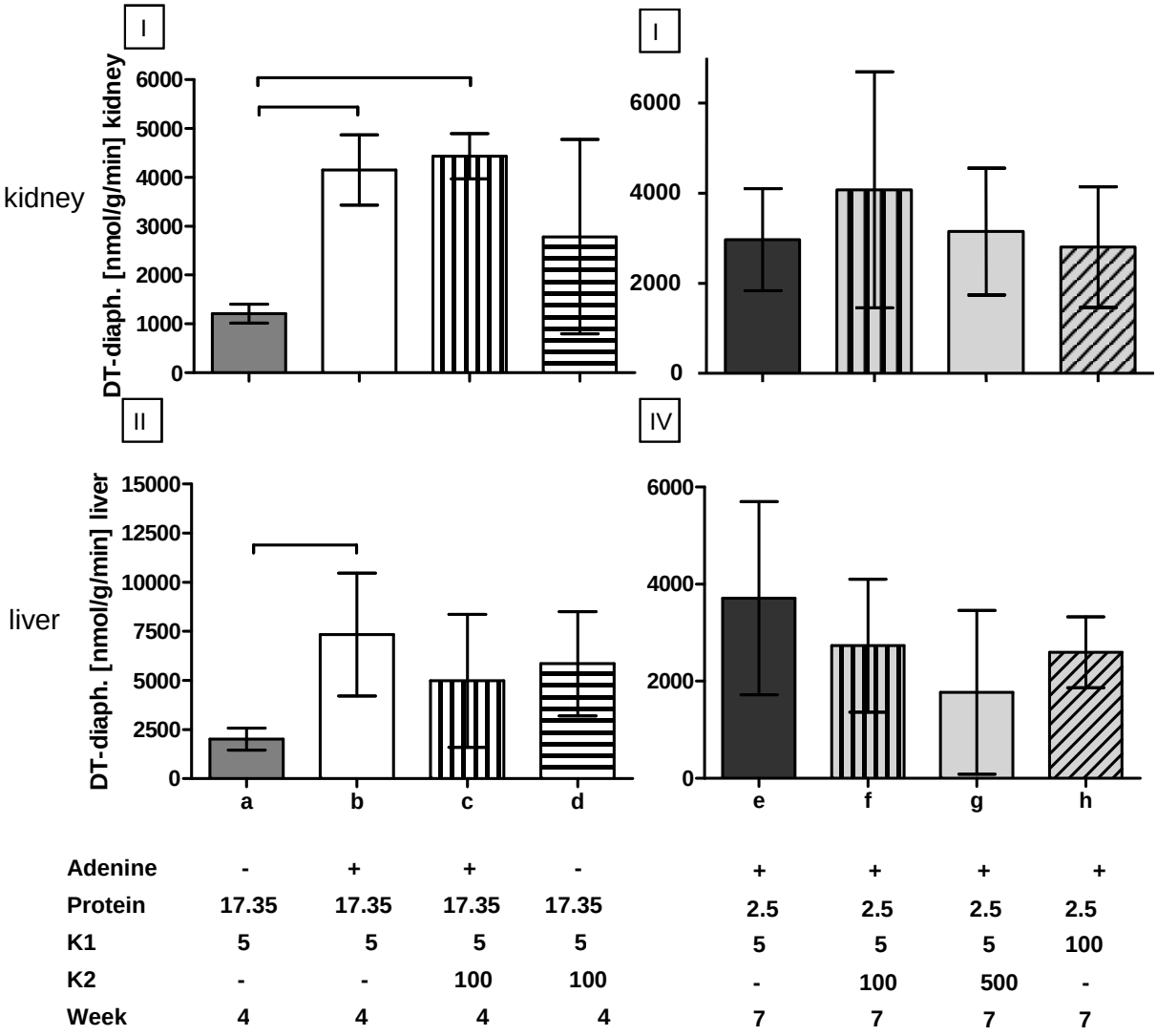

Figure 38: DT-diaphorase activity (mean ± SD) in kidneys [I after 4 weeks, II after 7 weeks of adenine diet] and liver [III after 4 weeks, IV after 7 weeks of adenine diet].

3.2.4 Calcium measurements

After 4 weeks of treatment, the aortic calcium content was significantly increased only in the adenine groups b) compared to healthy controls (groups a, d) (Figure 39I). After 7 weeks of adenine treatment, the aortic calcium content was significantly higher than in healthy controls (groups a and d) and after 4 weeks of adenine (group b) (Figure 39II). Aortic calcium deposition was reduced in the adenine plus high vitamin K groups (g, h) compared to CKD controls (group e) (Figure 39II). The cardiac calcium content increased after 7 weeks of

adenine treatment (group e CKD) and high dose vitamin K treatment significantly reduced cardiac calcium content (groups g, h) as compared to CKD (Figure 39IV). Kidney calcium content was significantly elevated after 4 weeks of adenine treatment without vitamin K substitution (group b CKD) as well as after 7 weeks with low dose vitamin K treatment (group f; 100 mg/kg, Figure 39V and 39VI). Kidney calcium content was significantly reduced by high dose vitamin K_2 (group g) supplementation or K_1 (group f) (Figure 39VI). In pulmonary tissue, no significant changes in the calcium content were detected.

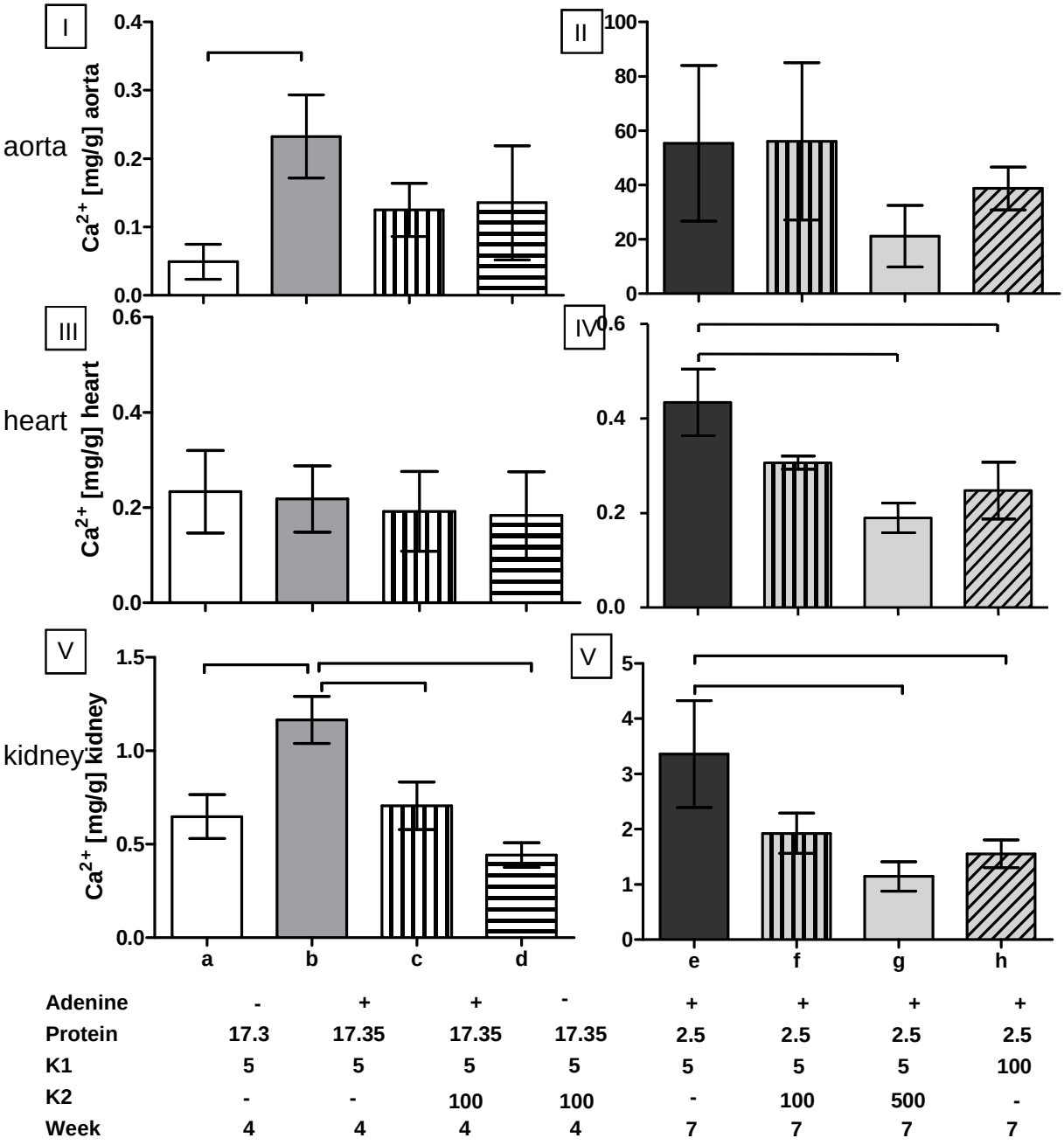

Figure 39: Calcium content in tissues (mean ± SD); Calcium content in aorta [I after 4 weeks; II after 7 weeks], heart [III after 4 weeks; IV after 7 weeks] and kidney [V after 4 weeks; V after 7 weeks].

3.2.5 Histochemistry

Quantification of calcified areas by *von Kossa* staining confirmed the results obtained by chemical calcium assessment, but none of the differences reached statistical significance. Overt vascular calcification was present after 7 weeks of adenine, and in *von Kossa*-stained

aortic specimens, the calcified area increased on average 7.7-fold compared to the status at 4 weeks (Figures 40).

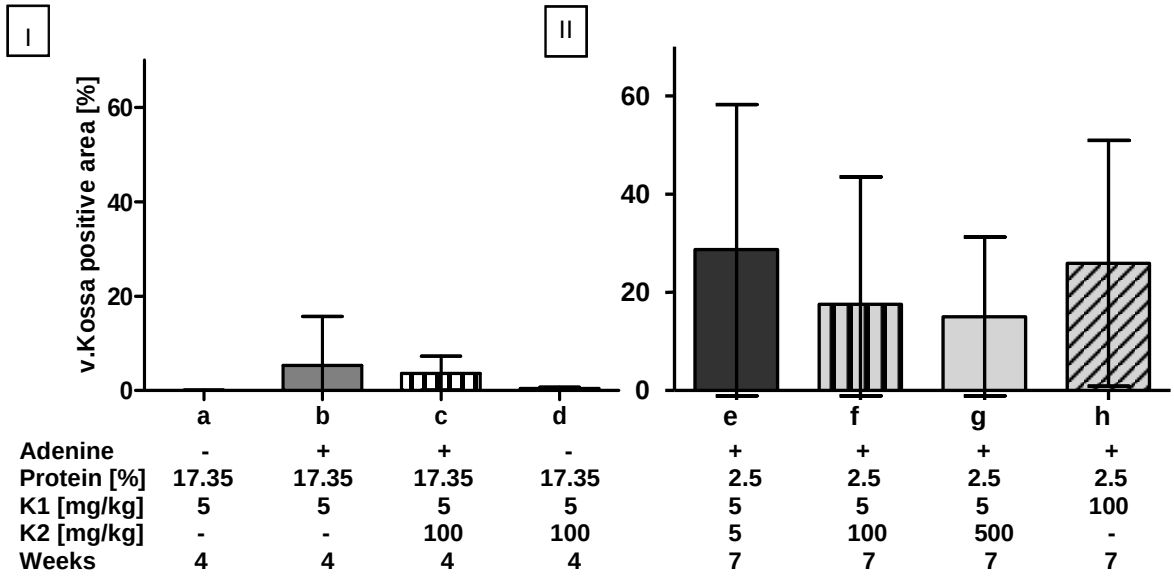

Figure 40: Quantification of *von Kossa* staining in rat aortic tissue (mean ± SD) after adenine diet.

Vascular media calcification co-localized with positive staining for ucMGP (Figure 41). Healthy animals did not show aortic calcification or positive staining for ucMGP by histology.

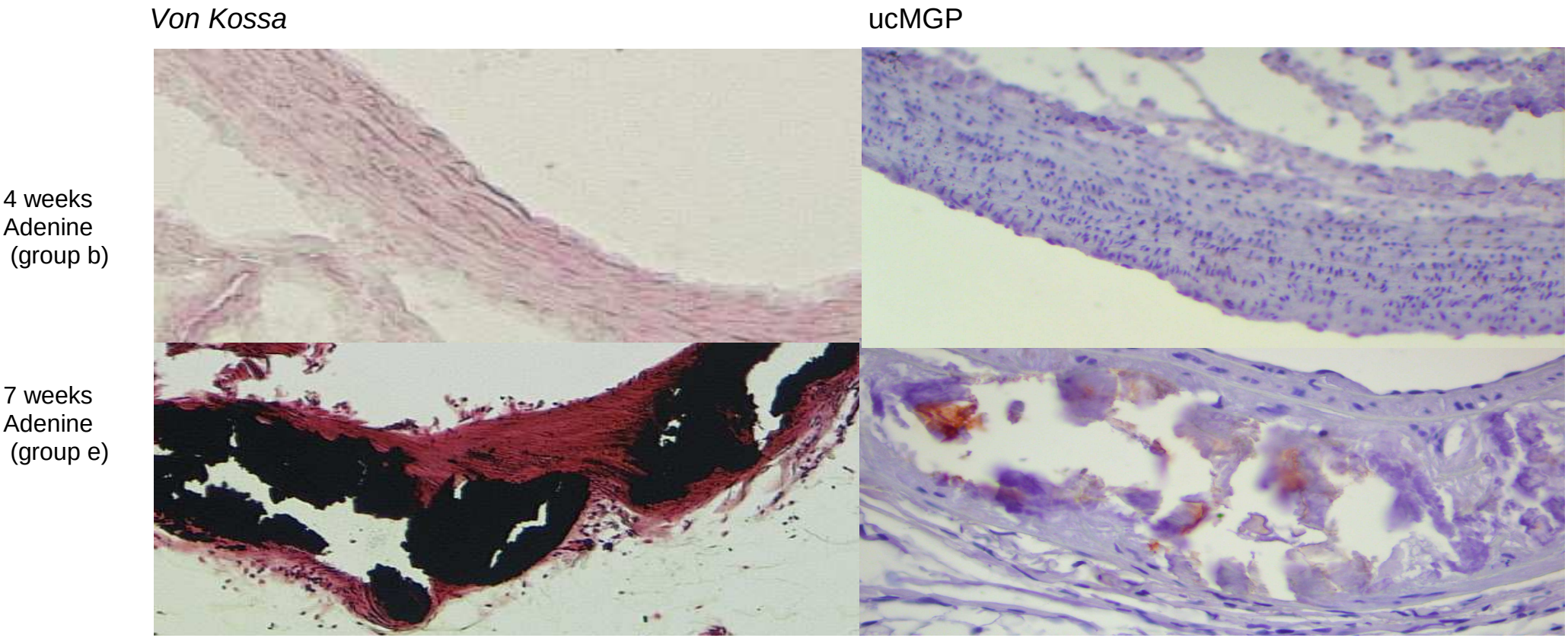

Figure 41: *Von Kossa* and ucMGP staining in rat aortic tissue (100 x): early calcification after 4 weeks of adenine (group b) and overt calcification after 7 weeks of adenine diet (group e). UcMGP positive staining (red colour) occurs at calcification sites (group e).

3.2.6 GGCX gene expression

The GGCX gene expression assessed by RT-PCR in liver tissue was similar in all groups after 4 weeks of adenine diet (Figure 42).

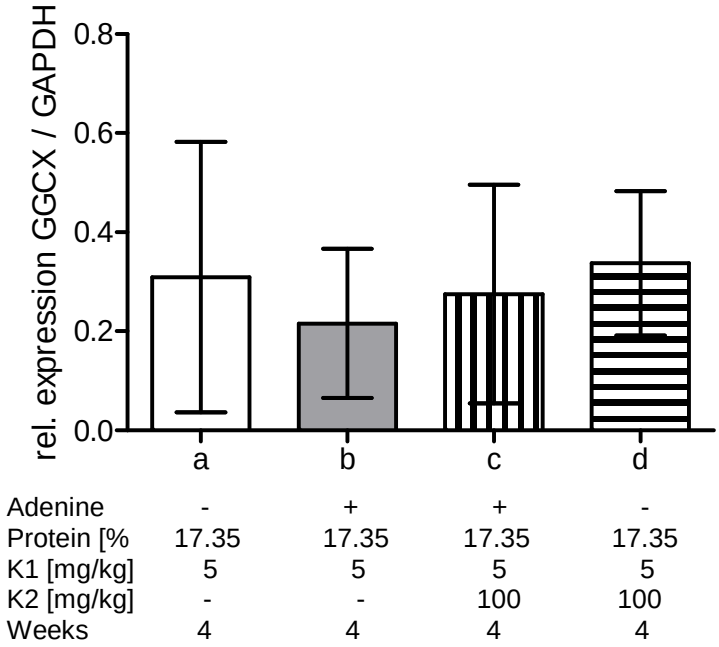

Figure 42: Relative expression of GGCX in rat liver. No changes were seen after 4 weeks of treatment.

3.3 Results for aim 7

In order to assess the role of Gas6 protein in vascular calcification processes, *in vitro* and *in vivo* models were used.

3.3.1 VSMC

In vitro, VSMC of WT and $Gas^{-/-}$ mice were challenged by supplementation of calcium and phosphate or warfarin on top. Using calcification medium the deposition of calcium in VSMC increased over time and after 120 h calcium content was 4-fold increased in WT and only 1.4 times in $Gas6^{-/-}$ (Figure 43a); however this difference was not significant. After 168 h of incubation the calcium load of VSMC increased further with no significant difference between VSMC from $Gas^{-/-}$ and from WT mice. (Figure 43a).

Warfarin treatment led to a significant increase of calcium deposition in WT cells after 120 h (WT t_o 1.40% ± 0.77%; WT t_{120}: 5.52% ± 5.17%). Again, there was no significant difference in calcium load between $Gas6^{-/-}$ and WT-derived VSMC (data not shown).

The rate of VSMC apoptosis in calcification medium ± warfarin supplementation increased over the time course; however the rate of apoptosis was not increased in $Gas6^{-/-}$ compared to WT VSMC (Figures 43b and 44).

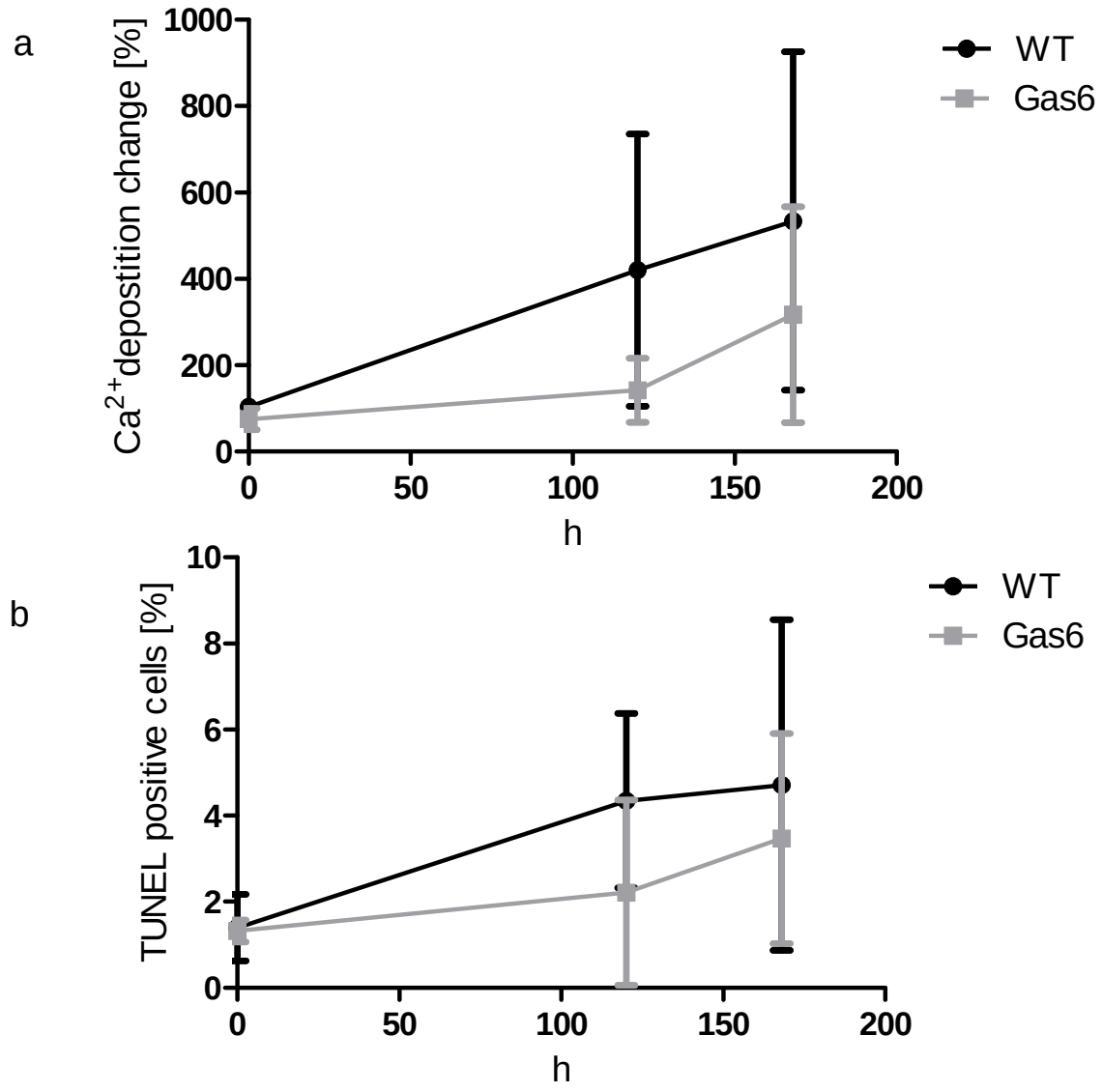

Figure 43: a) Ca^{2+} deposition in VSMC derived from $Gas6^{-/-}$ and WT mice after 168 hours (h) of exposure to phosphate and calcium enriched cell culture medium. b) TUNEL positive VSMC of $Gas6^{-/-}$ and WT mice after exposure to phosphate and calcium enriched cell culture medium.

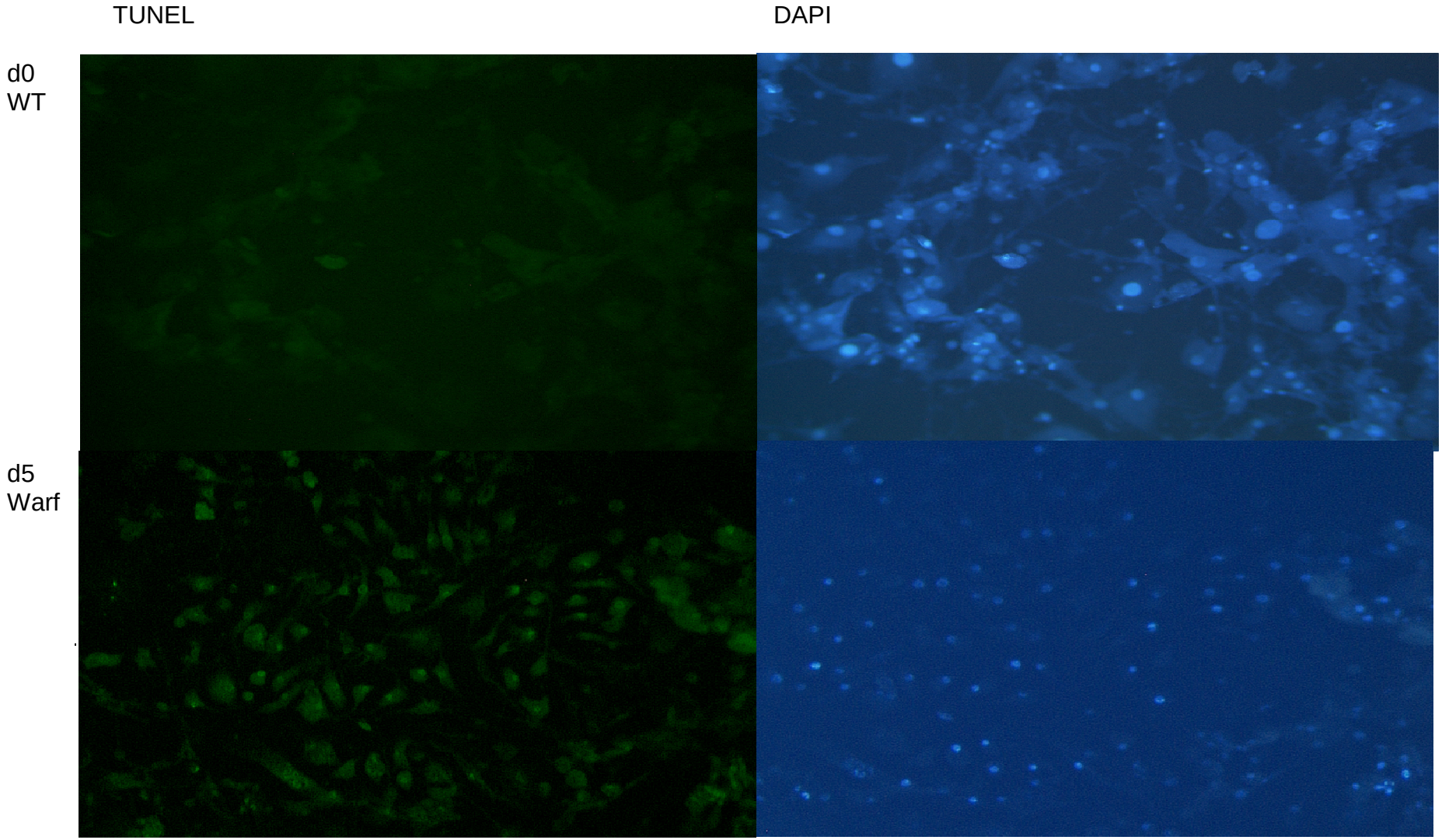

Figure 44: TUNEL and DAPI staining in VSMC from WT mice after 0 and 5 days of calcification medium plus warfarin

3.3.2 In vivo calcification models

In vivo animals of Gas6$^{-/-}$ were compared to WT mice.

All mice survived warfarin treatment without weight loss. In both strains 16% died after UniNx surgery. Somehow in the EC group all WT mice survived the surgical protocol. But only 40% of Gas6$^{-/-}$ mice survived to the end of the experiment (Figure 45).

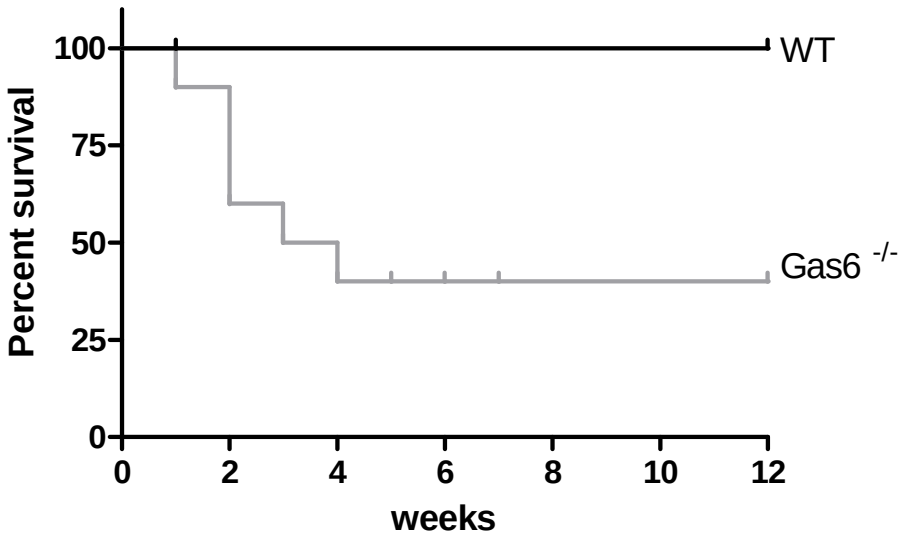

Figure 45: Kaplan-Meier curve after electrocautery surgery in WT and Gas6$^{-/-}$ mice.

3.3.2.1 Genotyping

Only DNA isolated from snap frozen WT and not Gas6$^{-/-}$ mice showed a distinct band at 500 bp (Figure 46).

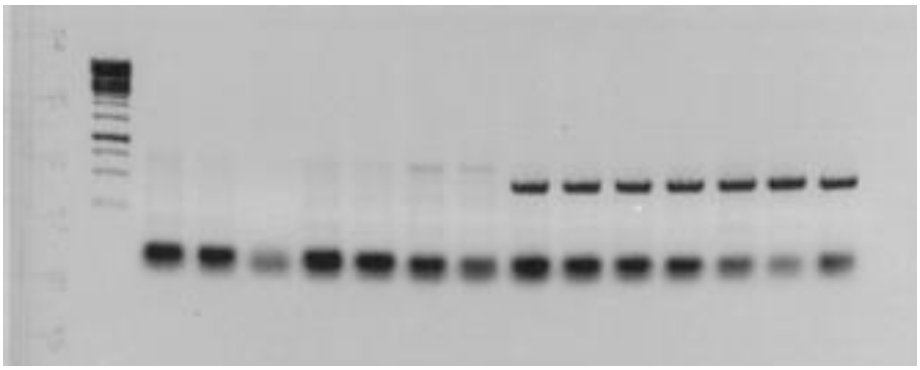

Figure 46: DNA gel for Gas6 gene; line 1: page ruler DNA ladder with a bright reference band at 1000 bp; lines 2-8 DNA isolated from Gas6$^{-/-}$; lines 9-15 DNA from WT mice,

3.3.2.2 Biochemistry

In healthy, untreated mice at the age of 8 weeks, alkaline phosphatase serum levels were lower in Gas6$^{-/-}$ than in WT mice (Table 6). Serum protein levels were higher in older mice and significantly lower in old Gas6$^{-/-}$ compared to old WT mice (Table 6).

Table 6: Baseline biochemical characteristics of healthy WT and Gas6$^{-/-}$ mice at different ages (Mean ± SD).

	8-12 weeks old, healthy		*34-36 weeks old, healthy*	
Parameter	**C57BL\6**	**Gas6$^{-/-}$**	**C57BL\6**	**Gas6$^{-/-}$**
Body weight [g]	20.2 ± 0.7	18.6 ± 1.6	30.06 ± 6.36	26.41 ± 4.19
haematology				
Urea [mmol/l]	13.26 ± 0.25	11.55 ± 1.92	6.65 ± 0.97	6.06 ± 0.91
Creatinine [µmol/l]	20.67 ± 0.58	24.50 ± 8.60	18.00 ± 5.89	26.25 ± 16.73
Calcium [mmol/l]	2.56 ± 0.09	2.23 ± 0.08	2.39 ± 0.13	2.39 ± 0.09
Phosphate [mmol/l]	2.46 ± 0.11	3.05 ± 0.82	2.88 ± 0.45	2.85 ± 0.34
Protein [g/dl]	5.00 ± 0.00	4.90 ± 0.15	6.00 ± 0.42	5.50 ± 0.26 *
Alkal. phosphatase [U/l]	332.67 ± 8.62	255.63 ± 34.55 *	142 ± 53.52	207.33 ± 69.45

* $p < 0.05$; to corresponding WT group

Serum protein levels increased significantly in both mouse strains after warfarin diet (Table 7). Serum creatinine levels increased after UniNx surgery compared to healthy animals in Gas6$^{-/-}$ and WT mice (+ 46% in WT and + 24% in Gas6$^{-/-}$, respectively) (Table 7). Serum calcium, phosphate and creatinine levels were significantly increased in WT and Gas6$^{-/-}$ mice after electrocautery compared to the corresponding healthy controls (Table 7).

Table 7: Biochemical heamatology and 24 h urine characteristics of wildtype and Gas6$^{-/-}$ mice after different treatments

Parameter	**C57BL\6**			**Gas6$^{-/-}$**		
model	**Warfarin**	**UniNx**	**Electrocautery**	**Warfarin**	**UniNx**	**Electrocautery**
body weight [g]	22.95 ± 1.57	24.42 ± 2.17 ‡	22.35 ± 1.64	18.90 ± 1.66	19.06 ± 3.19 *	18.45± 3.05
haematology						
Urea [mmol/l]	6.27 ± 0.63	10.26 ± 3.58	10.58 ± 1.62	6.43 ± 1.29	10.25 ± 2.56	17.1 ± 11.58
Creatinine [µmol/l]	22.00 ± 1.67	25.11 ± 2.37	30.28 ± 3.74	23.67 ± 6.32	29.91 ± 14.12	30.29 ± 3.86
Calcium [mmol/l]	2.58 ± 0.09	2.50 ± 0.12	2.73 ± 0.14 ‡	2.67 ± 0.17	2.50 ± 0.12	2.84 ± 0.27 ‡
Phosphate [mmol/l]	2.84 ± 0.22	2.78 ± 0.29	2.90 ± 0.30	3.68 ± 0.60	3.47 ± 0.89	3.91 ± 0.68
Protein [g/dl]	6.58 ± 0.38 ‡	5.74 ± 0.74	5.47 ± 0.49	6.03 ± 0.32 ‡	5.70 ± 0.31 ‡	5.41 ± 0.55
Alkal. phosphatase [U/l]	205 ± 26.59 ‡	173.11 ± 64.73 ‡	166.33 ± 35.90 ‡	227.67 ± 45.87	201.18 ± 63.97	187.00 ± 74.08
24h urine						
GFR [µl/min]	76.88 ± 36.88	55.17 ± 32.44	41.71 ± 21.31	56.63 ± 32.83	41.65 ± 28.06	40.38 ± 13.00
Protein [mg/dl]	25.88 ± 17.23	12.83 ± 4.58 ‡	6.66 ± 1.86 ‡	14.00 ± 4.93	9.50 ± 5.99 ‡	17.67 ± 4.16
Creatinine [µmol/l]	2071 ± 2005	3853 ± 2520	3062 ± 1133	4283 ± 3853	2175 ± 667	914 ± 179

* $p < 0.05$; to corresponding WT group; ‡ $p < 0.05$ to healthy control group

3.3.2.3. Calcium measurements

As ageing could be related to vascular pathology, older mice (at the age of 34 - 36 weeks) were tested for a possible different development of spontaneous vascular calcification. Calcium content was not significantly different in both old Gas6$^{-/-}$ and old WT mice (Figure 47). Von Kossa staining revealed only minor calcifications in both groups without significant differences (Figure 48).

Warfarin administration was used to induce calcification by blocking the posttranslational activation of MGP and potentially Gas6. After warfarin diet, no significant differences in soft tissue calcification between WT and Gas6$^{-/-}$ mice were detected (Figure 47a), except for a reduced cardiac calcium content in Gas$^{-/-}$ mice after 8 weeks of warfarin (Figure 47b).

UniNx (plus high phosphate diet) was used to initiate kidney damage. Spotty calcifications were present in the aorta (Figure 49a) and in cardiac tissue, however without obvious differences between Gas6$^{-/-}$ and WT mice. Within the heart calcifications were mainly located at the valves (Figure 49b). The most prominent calcification was found in kidney tissues in both strains, spreading throughout all structures with accumulation at the renal cortex (Figure 49c). Again, there was no significant difference between the models with respect to tissue calcium content (Figure 47c).

Electrocautery of the contralateral kidney was used in addition to UniNx (plus high phosphate diet) to further increase the extent of kidney damage. Calcium content in aortas and hearts of Gas6$^{-/-}$ mice was slightly higher than in WT, however without a significant difference (Figure 47). Calcification spots were found in a similar pattern than after UniNx in all kidney structures in both, WT and Gas6$^{-/-}$ mice.

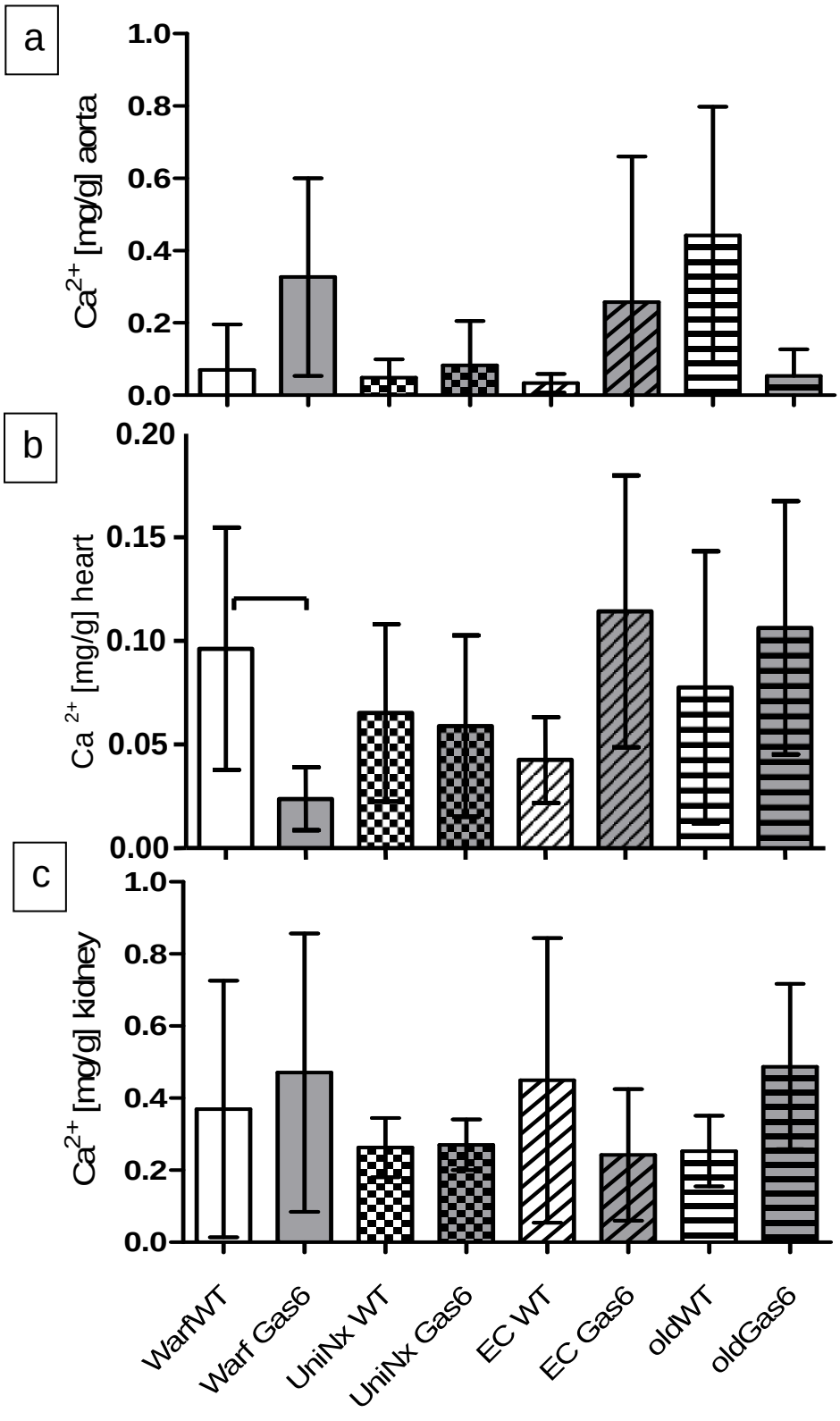

Figure 47: Ca^{2+} content in soft tissues after warfarin diet, UniNx, EC or in healthy aging WT (C57BL/6) and $Gas6^{-/-}$ mice. a) aorta, b) heart, c) kidney. UniNx (Uninephrectomy), EC (Electrocautery).

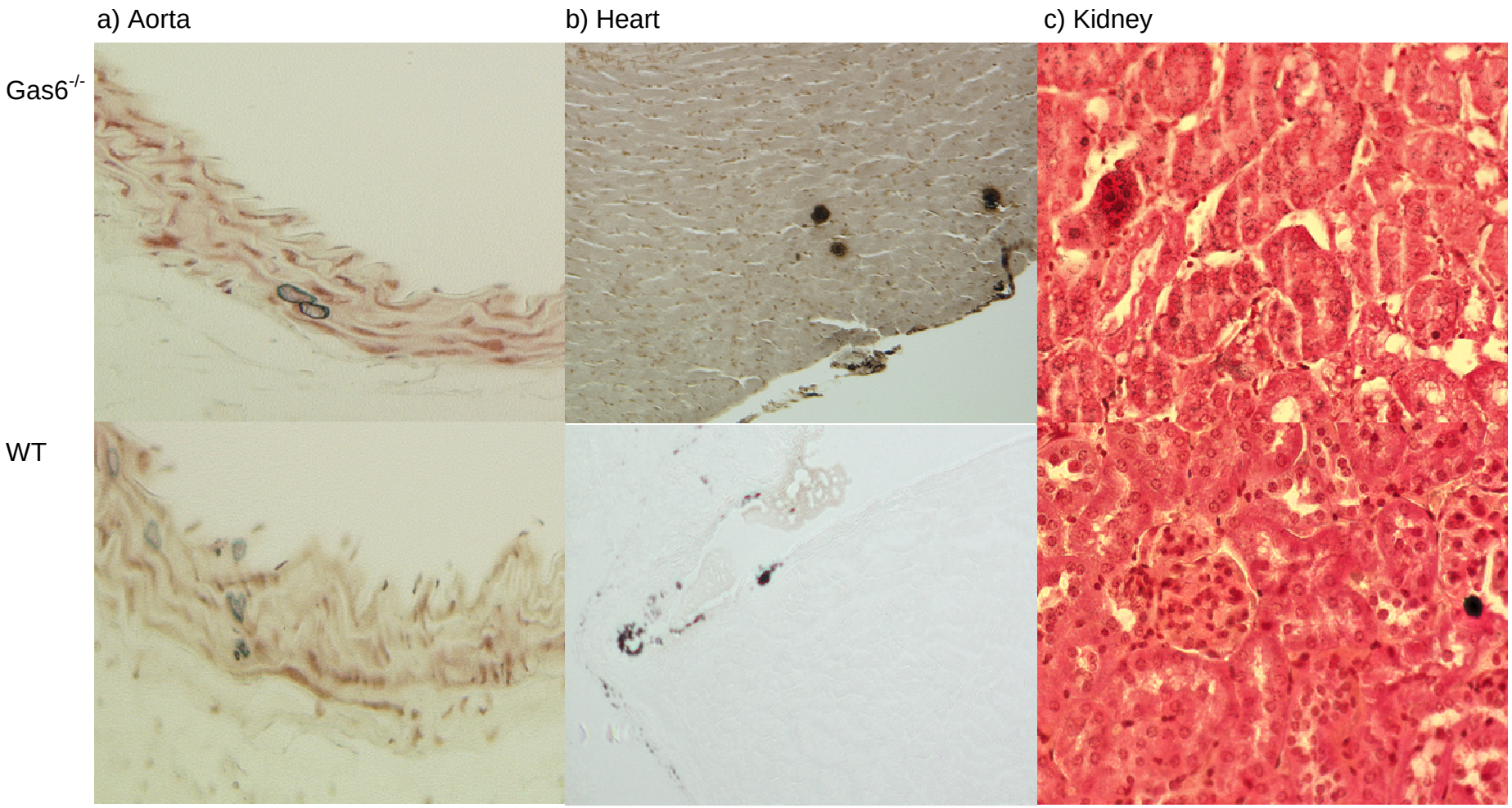

Figure 48: *Von Kossa* staining of aorta, heart and kidney in old WT compared to $Gas6^{-/-}$ mice (100 x).

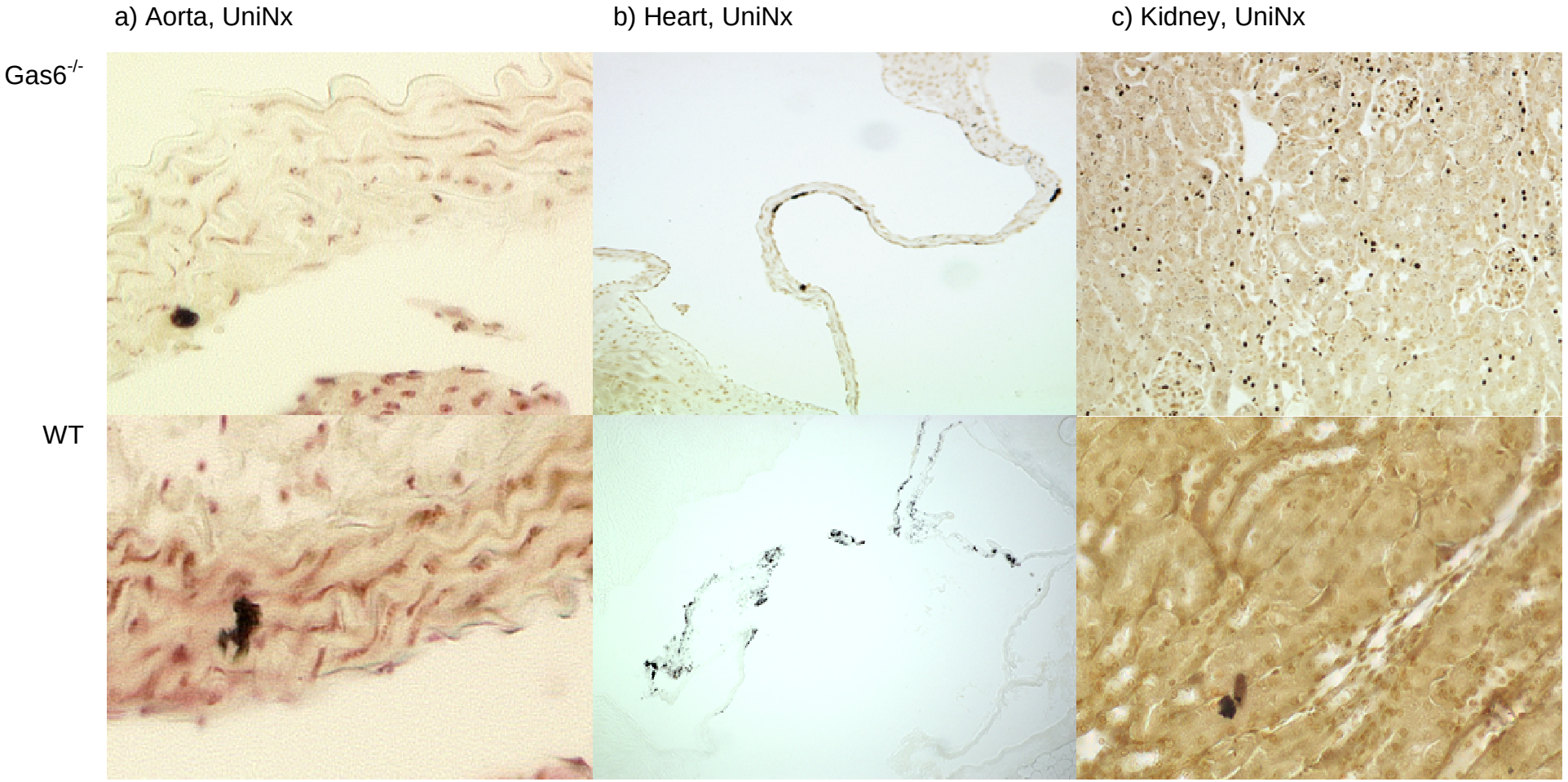

Figure 49: *Von Kossa* staining of aorta, heart and kidney after uninephrectomy in WT compared to $Gas6^{-/-}$ mice (100 x).

3.3.2.4 Echocardiography

The cardiac function of healthy young and ageing, warfarin treated, uninephrectomized and electrocoauterized mice was investigated. Echocardiography revealed a higher LV mass in healthy Gas6$^{-/-}$ compared to healthy WT mice at the age of 8 weeks (Table 8). After UniNx, EF in was significantly higher in Gas6$^{-/-}$ compared to WT (Table 9). UniNx and EC caused cardiac functional changes seen by decreased EF and SV in WT (Table 9). In all other groups, no significant differences were observed.

Table 8: Functional characteristics of healthy WT and Gas6$^{-/-}$ mice at different age

	8-12 weeks old, healthy		*34-36 weeks old, healthy*	
parameter	**C57BL\6**	**Gas6-/-**	**C57BL\6**	**Gas6-/-**
Echocardiography				
Left ventricular (LV) mass [mg]	50.82 ± 11.39	73.60 ± 9.72 *	98.55 ± 15.20	80.81 ± 29.50
Stroke volume (SV) [µl]	23.90 ± 9.05	20.30 ± 6.34	23.61 ± 6.23	19.77 ± 4.3
Ejection Fraction (EF) [%]	54.33 ± 11.49	45.64 ± 7.76	40.13 ± 9.65	41.50 ± 10.98
VACC [mm/ms]	2.09 ± 0.98	2.06 ± 1.15	2.13 ± 1.52	1.72 ± 0.72

(Mean ± SD); * significant to corresponding WT control group

Table 9: Functional characteristics of WT and Gas6$^{-/-}$ mice after different treatments

Parameter	**C57BL\6**			**Gas6-/-**		
model	**Warfarin**	**UniNx**	**Electrocautery**	**Warfarin**	**UniNx**	**Electrocautery**
Echocardiography						
Left ventricular (LV) mass [mg]	79.03 ± 22.00	60.67 ± 14.63	59.10 ± 11.80	69.21 ± 14.74	74.15 ± 28.46	61.36 ± 16.58
Stroke volume (SV) [µl]	22.00 ± 5.96	13.36 ± 2.68	10.44 ± 2.79	20.55 ± 4.33	24.37 ± 8.90	10.16 ± 6.19
Ejection Fraction (EF) [%]	46.60 ± 11.55	33.29 ± 13.79	33.75 ± 7.38	44.84 ± 2.66	58.43 ± 21.30*	38.36 ± 17.83
VACC [mm/ms]	1.97 ± 0.71	2.69 ± 1.01	1.78 ± 0.46	2.26 ± 2.14	3.03 ± 1.38	1.98 ± 0.37

(Mean ± SD), * significant to corresponding WT control group

3.3.2.5 TUNEL assay

To test for apoptosis the TUNEL assay was used. In all tested *in vivo* models (young healthy, senescent, warfarin, UniNx, EC), we could not observe different levels of apoptosis in aortas between the different groups (data not shown).

3.3.2.6 Collagen staining

As calcium content in WT mice after warfarin diet was higher only in cardiac tissue, we tested for differences in the associated cardiac collagen content by sirius red staining. The size of collagen positive areas in cardiac tissues was equal in warfarin treated mice in Gas6$^{-/-}$ and WT mice (Figure 50).

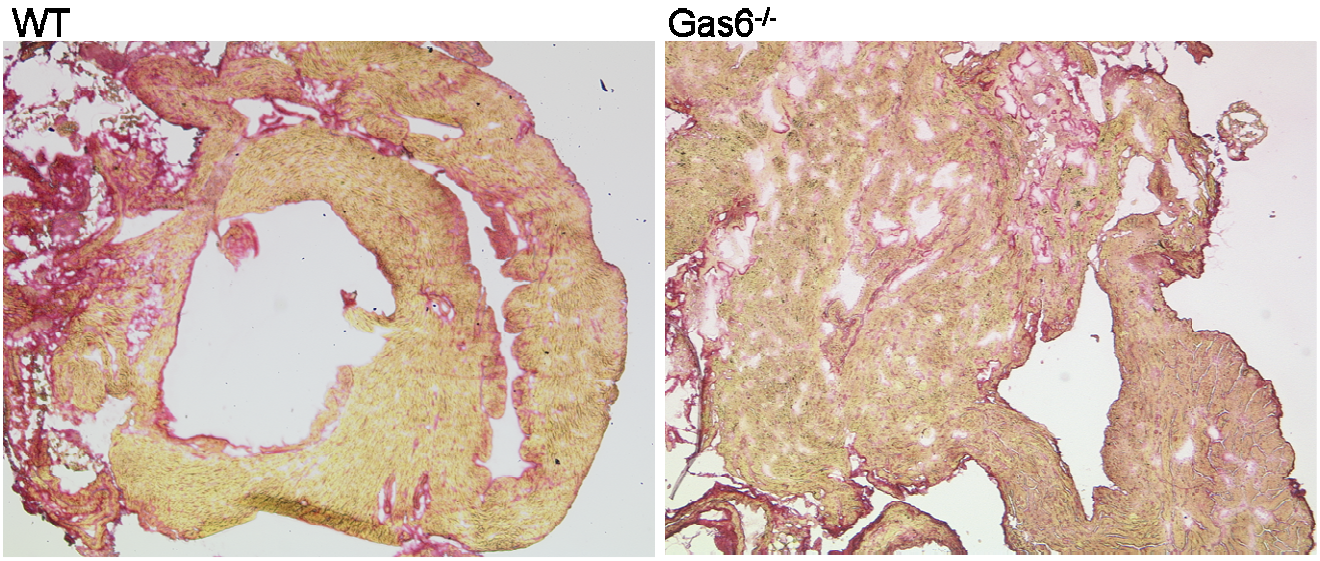

Figure 50: Collagen staining by sirius red in warfarin treated WT and Gas6$^{-/-}$ mice (50 x).

3.3.2.7 RT-PCR for MGP

Whether Gas6$^{-/-}$ mice show an upregulation of MGP gene expression in aortic tissues in all animal models (young healthy, ageing, warfarin, UniNx, EC) was investigated. However, a significant difference in MGP mRNA content in aortic tissue in all experimental groups was not detected (Figure 51).

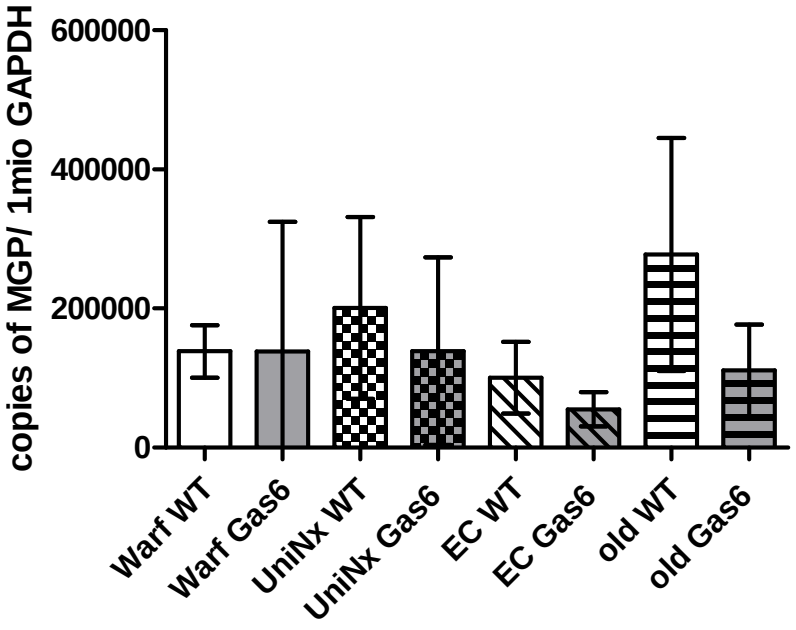

Figure 51: MGP gene expression measured by RT-PCR in WT versus Gas6$^{-/-}$ mice.

4. DISCUSSION

Aim 1 was the establishment of an appropriate method for safe and reproducible detection of GGCX activity in different tissues. Therefore I developed a fluorescence assay for the determination of the activity of the GGCX. This assay determines activities in nanomolar range (per gram protein per minute) in microsomes isolated from rat liver, kidney or aorta. The assay is based on the synthetically FITC labelled hexapeptide FLEFLK. It contains a single carboxylation site and interacts with the active centre of the GGCX enzyme. *In vivo* γ-carboxylation is essential for vitamin K dependent proteins. In most of these proteins a propetide region with 3 highly conserved amino acids seems to be important for the covalent binding with the GGCX enzyme (59). To further identify the interaction of FLEFLK-FITC with the GGCX the formation of the enzyme substrate complex could possibly be studied using nuclear magnetic resonance spectroscopy (60). The reversed phase-HPLC and MS measurements detect both the uncarboxylated as well as the carboxylated peptide as shown by the comparison between measured and calculated molecular weights (Table 2). This is indicated by different eluted peaks of FLEFLK-FITC and the more hydrophilic FLGLaFLK-FITC (Figure 18). The shorter retention time of the new appearing peak after *in vitro* carboxylation in rp-HPLC separation suggested a carboxylation of the substrate. This was proven by MS fragmentation. The comparison of mass spectrometric fingerprints of rp-HPLC eluted probes (Figures 17 and 20) with the calculated molecular weights of the carboxylated peptide revealed a high accordance. The additional peaks detected in HPLC (after 18.1 min and 18.6 min, Figure 20) may represent degradation products of the original peptide, molecular modifications like oxidation or residues from the microsomal matrix. Given the expected introduction of a carboxyl-group at the glutamic acid residues of the fragments, calculations of corresponding molecular weights are close to measured MW (measured fragments 576.7*, 581.5** and 1229.8*** MW, see Table 2 and Figure 20).

The variation of GGCX activity in liver tissues in the different healthy animals tested was quite high. This might be due to different expression levels or alterations of the activity caused by unknown conditions requiring further investigations. Age or body weight of the animals was similar excluding their influences on the GGCX activity. To our knowledge, individual differences in GGCX activity have not been investigated yet. In kidney tissues from different animals we found a quite constant enzyme activity.

The specificity of the assay is underlined by its highly significant inhibition by NEM. NEM is an inhibitor of the GGCX (49) by irreversibly alkylating sulfhydryl groups (61). The activity in liver tissues was reduced by NEM to 4% and in kidney tissues to 15% of the baseline

levels. These data are in line with previously reported results using the conventional radioactive carboxylase assay where NEM was found to inhibit the GGCX activity to 5 - 20% of baseline levels (49; 50).

The non-linearity of the substrate variation (i.e. decreased activity at higher concentrations) might be caused by an inhibiting effect of acetonitrile of the GGCX activity which is added in parallel to the substrate (Figure 26). To compare the efficiency of substrate carboxylation of FLEFLK-FITC with the frequently used pentapeptide FLEEL, the kcat/Km value was calculated from the slope of the curve of the $^{14}CO_2$ incorporation assay (Formula 1). Due to the inhibiting effect of acetonitrile on the GGCX and the limited solubility of the GGCX in an aqueous solution, the substrate concentration could not be further incrased to determine the Vmax directly. Based on the slope of the curve the calculated kcat/KM value that was 3.5 fold higher than the one reported for FLEEL (5068 vs. 1413 h^{-1} mM^{-1}) (58). This increased value might indicate a higher turnover of the GGCX in the new assay or a higher affinity for substrate FLEFLK-FITC. Nevertheless, the calculated kcat/KM value for FLEFLK-FITC indicates a sufficient carboxylation of the substrate. Further investigation on the binding between the substrate and the GGCX could explain these results.

The advantages of the new GGCX assay are the quick and direct measurement of the γ-carboxylated end product avoiding the hazardous use of radioactive labelled compounds. Purification of the substrate is achieved in a one-step procedure after incubation. The HPLC measurement yields reliable and reproducible results. This assay seems to be suitable for comparative studies between different treatment groups both of *in vitro* and *in vivo* experiments. It might also be interesting to identify possible GGCX-inhibitors or influences of gene mutations on the activity. Also of importance are VKOR/GGCX interactions. One reason for an insufficient γ-carboxylation are inhibiting effects on the VKOR as described for coumarins (62) but also seen for N-acteyl parabenzoquinone-imine a metabolite of the analgetic compound acetaminophen (paracetamol) (63). Determination of GGCX activity under several disease conditions might as well be of interest. This protocol is independent of the addition of a propeptide, underlining the practical aspect of the new assay. Measuring vitamin K dependent carboxylase activity by reversed phase HPLC enables us to calculate the activity in nmol/min/g protein, which offers the possibility to directly compare the results with the activities of DT-diaphorase and VKOR in one system.

The combination of the new GGCX assay with the assays to determine VKOR and DT-diaphorase activities enables one to investigate the complete vitamin K cycle in an *in vivo* model of CKD. For aim 2, the development of a rat model for uremia and vascular

calcification in rats, CKD was induced by 0.75% adenine diet. After 4 weeks of adenine diet, CKD was present as shown by increased creatinine und urea levels in serum (Table 3). Mild increase of the aortic calcium content was present after 4 weeks (Figure 38a) and to a calcification was established after 7 weeks of treatment (Figure 38b). The CKD rat model was also used to investigate aim 3 - the effect of uremia on the vitamin K cycle and aim 4 - the influence of vitamin K supplementation on vitamin K dependent enzyme activities. The activities of the enzymes of the vitamin K cycle were measured after 4 and 7 weeks of adenine diet. After 4 weeks – when the animals did not exhibit overt calcifications - , vitamin K deficiency was already present as evidenced by increased ucMGP serum levels (Figure 31). Typically, high serum levels of undercarboxylated proteins such as ucMGP indicate a vitamin K deficiency (64;65). At this time point the activity of the GGCX was already reduced at this stage of CKD (Figure 32), possibly contributing to the subsequent development of vascular calcification found at week 7 (Figure 38). After 4 weeks the VKOR activity was not reduced, and the DT-diaphorase was even more active, suggesting that in uremia GGCX is the rate-limiting enzyme in the vitamin K cycle and a potential major contributor to diminished vitamin K availability in tissues.

In addition, low dietary vitamin K intake has been noted in dialysis patients (7) augmenting vitamin K deficiency in uremia. Indeed, dietary vitamin K_2 supplementation (100 mg/kg, group c) in this present study lowered serum levels of ucMGP (Figure 31). These experimental observations parallel those made recently in hemodialysis patients where ucMGP serum levels were elevated and could be markedly reduced by dietary vitamin K_2 supplementation (64). Our 4 week CKD model contributes to the understanding of ucMGP action in the early stage. Vitamin K treatment resulted in significantly lower calcium tissue content in kidneys with a parallel trend in the aorta, strengthening the rationale for the planned vitamin K interventional trial *VitaVasK* targeting cardiovascular calcification in HD patients. For aim 5, the influence of oral vitamin K supplementation on vitamin K dependent enzyme activites, I assessed in a two-step approach whether correcting vitamin K deficiency in this setting rescues the uremic alterations and whether differences exist between treatment with vitamin K_1 or K_2.

To further analyze the influence of vitamin K treatment on tissue calcification, rats were also studied after 7 weeks of kidney failure, where overt vascular calcification was established as shown in *von Kossa* stained aortic specimens (Figure 40). The activity of the GGCX was still reduced after 7 weeks of adenine in kidney, liver and aortic tissues (Figure 32). High dietary

vitamin K_2 (500 mg/kg) or K_1 (100 mg/kg) restored and even over-stimulated the activity of the GGCX in several tissues. In addition, this treatment also significantly reduced calcification of the kidneys and heart. In aortic tissue we failed to reach significant differences in calcium contents by ANOVA testing which might be due to a high inter-individual variability in the extent of aortic calcification in this model. In the heart and kidneys, lower dosages of vitamin K_1 (100 mg/kg) than vitamin K_2 (500 mg/kg) were comparably effective in preventing calcification (Figure 38). Although prior observations favour vitamin K_2 above K_1 in acting on MGP and vascular calcification (66), our data suggest that vitamin K_1 is also active in these processes. Another possibility is that vitamin K_1 can be converted to K_2 inside the body as proposed before (67). Why in this study the supplementation of 100 mg/kg vitamin K_1 was even more potent than 100 mg/kg vitamin K_2 in increasing the GGCX activity and reducing calcifications needs further investigation. Recently, McCabe found increased calcium contents in aortas after adenine diet in rats and successfully reduced vascular calcification by dietary vitamin K_1 without elucidating the underlying mechanism, i.e. activity of the GGCX (68).

Compared to the daily dietary recommendation for humans (1 µg/kg body weight), the dosage of vitamin K supplements was markedly higher in these rat experiments (up to 15 mg/kg body weight). Such high dosages were chosen given that there is no evidence of toxicity from even very high vitamin K doses in man (69) and based on dosages in prior experimental studies (30).

Unexpectedly, after 7 weeks of adenine treatment, ucMGP levels were on average 16% lower than in healthy controls and 41% lower than after 4 weeks of adenine treatment. One explanation may be the accumulation of ucMGP in calcified areas in uremia (Figure 40). In addition, transdifferentiation of MGP-producing vascular smooth muscle cells into an MGP-negative osteoblastic phenotype might further reduce ucMGP serum levels as published before (70). Our workgroup (unpublished data) and others have observed that MGP-synthesising VSMC undergo apoptotic processes in calcification (71) which also may lead to reduced ucMGP serum levels.

Because altered GGCX mRNA expression - possibly leading to reduced activity - was not detected in all animal groups, the influence of uremic toxins on the low activity of the GGCX in CKD was assessed as aim 6. To assess post-transcriptional alterations, I focussed on carbamylation of this enzyme by the elevated urea concentrations in CKD. As urea levels rise in CKD, it is spontaneously transformed into cyanate which is known to irreversibly carbamylate lysine residues. Reversible modifications occur at tyrosine, serine, threonine or

cysteine residues, resulting in modification of the activities of enzymes (72). However, in the present study *in vitro* urea concentrations similar to uremic serum levels failed to affect GGCX enzyme activity (Figure 34). Two further uremic toxins tested *in vitro*, p-cresol and indoxylsulfate, did not result in altered GGCX activity either. Therefore, the mechanism of reduced GGCX activity presently remains unknown.

To summarize the influence of CKD and vitamin K supplementation on vascular calcification I found reduced activity of GGCX in uremia in several tissues possibly contributing to the observed functional vitamin K deficiency in dialysis patients. This might represent a key contributor to the increased ucMGP levels and excess cardiovascular calcification in CKD in rats. Vitamin K_1 and vitamin K_2 were able to increase GGCX activity and reduce extraosseous calcium content in the adenine nephropathy model. Thus, dietary vitamin K supplementation in CKD not only reverses the low intake but also rescues endogenous vitamin K recycling. By this dual action, the supplementation represents a promising therapeutic approach to the massively increased extraosseous calcification in CKD.

For aim 7, clarifying the role of Gas6 protein in vascular calcification I compared mice deficient for the protein Gas6 with WT mice. *In vitro*, VSMC from Gas6 deficient mice were challenged with calcification media and *in vivo* CKD was induced in mice to investigate uremic calcification. The main finding of this part of the study is that both *in vitro* and *in vivo* vascular as well as organ calcification of WT and $Gas6^{-/-}$ mice were not different between both genetic backgrounds (Figures 42 and 46).

Transformation of VSMC into an osteoblastic phenotype is a highly regulated process. Among these vitamin K dependent MGP carboxylation (73) and apoptosis (74;75) play a role in the calcification process. Previously, Gas6 mRNA stabilisation by statins was found to be a protective mechanism in cell culture experiments (21). In these *in vitro* experiments Gas6 protected against calcification. However, these findings were only seen *in vitro* and not reproduced *in vivo* yet.

Gas6 is also known to mediate antiapoptotic effects (20). In the experiments of this work I did not observe increased apoptosis in $Gas6^{-/-}$ mice *in vivo* and *in vitro* when compared to WT mice. The previous antiapoptotic findings of Gas6 mRNA cannot be confirmed by my results. Whether other antiapoptotic compensatory mechanisms are present remains speculative.

To test for potential other compensatory mechanisms avoiding the development of vascular calcification I analysed aortic MGP expression in $Gas6^{-/-}$ mice. MGP is known to be the most important local calcification inhibitor in the vessel wall (8) and could act as compensatory

mechanism the lack of Gas6. However, MGP was not upregulated in the vessel wall (Figure 49) indicating that Gas6 deficiency does not influence MGP production.

Interestingly, I observed a reduced survival of the knockout mice after electrocauterization compared to WT (Figure 44). But in mice reaching the designated end point of the treatment period, no augmented calcification was observed. As the mice died close to surgical procedures, calcification processes appear unlikely to be the reason for the increased mortality. One might speculate that inflammatory processes may play a role. Gas6 secretion is stimulated by TGF-ß (76) and Gas6 expressesion in atherosclerotic plaques was inversely associated with inflammation (76). In these experiments neither signs of inflammation in the vessel wall nor accumulation of collagen were observed. Other potential reasons could play a role for the decreased survival rate e.g. the lower body weight of the knockout animals. Alternatively, Gas6 knockout mice were reported to be protected from arterial thrombosis (77). Thus, it could be speculated that altered coagulation of the uremic $Gas6^{-/-}$ mice contributed to increased mortality. However, as we could not find tissue infarction or signs of bleeding, this mechanism does not seem to be responsible for the death rate of the $Gas6^{-/-}$ mice.

Interestingly, $Gas6^{-/-}$ mice had a higher left ventricular mass as assessed by heart ultrasound despite a smaller body weight (Table 6). This was accompanied with a lower, non significant reduction in ejection fraction (Table 8). Strikingly, calcium content of the myocardium was significantly lower in $Gas6^{-/-}$ mice compared to WT after warfarin diet (Figure 46). The reasons for this phenomenon remain speculative but one should consider that the detected cardiac calcium content ranging at 0.1 mg/g is very low and does not resemble overt calcification. Cardiac calcification is also associated with fibrosis (78) and cardiac fibroblast growth was found to be stimulated by Gas6 (19). Therefore we speculated that protective effects of lacking Gas6 might depend on a different collagen content of the hearts. Also, Gas6 was found to inhibit mRNA expression of collagen II (79). However, in our study collagen staining was equal in both $Gas6^{-/-}$ and WT mice.

One drawback of this part of the study is the use of the calcification resistant C57BL/6 genetic background of the mice in contrast to DBA/2 mice which are more prone to calcification (80). Mice deficient for Fetuin A on a C57BL/6 background (B6,129-*Ahsg*tm1Mbl) develop only minor ectopic microcalcifications in soft tissues (81). Fetuin A deficient mice backcrossed onto the DBA/2 background exhibit more severe calcification of different tissues (82). Nevertheless, in all of our models early calcification spots could be induced on the C57BL/6

background and the lack of aggravated calcification by depletion of Gas6 does not support a major role of Gas6 in vascular calcification pathogenesis.

5 CONCLUSIONS

The importance of vitamin K besides blood coagulation is a topic of current interest. All vitamin K dependent blood coagulation factors contain 9-12 Glu residues. Calcium binding is the crucial mechanism of all vitamin K dependent proteins. In their carboxylated form, Gla residues are capable to bind to phospholipid layers coupled with calcium ions. Vitamin K is regarded to prevent calcification of soft tissues by carboxylating MGP and the calcium binding property gained by this procedure is regarded as the main reason of MGP acting as a calcification inhibitor. A functional vitamin K deficiency is found in dialysis patients as shown by increased serum levels of ucMGP, ucOcn and PIVKAII. These patients exert pronounced vascular calcification which contributes to a highly increased mortality and morbidity. The reduced vitamin K deficiency under uremia is the topic of this work. Here I demonstrated that under uremic conditions the activity of the key enzyme of the vitamin K cycle γ-glutamyl carboxylase is reduced and can be reversed by high dose vitamin K supplementation whereas the remaining enzymes were unaffected by uremia. Further research will be needed to investigate the mechanism underlying the reduced GGCX activity in kidney disease. Vitamin K supplementation was able to reduce the extent of soft tissue calcification in rats with kidney failure. This was paralleled by an increase of the activity of the GGCX and a reduction of ucMGP serum levels. This suggests that increasing the amount of dietary vitamin K offers a therapeutic target to prevent calcification processes in patients with kidney disease. Not only for vitamin K deficient patients like kidney patients but also for healthy people a higher daily, dietary vitamin K recommendation should be taken under consideration. But special care might be taken in diabetic patients, because the carboxylated form of osteocalcin is associated with decreasing insulin sensitivity although data on a direct harmful effect is lacking.

Some studies suggest a role of the vitamin K dependent protein Gas6 in preventing vascular calcification. Here I did not detect any effects of Gas6 deficiency on the development of vascular calcification in mice.

Human interventional trials are still needed to clarify the efficacy of vitamin K treatment. Of interest are also potential beneficial effects of high vitamin K intake in healthy individuals as well as differences of vitamin K subforms on metabolic and clinical effects.

i Reference List

1. Souci, Fachmann, Kraut. Food Composition and Nutrition Tables. Deutsche Forschungsanstalt für Lebensmittelchemie, 2008.

2. Sato T, Yamada Y, Ohtani Y, Mitsu N, Murasawa H, Araki S. Production of Menaquinone (Vitamin K2)-7 by *Bacillus subtilis*. J Biosci Bioeng 2001;91:16-20.

3. Furie B, Furie BC. The Molecular Basis of Blood Coagulation. Cell 1988;53:505-18.

4. Thijssen HH, Drittij-Reijnders MJ. Vitamin K distribution in rat tissues: dietary phylloquinone is a source of tissue menaquinone-4. Br.J Nutr. 1994;72:415-25.

5. Shearer MJ, Newman P. Metabolism and cell biology of vitamin K. Thromb Haemost 2008;100:530-47.

6. Schlieper G, Westenfeld R, Krüger T et al. Circulating nonphosphorylated carboxylated matrix gla protein predicts survival in ESRD. J Am Soc Nephrol 2011;22:387-95.

7. Cranenburg E, Schurgers LJ, Uiterwijk HH et al. Vitamin K intake and status are low in hemodialysis patients. Kidney Int 2012;epub.

8. Lomashvili KA, Wang X, Wallin R, O`Neill C. Matrix Gla Protein Metabolism in Vascular Smooth Muscle and Role in Uremic Vascular Calcification. J.Biol.Chem. 2011;286:28715-22.

9. Luo G, Ducy P, McKee MD et al. Spontaneous calcification of arteries and cartilage in mice lacking matrix GLA protein. Nature 1997;386:78-81.

10. Zebboudj AF, Imura M, Bostrom K. Matrix GLA Protein, a Regulatory Protein for Bone Morphogenetic Protein-2. J.Biol.Chem. 2002;277:4388-94.

11. Briet M, Burns KD. Chronic kidney disease and vascular remodelling: molecular mechanisms and clinical implications. Clin Sci 2012;123:399-416.

12. Cranenburg EC, Brandenburg VM, Vermeer C et al. Uncarboxylated matrix Gla protein (ucMGP) is associated with coronary artery calcification in haemodialysis patients. Thromb Haemost. 2009;101:359-66.

13. London GM, Marchais SJ, Guérin AP, Métivier F. Arteriosclerosis, vascular calcifications and cardiovascular disease in uremia. Curr Opin Nephrol Hypertens 2005;14(6):525-31.

14. Levey AS, Coresh J. Chronic kidney disease. Lancet 2012;379:165-80.

15. Bellasi A, Raggi P. Vascular imaging in chronic kidney disease. Curr Opin Nephrol Hypertens 2012;21:382-8.

16. Shantouf RS, Budoff MJ, Ahmadi N et al. Total and Individual Coronary Artery Calcium Scores as Independent Predictors of Mortality in Hemodialysis Patients. Am J Nephrol 2010;31:419-25.

17. Ketteler M, Schlieper G, Floege J. Calcification and cardiovascular health: new insights into an old phenomenon. Hypertension 2006;47:1027-34.

18. Nakano T, Kawamoto K, Kishino J, Nomura K, Higashino K, Aarita H. Requirement of gamma-carboxyglutamic acid residues for the biological activity of Gas6: contribution of endogenous Gas6 to the proliferation of vascular smooth muscle cells. Biochem J 1997;323:387-92.

19. Stenhoff J, Dahlbäck B, Hafizi S. Vitamin K-dependent Gas6 activates ERK kinase and stimulates growth of cardiac fibroblasts. Biochem Biophys Res Commun. 2004;319:871-8.

20. Hasanbasic I, Rajotte I, Blostein M. The role of *ã*-carboxylation in the anti-apoptotic function of gas6. Journal of Thrombosis and Haemostasis 2005;2790-7.

21. Son BK, Kozaki K, Iijima K et al. Statins Protect Human Aortic Smooth Muscle Cells From Inorganic Phosphate-Induced Calcification by Restoring Gas6-Axl Survival Pathway. Circ Res 2006;01.

22. Shobeiri N, Adams MA, Holden RM. Vascular calcification in animal models of CKD: A review. Am J Nephrol 2010;31:471-81.

23. Neven E, D'Haese PC. Vascular Calcification in Chronic Renal Failure What Have We Learned From Animal Studies? Circ Res. 2011;108:249-64.

24. Price PA, Faus SA, Williamson MK. Warfarin-induced artery calcification is accelerated by growth and vitamin D. Arterioscler Thromb Vasc Biol. 2000;20:317-27.

25. Koos R, Mahnken AH, Muhlenbruch G et al. Relation of oral anticoagulation to cardiac valvular and coronary calcium assessed by multislice spiral computed tomography. Am J Cardiol. 2005;96:747-9.

26. Weijs B, Blaauw Y, Rennenberg R et al. Patients using vitamin K antagonists show increased levels of coronary calcification: an observational study in low-risk atrial fibrillation patients. Eur.Heart J 2011;32:2555-62.

27. Sadowski JA, Suttie JW. Mechanism of Action of Coumarins. Significance of Vitamin K Epoxide. Biochemistry 1974;13:3697-9.

28. Bruining N, van Domburg RT. Long-term application of vitamin K antagonists, more harm than good? The additional value of imaging. Eur.Heart J 2011;32:2473-5.

29. Chatrou MLL, Winckers K, Hackeng TM, Reutelingsperger C, Schurgers LJ. Vascular calcification: The price to pay for anticoagulation therapy with vitamin K-antagonists. Blood 2012;26:155-66.

30. Schurgers LJ, Spronk HM, Soute BA, Schiffers PM, DeMey JG, Vermeer C. Regression of warfarin-induced medial elastocalcinosis by high intake of vitamin K in rats. Blood 2007;109:2823-31.

31. Emson CT, Suttie JW. Vitamin K dependent Carboxylase. J.Biol.Chem. 1976;251:6238-43.

32. Buitenhuis HC, Soute BA, Vermeer C. Comparison of the vitamins K1, K2 and K3 as cofactors for the hepatic vitamin K-dependent carboxylase. Biochem.Biophys.Acta 1990;1034:170-5.

33. Tie J, Wu SM, Jin D, Nicchitta CN, Stafford DW. Atopological study of the human g-glutamyl carboxylase. Blood 2000;96:973-8.

34. Vermeer C. Gamma-carboxyglutamate-containing proteins and the vitamin K-dependent carboxylase. Biochem J 1990;266:625-36.

35. Berkner KL. Vitamin K-Dependent Carboxylation. Vitamins and Hormones 2008;78:131-56.

36. Wood GM, Suttie JW. Vitamin K-dependent Carboxylase. J Biol Chem 1988;263:3234-9.

37. Chu P, Huang TY, Williams J, Stafford DW. Purified vitamin K epoxide reductase alone is sufficient for conversion of vitamin K epoxide to vitamin K and vitamin K to vitamin KH2. Proc.Natl.Acad.Sci. 2006;103:19308-13.

38. Oldenburg J, Marinova M, Müller-Reible C, Watzka M. The Vitamin K Cycle. Vitamins and Hormones 2008;78:35-62.

39. Tie J, Jin D, Straight DL, Stafford DW. Functional study of the vitamin K cycle in mammalian cells. Blood 2011;117:2967-74.

40. Spronk HM, Soute BA, Schurgers LJ, Thijssen HH, De Mey JG, Vermeer C. Tissue-specific utilization of menaquinone-4 results in the prevention of arterial calcification in warfarin-treated rats. J Vasc Res 2003;40:531-7.

41. Fasco MJ, Principe LM, Walsh WA, Friedman PA. Warfarin Inhibition of Vitamin K 2,3-Epoxide Reductase in Rat Liver Microsomes. Biochemistry 1983;22:5655-60.

42. Preusch PC, Siegel D, Gibson NW, Ross D. A note on the inhibition of the DT-diaphorase by dicoumarol. Free Radical Biology & Medicine 1991;11:77-80.

43. Stafford DW. The vitamin K cycle. J Thromb Haemost. 2005;3:1873-8.

44. Krueger T, Westenfeld R, Ketteler M, Schurgers LJ, Floege J. Vitamin K deficiency in CKD patients: a modifiable risk factor for vascular calcification? Kidney Int 2009.

45. Ulrich MW, Furie B, Jacobs MR, Vermeer C, Fu B. Vitamin K-dependent Carboxylation. J.Biol.Chem. 1988;263A :9697-702.

46. McTigue JJ, Dahaon MK, Rich DH, Richardson M, Suttie JW. Vitamin K-dependent Carboxylase. Biochem.J. 1984;259 :4272-8.

47. Morris DP, Soute BAM, Vermeer C, Stafford DW. Characterization of the Purified Vitamin K-dependent Gamma-Glutamyl Carboxylase. J Biol Chem 1993;268:8735-42.

48. Sadowski JA, Emson C.T., Suttie JW. Vitamin K-dependent Carboxylase. J.Biol.Chem. 1975;251:2770-6.

49. Canfield LM. Vitamin K-dependent oxygenase/carboxylase; differential inactivation by sulfhydryl reagents. Biochem Biophys Res Commun. 1987;148:184-91.

50. Lipsky JJ. Mechanism of the inhibition of the y-carboxylation of glutamic acid by N-methylthiotetrazole-containing antibiotics. Proc.Natl.Acad.Sci. 1984;81:2893-79.

51. Mutucumarana VP, Stafford DW, Stanley TB et al. Expression and Characterization of the Naturally Occurring Mutation L394R in Human g-Glutamyl Carboxylase. J Biol Chem 2000;275:32572-7.

52. Cranenburg E, Brandenburg VM, Vermeer C et al. Uncarboxylated matrix Gla protein (ucMGP) is associated with coronary artery calcification in haemodialysis patients. Thromb Haemost 2009;101:359-66.

53. Prochaska HJ, Santamaria AB. Direct Measurement of NAD(P)H:Quinone Reductase from Cells Cultured in Microtiter Wells: A Screening Assay for Anticarcinogenic Enzyme Inducers. Anal.Biochem. 1988;169:328-36.

54. Westenfeld R, Schaefer C, Smeets R et al. Fetuin-A (AHSG) prevents extraosseous calcification induced by uraemia and phosphate challenge in mice. Nephrol Dial.Transplant. 2007;22:1537-46.

55. Schurgers LJ, Teunissen KJ, Knapen MH et al. Novel conformation-specific antibodies against matrix gamma-carboxyglutamic acid (Gla) protein: undercarboxylated matrix Gla protein as marker for vascular calcification. Arterioscler Thromb Vasc Biol 2005;25:1629-33.

56. Gagnon RF, Duguid WP. A Reproducible Model for Chronic Renal Failure in the Mouse. Urol Res. 1982;11:11-4.

57. Westenfeld R, Schafer C, Kruger T et al. Fetuin-A protects against atherosclerotic calcification in CKD. J Am Soc Nephrol 2009;20:1264-74.

58. Mutucumarana VP, Achers F, Straight DL, Jin DY, Stafford DW. A Conserved Region of Human Vitamin K-dependent Carboxylase between Residues 393 and 404 Is Important for Its Interaction with the Glutamate Substrate. J Biol Chem 2003;278:46488-93.

59. Berkner KL. The Vitamin K-Dependent Carboxylase. J.Nutr. 2000;130:1877-80.

60. Roberts GCK. The Other Kind of Biological NMR -Studies of Enzyme-Substrate Interactions. Neurochemical Research 1996;21:1117-24.

61. Smyth DG, Blumenfeld OO, Konigsberg W. Reactions of N-Ethylmaleimide with Peptides and Amino Acids. Biochem J 1964;91:589-95.

62. Sadowski JA, Suttie JW. Mechanism of Action of Coumarins. Signisifcance of Vitamin K Epoxide. Biochemistry 1974;13:3697-9.

63. Thijssen HH, Soute BA, Vervoort LM, Claessens JG. Paracetamol (acetaminophen) warfarin interaction: NAPQI, the toxic metabolite of paracetamol, is an inhibitor of enzymes in the vitamin K cycle. Thromb Haemost. 2013;92:797-802.

64. Westenfeld R, Krüger T, Schlieper G et al. Effect of Vitamin K2 Supplementation on Functional Vitamin K Deficiency in Hemodialysis Patients: A Randomized Trial. Am J Kidney Dis. 2012;59:186-95.

65. Shea MK, O'Donnell CJ, Vermeer C et al. Circulating Uncarboxylated Matrix Gla Protein Is Associated with Vitamin K Nutritional Status, but Not Coronary Artery Calcium, in Older Adults. J Nutr. 2011;141:1529-34.

66. Geleijnse JM, Vermeer C, Grobbee DE et al. Dietary intake of menaquinone is associated with a reduced risk of coronary heart disease: the Rotterdam Study. J Nutr. 2004;134:3100-5.

67. Al Rajabi A, Booth SL, Peterson JW et al. Deuterium-labeled phylloquinone has tissue-specific conversion to menaquinone-4 among fischer 344 male rats. J Nutr. 2012;142:841-5.

68. McCabe KM, Booth SL, Fu X et al. Dietary vitamin K and therapeutic warfarin alter the susceptibility to vascular calcification in experimental chronic kidney diesease. Kidney Int 2013;83:835-44.

69. Truong J, Booth SL. Emerging Issues in Vitamin K Research. JEBCAM 2011;26:73-9.

70. Montezano AC, Zimmerman D, Yusuf H et al. Vascular Smooth Muscle Cell Differentiation to an Osteogenic Phenotype Involves TRPM7 Modulation by Magnesium. Hypertension 2010;56:453-362.

71. Shroff RC, McNair R, Skepper JN et al. Chronic Mineral Dysregulation Promotes Vascular Smooth Muscle Cell Adaption and Extracellular Matrix Calcification. J Am Soc Nephrol 2010;21:103-12.

72. Kraus LM, Kraus AP. Carbamoylation of amino acids and proteins in uremia. Kidney Int 2001;59:102-7.

73. Schurgers LJ, Spronk HM, Skepper JN et al. Post-translational modifications regulate matrix Gla protein function: importance for inhibition of vascular smooth muscle cell calcification. J Thromb Haemost. 2007;5:2503-11.

74. Shanahan CM, Crouthamel MH, Kapustin A, Giachelli CM. Arterial Calcification in Chronic Kidney Disease: Key Roles for Calcium and Phosphate. Circ Res. 2011;109:697-711.

75. Clarke MCH, Littlewood TD, Figg N et al. Chronic Apoptosis of Vascular Smooth Muscle Cells Accelerates Atherosclerosis and Promotes Calcification and Medial Degeneration. Circ Res 2008;102:1529-38.

76. Clauser S, Meilhac O, Bièche I et al. Increased secretion of Gas6 by smooth muscle cells in human atherosclerotic carotid plaques. Thromb Haemost 2012;107:140-9.

77. Angelillo-Scherrer A, Garcia de Frutos P, Aparicio C et al. Deficiency or inhibition of Gas6 causes platelet dysfunction and protects mice against thrombosis. Nature 2001;7:215-21.

78. Merx MW, Schafer C, Westenfeld R et al. Myocardial stiffness, cardiac remodeling, and diastolic dysfunction in calcification-prone fetuin-A-deficient mice. J.Am.Soc.Nephrol. 2005;16:3357-64.

79. Motomura H, Niimi H, Sugimori K, Toshihisa O, Kimura T, Kitajima I. Gas6, a new regulator of chondrogenic differentiation from mesenchymal cells. Biochem Biophys Res Commun. 2007;357:997-1003.

80. Moe SM. Vascular Calcification: The Three-Hit Model. J Am Soc Nephrol 2009;20:1162-4.

81. Jahnen-Dechent W, Schinke T, Trindl A et al. Cloning and Targeted Deletion of the Mouse Fetuin Gene. J Biol Chem 1997;272:31496-503.

82. Schaefer C, Heiss A, Schwarz A et al. The serum protein alpha 2-Heremans-Schmid glycoprotein/fetuin-A is a systemically acting inhibitor of ectopic calcification. J Clin.Invest 2003;112:357-66.

ii Danksagungen

Ein ganz herzlicher Dank gilt allen, die das Gelingen dieser Arbeit überhaupt erst möglich gemacht haben! Insbesondere möchte ich mich bedanken bei:

Dr. med. Thilo Krüger für die nette umfassende Betreuung im Labor, spaßigen Dienstreisen und Unterstützung in allen Lebenslagen.

Frau Prof. Brigitte Schmitz für die Übernahme des Erstgutachtens und ihr Bemühen zu Zeiten des thematischen Wechsels.

Frau Prof. Simone Diestel für die Übernahme des Zweitgutachtens.

PD Dr. med. Vincent Brandenburg für die unterhaltsame Betreuung, allzeit verlässliche Rückendeckung und vor allem seinen unermüdlichen Einsatz gegen die dunkle Seite der Macht.

PD Dr. med. Georg Schlieper für die nette Betreuung und sein organisatorisches Talent.

CTA Katrin Härthe für die nette Aufnahme im Labor, stets offenen Ohren, technischen Support insbesondere bei den molekularbiologischen Methoden, bastlerisches Geschick und kompetentes brainstorming für neue Experimente.

Herr Prof. Dr. med. Jürgen Floege für die Aufnahme ins Team der Med. Klinik II.

Herr Dr. rer. nat. Thomas Schettgen für die Überlassung des HPLC Arbeitsplatzes und die MS Messungen.

Petra Dewes für die Einarbeitung in die HPLC.

Elke Magdeleyns und Marjolein Herfs für die ucMGP Messungen.

Svenja Immendorf für die Kultivierung der murinen VSMC.

Chun Ouyang für die Unterstützung bei der Elektrokauterisuerung der Nieren.

Vasantha Mutucumarana für die $^{14}CO_2$ Incorporsationsmessung und die Berechnung des zugehörigen kcat/Km.

Prof. Peter Carmeliet für die Überlassung zweier Gas6$^{-/-}$ Zuchtpaare.

Allen Kollegen der Medizinischen Klinik II für das freundschaftliche Miteinander.

Zu guter letzt Daniel für die letzten 15 Jahre.